

Dissertation

der Fakultät für Biologie
der Ludwig-Maximilians-Universität München

**Characterization of Neuropeptide S (NPS)
in view of its potential as
a novel anxiolytic therapy for anxiety disorders**

vorgelegt von
Irina Alexandra Ionescu

München, 28. Februar 2012

Erstgutachter: Professor Dr. Rainer Landgraf

Zweitgutachter: Professor Dr. Lutz Wiegrebe

Datum der mündlichen Prüfung: 30. Juli 2012

Men ought to know that from nothing else but the brain come joys, delights, laughter and sports, and sorrows, griefs, despondency, and lamentations. ... And by the same organ we become mad and delirious, and fears and terrors assail us, some by night, and some by day, and dreams and untimely wanderings, and cares that are not suitable, and ignorance of present circumstances, desuetude, and unskillfulness. All these things we endure from the brain, when it is not healthy...

Hippocrates, *On the Sacred Disease* (400 BCE)

***To my parents and my grandparents,
who never doubted me,
with all my love.***

Abstract

Anxiety disorders, such as posttraumatic stress disorder (PTSD), are characterized by a high prevalence and debilitating symptoms. However, the current first-line treatment for these conditions, which consists of selective serotonin reuptake inhibitors (SSRIs) and cognitive behavioral therapy, alongside symptomatic treatment with benzodiazepines, does not represent by far a functional solution for all affected patients. Therefore, identifying and characterizing novel candidates for alternative anxiolytic therapies are a crucial focus of psychiatric and neurobiological research.

This study focuses on Neuropeptide S (NPS), a newly identified endogenous neuropeptide that has been shown to exert strong anxiolytic effects upon intracerebral injection in rodents. In an approach that combines basic research with incipient clinically relevant application, novel mechanisms and brain targets of NPS-mediated anxiolytic effects were identified, and a noninvasive application procedure also applicable in patients, namely the intranasal administration, was established for the first time for NPS in mouse models.

In a first step, the feasibility of intranasal NPS delivery was established in mice using fluorophore-coupled NPS to allow intracerebral tracking. This method permitted for the first time tracking of intranasally applied substances within the brain at a single-cell resolution. These results not only proved the applicability of intranasal NPS administration in the mouse, but also allowed identification and characterization of hitherto undescribed cerebral NPS target cells, which were shown to be most likely exclusively neurons. Moreover, specific uptake of fluorescently labeled NPS in the hippocampus provided the first direct evidence linking this brain region, a well-known major player in the regulation of fear expression, to the NPS circuitry. Further investigation into the functional role of the hippocampus in NPS-elicited anxiolytic effects revealed that local microinjections of NPS into the ventral CA1 (vCA1) region are sufficient to elicit anxiolysis in C57BL6/N mice on the elevated plus maze (EPM).

In a second step, behavioral and molecular effects of intranasal NPS treatment were characterized in C57BL/6N mice. Intranasal application of NPS was shown here to produce anxiolytic effects similar to those described by others after intracerebral injection. This finding represents the basis for the implementation of a future NPS-

based therapy via nasal sprays in patients suffering from anxiety disorders. Furthermore, the molecular effects of NPS treatment on cerebral protein expression were examined here for the first time. This research led to identification of novel downstream targets of NPS-mediated regulation in the hippocampus and the prefrontal cortex. These new targets include proteins involved in the glutamatergic system and in synaptic plasticity, both of which are known to be dysregulated in anxiety disorders.

Finally, the effects of intranasal NPS treatment, hitherto described only in non-pathological animal models, were examined for the first time in mouse models of anxiety disorders, namely the high anxiety behavior (HAB) mice and a mouse model of PTSD. In HAB mice, NPS treatment elicited anxiolytic effects similar to those observed in C57BL/6N mice. In the mouse model of PTSD, NPS counteracted disease-related changes in expression levels of hippocampal synaptic proteins.

To sum up, this work expands the current state-of-knowledge concerning the molecular and mechanistic background of NPS-mediated anxiolysis by characterizing the role of the hippocampus in the NPS circuitry and by identifying novel downstream targets of NPS. The data on anxiolytic effects of intranasal NPS treatment especially in mouse models of anxiety disorders furthermore establishes the therapeutic potential of NPS as a novel anxiolytic treatment.

ABSTRACT	I
TABLE OF ABBREVIATIONS IN ALPHABETICAL ORDER	VII
1. INTRODUCTION	1
1.1. The endocrine stress response	1
1.2. The HPA axis in psychiatric disorders	3
1.3. Anxiety disorders	4
1.3.1. Posttraumatic stress disorder (PTSD)	5
1.4. Neuropeptide S and its receptor, NPSR	8
1.5. Intranasal application	11
1.6. Mouse models of anxiety disorders	12
1.6.1. The HAB mice, a mouse model for inbred anxiety	13
1.6.2. The mouse model of PTSD	14
1.7. Goals	15
2. METHODS AND MATERIALS	16
2.1. Cell biology	16
2.1.1. Generation of tagged NPSR constructs	16
2.1.1.1. Isolation of total mRNA from murine brain regions.....	16
2.1.1.2. Reverse transcription of total mRNA into cDNA.....	17
2.1.1.3. Amplification of NPSR cDNA from total cDNA	18
2.1.1.4. Cloning insert into plasmid	19
2.1.2. Transfection of HEK cells with the NPSR constructs	21
2.1.2.1. Expression of NPSR constructs on mRNA level	22
2.1.2.2. Immunofluorescence of NPSR constructs.....	23
2.1.3. Stimulation with Cy3-NPS	24
2.2. ICV and intranasal application of fluorescent NPS conjugates in mice	25
2.2.1. Animals.....	25
2.2.2. Stereotactic surgery and ICV injection	25
2.2.3. Intranasal application of fluorescent NPS conjugates	26

2.2.4. Brain removal and immunohistochemistry	27
2.3. Analysis of behavioral and molecular effects of intranasal NPS application	28
2.3.1. Animals.....	28
2.3.2. Intranasal NPS application in C57BL/6N and HAB mice.....	29
2.3.2.1. Behavioral assays	30
2.3.2.1.1. Statistical analysis	30
2.3.2.2. Analysis of molecular changes after NPS treatment	31
2.3.2.2.1. Preparation of single brain regions and selection of candidates	31
2.3.2.2.2. mRNA isolation and real-time PCR	31
2.3.2.2.2. Protein isolation and immunoblotting.....	32
2.3.2.2.3. Statistical analysis	35
2.3.3. Intranasal NPS application in a mouse model of PTSD	35
2.3.3.1. Behavioral assays	35
2.3.3.2. Protein and mRNA expression in Hc and Pfc.....	36
2.3.3.3. Measurement of corticosterone plasma levels	36
2.3.3.4. Statistical evaluation.....	37
2.3.3.4.1. Behavioral assays	37
2.3.3.4.2. Protein and mRNA data.....	37
2.3.3.4.3. Corticosterone plasma levels	37
2.4. Behavioral effects of NPS treatment via injection into the ventral CA1 region (vCA1).....	38
2.4.1. Stereotactic surgery	38
2.4.2. Injection of Cy3-NPS into vCA1	38
2.4.3. Behavioral assays	38
2.4.3.1. Statistical analysis	39
3. RESULTS.....	40
3.1. Cloning of NPSR and <i>in vitro</i> analysis of NPSR-NPS interaction.....	40
3.1.1. Visualization of EGFP-NPSR and FLAG-NPSR in HEK cells	41
3.1.2. Stimulation of NPSR-expressing HEK cells with Cy3-NPS	42
3.2. Brain target regions and target neurons of NPS.....	44
3.2.1. Identification of brain target regions and cells of NPS by intracerebroventricular (ICV) administration of Cy3-NPS.....	44
3.2.2. Specificity of Cy3-NPS uptake	47
3.2.3. Characterization of cell types taking up Cy3-NPS.....	51
3.2.4. Intranasal administration of Cy3-NPS	53

3.2.5. Identification of the hippocampus as a novel target brain region of NPS	56
3.3. Behavioral and molecular effects of intranasally applied NPS.....	57
3.3.1. Behavioral phenotype after intranasal NPS application	58
3.3.2. Regulatory effects of NPS on protein and mRNA expression of proteins involved in the glutamatergic system and synaptic plasticity	60
3.4. The role of the ventral hippocampus in NPS-elicited anxiolytic effects	63
3.4.1. Cy3-NPS distribution is restricted to the ventral CA1 region (vCA1) after local injection	64
3.4.2. NPS injection into vCA1 leads to anxiolytic locomotion-independent effects	65
3.5. Acute intranasal NPS treatment in high anxiety behavior (HAB) mice, a mouse model for pathological anxiety	67
3.5.1. Behavioral phenotype after intranasal NPS application	68
3.5.2. Regulatory effects of NPS on protein and mRNA expression of proteins involved in the glutamatergic system and synaptic plasticity	69
3.6. Acute intranasal NPS treatment in a mouse model of PTSD	71
3.6.1. Behavioral results	72
3.6.2. Analyses of mRNA and protein expression in hippocampus and prefrontal cortex in the PTSD mouse model	73
3.6.3. Corticosterone plasma levels	75
4. DISCUSSION	76
4.1. Anxiolytic effects of intranasally applied NPS in C57BL/6N and HAB mice.....	76
4.2. Identification of target brain regions and target neurons of NPS by NPSR-mediated internalization of Cy3-NPS	78
4.3. The hippocampus: A novel player in NPS-mediated anxiolytic effects	80
4.4. NPS and the glutamatergic system in C57BL/6N and HAB mice.....	83
4.5. Effects of NPS treatment on cerebral protein expression in a mouse model of PTSD.....	85
4.6. Summary	86
5. SUPPLEMENTARY MATERIAL	88
6. REFERENCES	97

ACKNOWLEDGMENTS.....	112
CURRICULUM VITAE.....	114
LIST OF PUBLICATIONS.....	116
DECLARATION / ERKLÄRUNG.....	117

Table of abbreviations in alphabetical order

ACTH	adrenocorticotrophic hormone
AMPA	α -amino-3-hydroxy-5-methyl-4-isoxazolepropionic acid
ANOVA	analysis of variance
APS	ammonium persulfate
ASR	acoustic startle response
BCA	bicinchoninic acid
BLA	basolateral amygdala
BSA	bovine serum albumin
cAMP	cyclic adenosine monophosphate
cDNA	complementary DNA
CNS	central nervous system
CREB	cAMP-response element binding protein
CRH	corticotropin-releasing hormone
CSF	cerebrospinal fluid
Cy3	cyanine 3
DAPI	4',6-diamidino-2-phenylindole
DCS	D-cycloserine
DEPC	diethylpyrocarbonate
DMEM	Dulbecco's Modified Eagle's medium
DNA	deoxynucleic acid
dNTP	deoxy-nucleoside triphosphate
DSM-IV	fourth edition of the Diagnostic and Statistical Manual of Mental Disorders
<i>E. coli</i>	<i>Escherichia coli</i>
EDTA	ethyleendiaminetetraacetic acid
EGFP	enhanced green fluorescent protein
ELISA	enzyme-linked immunoabsorbent assay
EPM	elevated plus maze
EtBr	ethidium bromide
FCS	fetal calf serum
FKBP5	FK506 binding protein 5
GABA	γ -amino butyric acid
GABA _A	GABA receptor subtype A
GAD	generalized anxiety disorder
GAPDH	glyceraldehyde 3-phosphate dehydrogenase
GFAP	glial fibrillary acidic protein
GlT-1	glutamate transporter type 1
GluR1/2	subunits 1 and 2 of the AMPA receptor
GPCR	G-protein coupled receptor
GR	glucocorticoid receptor
HA	hemagglutinin

Table of abbreviations

HAB	high anxiety behavior
Hc	hippocampus
HEK	human embryonic kidney
HPA	hypothalamo-pituitary-adrenal
HRP	horseradish peroxidase
Iba-1	ionized calcium binding adaptor molecule 1
ICV	intracerebroventricular
ISH	in situ hybridization
LAB	low anxiety behavior
LB	lysogeny broth
LC	locus coeruleus
MAPK	mitogen-activated protein kinase
MDB	membrane desalting buffer
MR	mineralocorticoid receptor
mRNA	messenger ribonucleic acid
NAB	normal anxiety behavior
NF	neurofilament
NMDA	N-methyl-D-aspartate
NPS	Neuropeptide S
NPSR	NPS receptor
NPY	Neuropeptide Y
PBS	phosphate buffered saline
PCR	polymerase chain reaction
PD	panic disorder
PFA	paraformaldehyde
Pfc	prefrontal cortex
PTSD	posttraumatic stress disorder
PV	paraventricular nucleus of the hypothalamus
rDNase	reconstituted DNase
REM	rapid eye movement
rpm	rotations per minute
RT	room temperature
SDS-PAGE	sodium dodecyl sulfate polyacrylamide gel electrophoresis
SHA 68	3-oxo-1,1-diphenyl-tetrahydrooxazolo-[3,4-a]pyrazine-7-carboxylic acid 4-fluoro-benzylamide
SNP	single nucleotide polymorphism
SOB	Super Optimal Broth
SSRI	selective serotonin reuptake inhibitor
TBE	tris/borate/EDTA
TBST	Tris-buffered saline with Tween 20
TEMED	tetraethylmethylenediamine
TMB	tetramethylbenzidine
vCA1	ventral CA1 region

1. Introduction

1.1. The endocrine stress response

The term “stress”, used for a long time only in physical sciences as a synonym for “tension”, was coined in its physiological sense by Hans Selye as late as the 1930s. Nowadays, it is applied almost exclusively to designate the biological phenomenon that Selye defined as “the non-specific response of the body to any demand placed upon it” (Selye, 1956).

The most important characteristic of stress is the disruption of systemic homeostasis (Cannon, 1932). The human organism can respond to stressors on different levels. In most cases, this response is beneficial (Chrousos and Gold, 1992), since it allows adaptation to extraordinary circumstances via two well-described different endocrine pathways, known as the central stress pathways (Praag et al., 2004; Steckler et al., 2005): 1) activation of the sympathetic nervous system, a fast process leading to immediate response readiness; and 2) activation of the hypothalamo-pituitary-adrenal (HPA) axis, a slower reaction resulting in long-term readjustment of internal processes.

The sympathetic nervous system is activated to achieve a fight-or-flight response to an imminent threat. This leads to increased release of catecholamines, especially adrenaline (from the adrenal medulla) and noradrenaline (released peripherally from the adrenal medulla and centrally from the locus coeruleus (LC)). Adrenaline increases cardiac frequency and blood pressure, dilates the bronchi, and activates lipolysis and glucose release and biosynthesis. Noradrenaline, on the other hand, also possesses a neurotransmitter function, by which it can increase arousal and modulate cognitive and affective processes (Steckler et al., 2005).

Long-term adaptation to stressors is additionally mediated via increased activity of the HPA axis (see Figure 1). The HPA axis involves complex interactions between various brain structures and glands. Stressors act as stimuli which lead to increased secretion of the neuropeptides vasopressin and corticotropin-releasing hormone (CRH) from the paraventricular nucleus (PV) of the hypothalamus. These in turn are transported from the median eminence to the pituitary and stimulate, in the anterior

lobe of the pituitary, release of adrenocorticotrophic hormone (ACTH), which ultimately activates the adrenal cortex to upregulate synthesis of glucocorticoid hormones such as cortisol (or corticosterone in rats and mice). These glucocorticoids then exert, mainly via the glucocorticoid receptor (GR) and the mineralocorticoid receptor (MR), a variety of actions, such as suppression of immune activity and increased glucose availability to adapt to stressful environmental cues. Interestingly, effects of glucocorticoids on synaptic plasticity have also been postulated as potential players in stress-induced changes in synaptic plasticity via regulation of the glutamatergic system (Krugers et al., 2010). This process occurs at least partly by corticosterone-mediated increase 1) in the release of glutamate (Karst et al., 2005); 2) in the availability of subunits 1 and 2 (GluR1 and GluR2) of the α -amino-3-hydroxy-5-methyl-4-isoxazolepropionic acid (AMPA) receptor (a ionotropic glutamate receptor) at the postsynaptic site (Groc et al., 2008); and 3) in the synaptic insertion of GluR2-containing AMPA receptors (Karst et al., 2005; Martin et al., 2009).

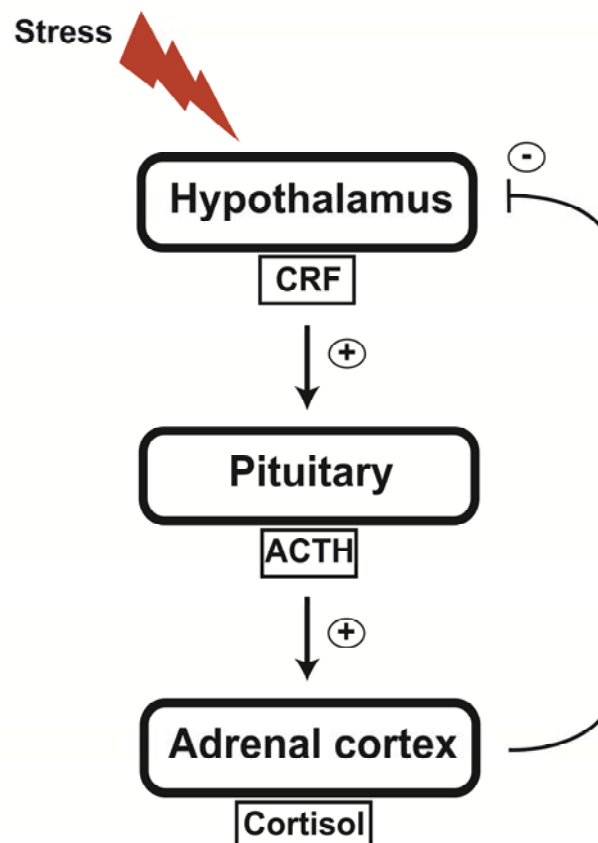


Figure 1. Schematic overview of the HPA axis response to stress.

A mechanism for avoiding pathological changes due to stress is the strict regulation of the HPA axis by negative feedback such as GR-mediated decrease in

hypothalamic CRH production (Holsboer, 1999), which allows restoration of homeostasis in hormone and neurotransmitter levels. Thus, there are no adverse consequences for the organism (Chrousos and Gold, 1992). Chronic stress, however, can lead to impairment of this negative feedback loop: hypothalamic CRH expression can no longer be suppressed by glucocorticoids (Praag et al., 2004). This is the case in many patients suffering from affective disorders like depression and anxiety disorders.

1.2. The HPA axis in psychiatric disorders

Major signs of a dysregulated HPA axis include changes in circulating levels of CRH, vasopressin, ACTH and cortisol, which are due inter alia to differential regulation of their transcription and translation rates. Thus, in major depression, the HPA system was found to be hyperactive, with increased CRH production (Raadsheer et al., 1995) and increased levels of circulating ACTH (Deuschle et al., 1997); on the other hand, CRH deficiency has also been observed in a minority of patients (Posener et al., 2000). Panic disorder (PD) and generalized anxiety disorder (GAD) have been associated with increased concentrations of cortisol in the cerebrospinal fluid (CSF) and hypertrophy of the pituitary and adrenal glands due to hyperactivity (Chalmers et al., 1996).

The long-lasting changes in CRH and cortisol levels found in affective disorders have also been postulated to trigger behavioral effects, including increased anxiety. Anxiety is defined as pathological and generalized fear and manifests itself as a persistent, unpleasing and often unsubstantiated feeling of worriedness, in the absence of any acute stimulus that might trigger fear (American Psychiatric Association, 2000). It is comorbid with many psychiatric conditions, such as depression (Pini et al., 1997). In animal models, high doses of CRH have been shown to elicit anxiogenic effects, such as decrease in exploration of novel environments and increased freezing and acoustic startle response (ASR) (Heinrichs et al., 1997); similarly, transgenic mice that overproduce CRH are hyperanxious (Stenzel-Poore et al., 1994).

1.3. Anxiety disorders

Anxiety in itself can also constitute an independent pathological condition, as in the case of anxiety disorders. According to the fourth edition of the Diagnostic and Statistical Manual of Mental Disorders (DSM-IV), these include panic disorder (PD), generalized anxiety disorder (GAD), phobias (social, specific and agoraphobia), acute stress disorder and posttraumatic stress disorder (PTSD) (American Psychiatric Association, 2000). The lifetime prevalence of any anxiety disorder is 28.8 % (Kessler et al., 2005) and the symptoms are debilitating. Thus, in PD, patients are prone to recurrent panic attacks which involve acute fear and discomfort occurring in the absence of true danger and coupled to activation of the sympathetic nervous system (American Psychiatric Association, 2000).

Anxiety and fear regulation involve activation of and interaction between various brain structures. Most important among them are the amygdala, the prefrontal cortex and the hippocampus. A combination of patient and animal studies have pinpointed the amygdala as the primary region involved in the response to fearful stimuli (Mathew et al., 2008; Shin and Liberzon, 2009); together with the hippocampus, it has been related to learning of fear conditioning (Kjelstrup et al., 2002; Maren and Holt, 2004; McHugh et al., 2004). The prefrontal cortex on the other hand seems to play a large role in fear extinction, which also requires formation of new memories (Santini et al., 2004; Kim et al., 2010). These structures have been shown to be involved in the pathology of anxiety disorders. In PD, amygdala hyperactivity has been reported in subgroups of PD patients (Domschke et al., 2008), and in the medial prefrontal cortex, gray matter volumes were found to be reduced (Asami et al., 2008; Uchida et al., 2008).

Dysregulations of endocrine and neurotransmitter systems in anxiety disorders include among others: 1) dysregulation of the HPA axis, leading to altered levels in CRH, ACTH and cortisol (see also 1.2.); 2) increased activity of the glutamatergic system; 3) reduction in levels of monoamine transmitters such as noradrenaline and serotonin; and 4) changes in levels of neuropeptides, such as Substance P and Neuropeptide Y (NPY) (Mathew et al., 2008).

Currently, treatment of anxiety disorders consists in a combination of psychotherapy, where the gold standard is cognitive-behavioral therapy (Mathew et al., 2008), and pharmacotherapy. The first-line pharmacological treatment are selective serotonin reuptake inhibitors (SSRIs), alongside symptomatic treatment with benzodiazepines (Ravindran and Stein, 2010b). The SSRIs work mainly by inhibiting the reuptake of serotonin from the presynaptic cleft via the presynaptic serotonin transporter, thus increasing overall cerebral levels of serotonin. Benzodiazepines target a specific binding site of the ionotropic γ -amino butyric acid subtype A (GABA_A) receptor and enhance the effect of the inhibitory neurotransmitter GABA, reducing amygdala activation and thereby achieving anxiolysis. However, these medications do not represent a functional solution for all anxiety disorders. For instance, in PTSD patients, while SSRI treatment generally has good results in the case of civilian trauma, it failed to be effective in most studies with combat-related PTSD (Shiromani et al., 2009).

1.3.1. Posttraumatic stress disorder (PTSD)

Posttraumatic stress disorder (PTSD) is one of the most common anxiety disorders (Steckler et al., 2005) and affects a minority of persons exposed to a trauma such as rape, assault or combat, as well as natural disasters and accidents (Yehuda and LeDoux, 2007). Approximately 6.8 % of people exposed to a traumatic event develop PTSD, whereas around 75 % of the total population are exposed to trauma once in their life (Kessler et al., 1995, 2005). Given the wide range of causes that may lead to PTSD, the risk of developing this disorder applies to the entire population.

DSM-IV defines the core symptoms of PTSD as: 1) persistent reexperiencing of the traumatic event; 2) persistent avoidance of trauma-related stimuli and numbing of general responsiveness following trauma; and 3) hyperarousal following trauma (American Psychiatric Association, 2000). For fulfillment of these diagnostic criteria, this symptom complex has to persist for at least 1 month. PTSD symptoms can occur starting several weeks up to decades after the event.

Since PTSD is not a mandatory consequence of experiencing a trauma, research has also been focusing on identifying pre-traumatic factors that may influence the development of this disease. These factors include structural brain abnormalities

(Yehuda and LeDoux, 2007) and environmental, genetic, and epigenetic contributions (Afifi et al., 2010; Schmidt et al., 2011; Yehuda et al., 2011). Thus, hippocampal volume was found to be reduced in PTSD patients (Rauch et al., 2006; Bremner, 2007), but additionally, smaller hippocampal volumes have also been correlated to higher risk of developing PTSD (Gilbertson et al., 2002; Pitman et al., 2006). These results indicate a role of the hippocampus in PTSD vulnerability (Pitman et al., 2001). Twin studies have shown significantly greater risk for developing PTSD in monozygotic twins independent of differences in environment (True et al., 1993). However, gene-environment interactions generally play a major role in creating a predisposition for developing PTSD (Afifi et al., 2010). Thus, the effect of gene variants and environment has been examined in PTSD especially for genes associated with regulation of the HPA axis and coding inter alia for CRH (Tyrka et al., 2009), GR (Bachmann et al., 2005) and FK506 binding protein 5 (FKBP5) (Binder et al., 2008). In the gene coding for FKBP5, which regulates cortisol-binding affinity to GR and nuclear translocation of GR, four single nucleotide polymorphisms (SNPs) were found to interact with the severity of child abuse as predictor of adult PTSD symptoms. Changes in gene expression may also occur via epigenetic modifications, which are in themselves a consequence of environmental influences, especially in early life-phases (Schmidt et al., 2011). A strong hint in this direction is provided by analysis of gene expression patterns in survivors of the terrorist attacks on the World Trade Center, which revealed different gene expression of e.g. FKBP5 in patients with current PTSD (Yehuda et al., 2009).

The ongoing search for alternative PTSD medication is of great importance, since the current therapy situation is not satisfactory. Despite a wide variety of available therapeutics ranging from SSRIs to symptomatic treatment with benzodiazepines (Ravindran and Stein, 2009, 2010b; Steckler and Risbrough, 2011), specific targeting of PTSD core symptoms is as yet still not possible. Although treatment of anxiety disorders with either antidepressants or a combination of antidepressants and cognitive therapy is usually effective, it requires weeks for onset of action and furthermore often leads only to partial remission (Furukawa et al., 2006; Ravindran and Stein, 2009; Rodrigues et al., 2011). Benzodiazepines on the other hand act very fast, however, due to their high abuse potential as well as other negative side-effects including sedation and dependency, they are not optimal as a long-term anti-anxiety

therapy (Cloos and Ferreira, 2009; Ravindran and Stein, 2009; Tan et al., 2010). It is therefore essential to develop effective anxiolytics with a rapid onset of action and lacking the undesirable side-effects of benzodiazepines (Ravindran and Stein, 2010a; Rudolph and Knoflach, 2011; Steckler and Risbrough, 2011). In order to achieve this goal, it is crucial to work towards a better understanding of PTSD pathology and thereby identify new potential drug targets.

The neurobiological underpinnings of PTSD are as yet imperfectly understood, as is the case with most psychiatric disorders. Some players have however already been identified, such as the serotonin system and the HPA axis. The serotonin system, target of SSRI therapeutic actions, is also a major player in PTSD pathology (Praag et al., 2004). Activation of the serotonergic receptor system leads to rapid anxiolytic effects; in PTSD, however, decreased levels of serotonin coupled to impaired receptor activation and redistribution of receptor expression may contribute to symptoms like hyperarousal and intrusive memories (Southwick et al., 1999b). The HPA axis is the most extensively characterized system with regard to PTSD (Ehlert et al., 2001; Shea et al., 2005; de Kloet et al., 2006). For instance, some studies have shown overall hypocortisolism in PTSD patients (Yehuda et al., 1995), accompanied by changes in the noradrenergic system, which may be partly responsible for the state of hyperarousal and facilitated retrieval of traumatic memories (flashbacks) experienced in PTSD (Southwick et al., 1999a).

Apart from the HPA axis and the serotonin system, PTSD also goes along with disturbance of the balance in various other neurotransmitter systems. Dysregulation has been found in the glutamatergic system (Heim and Nemeroff, 2009; Rossi et al., 2009), as well as in synaptic plasticity (Alfarez et al., 2006; Kozlovsky et al., 2007; Ježek et al., 2010; Acheson et al., 2011). Other neurotransmitters that have been associated with PTSD include neuropeptides. For example, NPY was found to be decreased in the plasma and CSF of combat veterans with PTSD (Rasmusson et al., 2000; Sah et al., 2009); galanin mRNA expression was reduced in the hippocampus and frontal cortex in a mouse model of PTSD (Kozlovsky et al., 2009); and endogenous opioids have been associated with some symptoms of PTSD (Heim and Nemeroff, 2009).

Novel approaches for PTSD treatment aim at restoring homeostasis in these neurotransmitter circuits. Examples include modulating the activity of the glutamatergic system for instance via N-methyl-D-aspartate (NMDA) receptor antagonists (Steckler and Risbrough, 2011) and D-cycloserine (DCS), an NMDA receptor agonist, which enhances extinction and/or replacement of traumatic memories (Yamamoto et al., 2008). Neuropeptides have also emerged as promising candidates for alternative anxiolytic therapies (Hökfelt et al., 2003). For instance, the aforementioned NPY was associated with resistance to and recovery from PTSD both in humans (Yehuda et al., 2006) and in animal models of PTSD (Cohen et al., 2011). Consequently, a variety of ligands and activity modulators for the various NPY receptor subtypes have been designed (Brothers and Wahlestedt, 2010). However, the wide variety of NPY receptor subtypes makes specific modulation of the NPYergic system with a view towards reducing anxiety a challenge that has not as yet been overcome. Ideally, therapeutic substances would target only one type of receptor very specifically in the central nervous system (CNS).

1.4. Neuropeptide S and its receptor, NPSR

In contrast to NPY, animal experiments showed that Neuropeptide S (NPS) exerts its effects via one receptor only (Zhu et al., 2010). This neuropeptide was identified by reverse pharmacology as the ligand for a previously orphan G-protein coupled receptor (GPCR), GPR154, that henceforth became known as the NPS receptor (NPSR) (Xu et al., 2004). NPS is a 20 amino acid long neuropeptide, with a highly conserved sequence among various species of vertebrates (Figure 2A), which hints at its crucial importance in the brain circuitry (Xu et al., 2004; Reinscheid, 2007). The name of the peptide is derived from the aminoterminal residue in its sequence, serine, which is conserved across all species. Structure-activity studies on NPS showed its aminoterminal structures (NPS 1-10), which are also the best conserved across species, to be especially relevant for its biological activity and for activation of the cognate receptor; the C-terminal structures may however be required for *in vivo* activity (Roth et al., 2006).

NPSR, the only known NPS receptor, is coupled to either G_s or G_q (Reinscheid et al., 2005). Upon binding to its receptor, NPS leads to intracellular increase in cyclic adenosine monophosphate (cAMP) and Ca²⁺ levels, and to activation of the mitogen-

activated protein kinase (MAPK) cascade (Reinscheid et al., 2005) (Figure 2B). These effects hint at a potential role of NPS in the regulation of cell proliferation.

NPS can interact with and modulate various neurotransmitter systems (Raiteri et al., 2009; Boeck et al., 2010; Mochizuki et al., 2010; Si et al., 2010), most important among which is the glutamatergic system (Han et al., 2009; Okamura et al., 2010). Furthermore, NPS treatment has regulatory effects on the HPA axis (Figure 2C), increasing plasma ACTH and corticosterone concentrations *in vivo* in rats after intracerebral injection, and stimulating CRH and vasopressin after incubation with hypothalamic explants (Smith et al., 2006). Most importantly, NPS effects do not seem to be mediated via the benzodiazepine binding site of the GABA_A receptor (Leonard et al., 2008), which suggests that NPS treatment will not have the common side effects of benzodiazepine treatment (Cloos and Ferreira, 2009; Tan et al., 2010; Ravindran and Stein, 2010b).

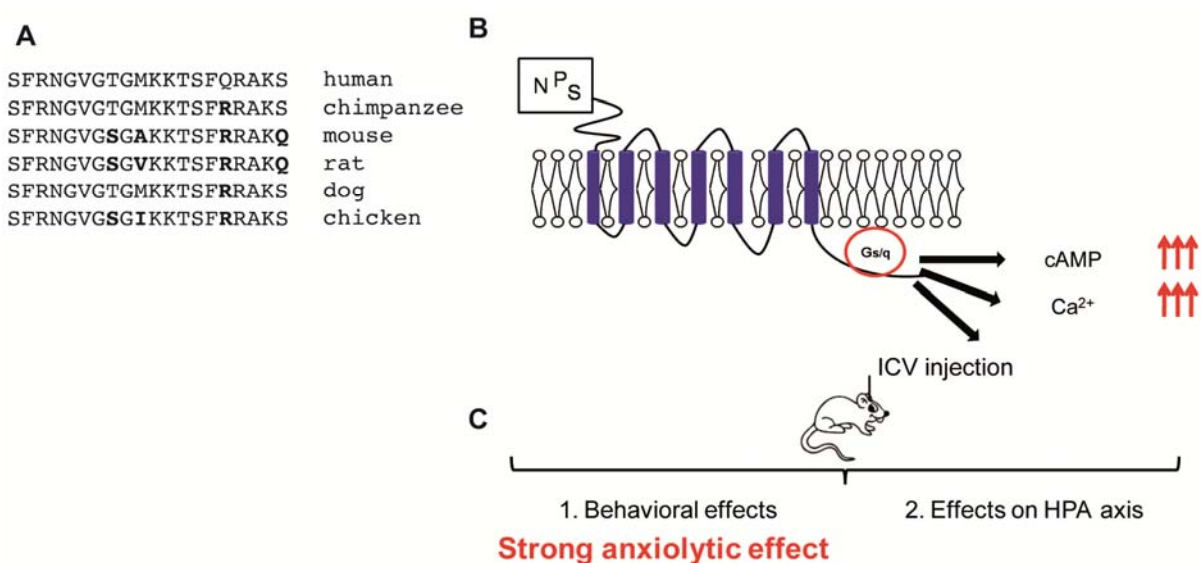


Figure 2. NPS, NPSR and NPS-elicited effects. **A** Sequence of active NPS in various species (Xu et al., 2004). **B** Effects of NPS upon binding to NPSR on the intracellular level as described in (Reinscheid et al., 2005). **C** Effects of NPS on a systemic level upon intracerebroventricular (ICV) injection in rodents: behavioral effects as described in (Xu et al., 2004; Leonard et al., 2008) and effects on the HPA axis as described in (Smith et al., 2006).

Despite the variety of its effects, NPS expression in the rat is restricted almost exclusively to three brain regions: the peri-locus coeruleus, the parabrachial nucleus and the principal sensory 5 nucleus of the trigeminus (Xu et al., 2004, 2007). Also, in the mouse, NPS precursor mRNA is found in only two brain regions: the Kölliker-

Fuse nucleus and the pericoerulear area (Clark et al., 2011). NPSR, on the other hand, is widely expressed throughout the brain in regions ranging from cortical areas such as the olfactory, somatosensory and motor cortex to deep subcortical structures such as the amygdaloid and thalamic nuclei (Xu et al., 2007). There are however discrepancies between reports on NPSR mRNA and protein expression patterns in the rat brain, as well as between murine and rat NPSR mRNA expression. In the rat, in situ hybridization (ISH) studies reveal no NPSR mRNA expression in the CA1, CA2 and CA3 regions and in the dentate gyrus (Xu et al., 2007). In contrast, protein expression studies performed using an NPSR antibody describe presence of NPSR protein in those same areas, albeit at low expression levels (Leonard and Ring, 2011). Similarly, NPSR mRNA was found to be expressed in the murine basolateral amygdala (BLA), where also strong effects on neuronal activity were elicited after local treatment with this substance (Jüngling et al., 2008; Clark et al., 2011), whereas in the rat BLA, NPSR mRNA expression was very low and protein expression was completely absent. Due to these conflicting reports, the ultimate identity of the NPS target neurons and target brain regions that contribute to its behavioral effects still remains elusive.

Intracerebroventricular (ICV) injection into mice revealed that NPS elicits a variety of behavioral effects, including increased locomotion and hyperarousal (Xu et al., 2004; Rizzi et al., 2008). Most relevant for the thesis at hand however are the well-described strong anxiolytic effects of NPS treatment (Figure 2C), which highlight the potential of NPS as a novel alternative therapy for anxiety disorders, including PTSD (Xu et al., 2004; Jüngling et al., 2008; Leonard et al., 2008; Rizzi et al., 2008; Fendt et al., 2010). Also, a transcriptionally and functionally hyperactive NPSR variant expressing an A/T SNP in the coding region has been associated with panic disorder (Okamura et al., 2007; Domschke et al., 2010) and overinterpretation of fear-related experiences (Raczka et al., 2010; Dannlowski et al., 2011; Lennertz et al., 2011). Moreover, NPS-producing neurons have also been reported to become activated upon stress exposure (Liu et al., 2011). All these findings support the hypothesis that endogenous NPS plays an important role in the anxiety circuit and has strong potential as an alternative therapy of anxiety-related symptoms.

1.5. Intranasal application

In order to further investigate the therapeutic potential of NPS with a view towards implementing it as a therapy in patients suffering from pathological anxiety, one of the first steps consists in establishing a noninvasive administration method that can be easily applied in humans. One such possible alternative to the intracerebral injection commonly used in animal models is the intranasal application.

Intranasal application has been shown both in humans and in animals to be appropriate for targeting the CNS in the case of several substances, including neuropeptides (e.g. oxytocin and vasopressin) (Gozes et al., 2000; Born et al., 2002; Dufes et al., 2003; Guastella et al., 2010; Shi et al., 2010). Use of radioactively labeled ligands (Figure 3) has led to identification of two different pathways which substances can follow in order to reach the brain after intranasal application (Thorne et al., 1995, 2004). Along one pathway, substances are transported along the olfactory nerve via the olfactory bulb to rostral and subcortical brain regions. The second pathway follows the myelin sheaths of the trigeminal nerves to target caudal cerebral structures such as the brainstem and the cerebellum. Timeline studies have shown this process to be surprisingly rapid, with substances reaching the brain within minutes of administration and remaining detectable up to hours after treatment (Thorne et al., 2004; Dhuria et al., 2009).

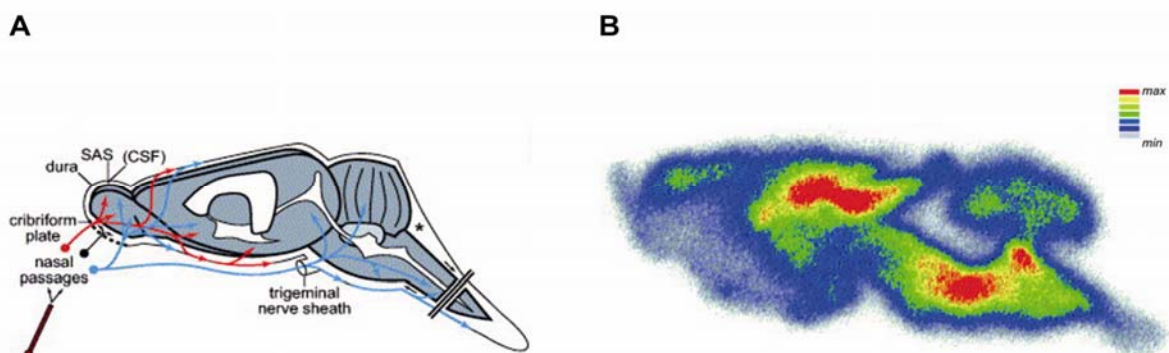


Figure 3. Targeting of CNS via intranasal application (adapted from (Thorne et al., 2004)). **A** Cerebral substance distribution after intranasal application follows two different pathways: the peripheral olfactory system to the olfactory bulb and rostral brain (red) and the peripheral trigeminal system to the brainstem (blue). **B** Autoradiography of representative sagittal brain section after intranasal application of radioactively labeled ligand.

Given the previous success of intranasal therapy with some neuropeptides (Born et al., 2002; Guastella et al., 2010), NPS seems to be a prime candidate for intranasal application. However, since the nose-brain barrier permeability of substances is highly influenced by their polarity and molecular weight (Ozsoy et al., 2009; Dhuria et al., 2010), it is very difficult to predict whether a given compound will successfully reach the brain upon intranasal instillation. Consequently, the feasibility of this procedure has to be established afresh for every substance of interest. In addition, due to the largely unknown pharmacodynamics and pharmacokinetics which differ substantially between intranasally administered and intracerebrally injected agents (Thorne et al., 1995; Thorne and Frey, 2001), new protocols have to be established for characterizing the treatment-induced phenotype.

1.6. Mouse models of anxiety disorders

To test the potential of intranasally applied NPS as a therapeutic, it is necessary to examine its effects in animal models of the pathological conditions that should subsequently be treated in patients. While it is not possible to check for paranoia in mouse models of schizophrenia or for flashbacks in mouse models of PTSD, it is possible, using various behavioral paradigms, to describe changes in the anxiety- and fear-related behavior inherent to the animals. It has also been proven in many cases that this type of behavior can be influenced by anxiolytic and anti-depressive medication (Garcia et al., 2008) similarly to patients (Autry et al., 2011), which supports the validity of these models. Most importantly, these models allow for differentiating between trait and state anxiety. Trait anxiety is defined as an individual predisposition to respond, whereas state anxiety is a context-dependent response to certain stimuli and is accompanied by physiological arousal as described above (see 1.1.) (Endler and Kocovski, 2001). Trait and state anxiety can both be pathologically altered.

In this work, two different mouse models exhibiting increased anxiety-like behavior were used to test the anxiolytic effects of intranasally applied NPS: 1) high anxiety behavior (HAB) mice, which model the condition of trait anxiety; and 2) a mouse model of PTSD, which represents the condition of state anxiety.

1.6.1. The HAB mice, a mouse model for inbred anxiety

HAB mice are a mouse model of pathologically high anxiety, inbred for over 40 generations in a CD1 background (Krömer et al., 2005; Landgraf et al., 2007; Bunck et al., 2009; Hamsch et al., 2010). HAB mice are selected at 7-13 weeks for their specific high anxiety behavior on the elevated plus-maze (EPM) in comparison to low behavior anxiety (LAB) mice, which are similarly inbred; outbred CD1 mice are employed as normal anxiety behavior (NAB) controls (Krömer et al., 2005). The EPM, an elevated platform with two open and two enclosed arms (see Figure 4A) allows for precise quantification of anxiety-like behavior by comparing the time mice spend in the closed arms to the time they spend in the open arms (Lister, 1987) (see Figure 4B). Mice tend to explore new environments; however, they also instinctively prefer to remain in the closed arms where they feel more protected than in the open. In exceptionally anxious mice, the amount of time spent exploring is significantly biased in favor of the closed arms. In mice characterized by lower-than-typical anxiety, the bias is reversed. The behavior on the EPM at the age of testing is considered to predict later anxiety and stress-coping behavior (Krömer et al., 2005).

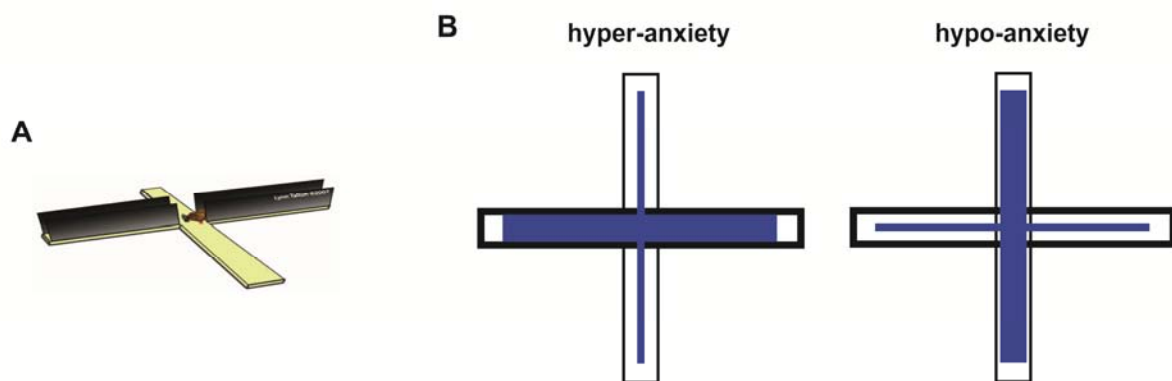


Figure 4. Overview of the EPM. **A** Setup. **B** Schematic overview of mouse behavior on the EPM: hyper-anxious mice will tend to restrict themselves to the closed arms, while mice showing low anxiety will preferentially explore the open arms.

The comparability of this model to the situation in patients has been established on the molecular level as well. For instance, it was found that HAB and LAB mice show significant differences in expression of various proteins associated with stress responsiveness, as well as metabolic differences (Landgraf et al., 2007; Filiou et al., 2011; Zhang et al., 2011; Filiou and Turck, 2012). Thus, in HAB mice, expression and release of vasopressin, a neuropeptide with a major role in the HPA axis (see 1.1.),

are strongly upregulated due to a SNP in the vasopressin promoter region, whereas the opposite situation is observed in LAB mice (Landgraf et al., 2007). This model is especially interesting since it allows for investigation of high trait anxiety on a very complex level of interactions between neuroendocrine, behavioral and genetic factors (Landgraf et al., 2007). Therefore, it complements very well the mouse model of PTSD, which represents a model of state anxiety.

1.6.2. The mouse model of PTSD

The mouse model used here has been established in the C57BL/6N strain and is based on an electrical footshock as one-time trauma exposure (Siegmund and Wotjak, 2007). The difference to classical Pavlovian conditioning, which also uses a footshock as conditioning stimulus, consists in that, in the case described here, the electrical current applied is more than twice as high (1.5 mA as opposed to 0.7 mA), and ca. five times higher than the pain threshold of C57BL/6N mice (Siegmund et al., 2005), making this experience considerably more painful and therefore traumatic. Differences in behavior were considered relevant 28 days after shock, an incubation period which allows for attenuation of acute and PTSD-non-related effects and also takes into consideration the possibility of delayed phenotype onset. 28 days after trauma, shocked mice have been shown to develop a PTSD-like phenotype (Siegmund and Wotjak, 2007). This is characterized by: 1) increased sensitized fear as measured by their freezing behavior in a neutral context, corresponding to the physiological response in patients upon exposure to trauma-related stimuli that may symbolize or resemble an aspect of the traumatic event (trigger phenomenon); 2) reduced social response accompanied by social withdrawal in a social interaction test, corresponding to significant impairment in the social behavior of patients; and 3) hyperarousal as shown by heightened startle reaction in response to neutral tones of increasing intensities, exactly as observed in PTSD patients (Siegmund and Wotjak, 2007; Golub et al., 2011). Additionally, cerebral changes that have been described in PTSD patients are also found in shocked mice, such as hippocampal shrinkage (Wignall et al., 2004; Golub et al., 2011).

1.7. Goals

Anxiety disorders are among the most common psychiatric conditions, with a high prevalence and severe impact not only on the life quality of the individual, but also on the well-being of society as a whole. The current treatment situation is unsatisfactory, and in consequence, developing alternative medication and better characterizing its mode of action is of crucial importance.

The present work is situated at the crossroad between basic and applied research. Therefore, the main purpose consisted in characterizing the mechanisms of action and the targets of NPS, a novel and promising candidate for the development of alternative anxiolytic therapeutics, as well as in validating a therapeutic procedure that can easily be applied in humans.

The first goal was establishing the feasibility of intranasal NPS treatment in mice. Here, two important points had to be proved: (1) that intranasally applied NPS can bypass the nose-brain barrier to reach the brain, especially the regions known to be involved in the anxiety circuit like amygdala and hippocampus; and (2) that intranasal application of NPS elicits similar anxiolytic effects as intracerebral injection.

The second focal point of investigation concerned the regulatory effects of NPS treatment on cerebral protein expression. This was especially relevant in the case of systems that have already been associated with NPS effects and that were shown to be dysregulated in PTSD, such as the glutamatergic system and proteins involved in synaptic plasticity.

Finally, the therapeutic potential of NPS was examined in mouse models of two different pathological conditions, i.e. the HAB mice and the mouse model of PTSD.

2. Methods and materials

For a complete list of all devices, materials, substances, kits, buffer recipes and software used in this work please see Supplementary Tables 1-6.

2.1. Cell biology

2.1.1. Generation of tagged NPSR constructs

In order to investigate the trafficking of NPSR and its interactions with its ligand *in vitro*, it was necessary, given the lack of a functioning NPSR antibody, to generate tagged NPSR constructs. This process was performed in multiple steps: 1) isolation of total mRNA from murine brain regions known to express NPSR mRNA; 2) reverse transcription of total mRNA into cDNA; 3) amplification of NPSR cDNA with specific NPSR primers; and 4) cloning of NPSR cDNA into plasmids to produce recombinant NPSR tagged with either enhanced green fluorescent protein (EGFP) or FLAG.

2.1.1.1. Isolation of total mRNA from murine brain regions

Total mRNA was isolated from a section of the murine brain which contained regions where NPSR mRNA had been previously described, such as the hippocampus, the paraventricular hypothalamic nucleus, cortical regions and amygdaloid nuclei (Figure 5). The isolated brain part was estimated generously to include as many regions with NPSR expression as possible, in order to maximize NPSR mRNA yield.

Total mRNA was isolated according to the TRIzol protocol established in our laboratory. The brain tissue sample was taken up in 2 ml RNase-free plastic tubes, 1 ml TRIzol was added and the sample was homogenized with a turrax at room temperature (RT). The homogenized sample was shaken vigorously by hand and incubated for 5 min at RT. For phase separation, 200 µl chloroform were added, the sample was shaken vigorously by hand for 15 seconds and then incubated for 2-3 min at RT. Subsequently, the sample was centrifuged at 13000 rotations per minute (rpm) for 15 min at 4 °C, and the watery colorless phase was transferred into a new tube. For precipitation, 0.5 ml isopropanol were added and the solution was mixed by inverting the tube 10 times. After 10 min incubation at RT, the sample was centrifuged at 13 krpm and 4 °C for 10 min and the supernatant was discarded. This

was followed by a washing step on ice. 1 ml 70 % ethanol was added and the pellet washed by inverting and flicking the tubes. After centrifugation at 13 krpm and 4 °C for 10 min, the supernatant was discarded and the pellet was dried at RT for ca. 60 min (until all visible traces of ethanol had disappeared). The pellet was then redissolved in 50 µl H₂O treated with diethylpyrocarbonate (DEPC) (DEPC-H₂O) and stored at -80 °C. Total mRNA concentration was determined by measurement with a Nanophotometer.

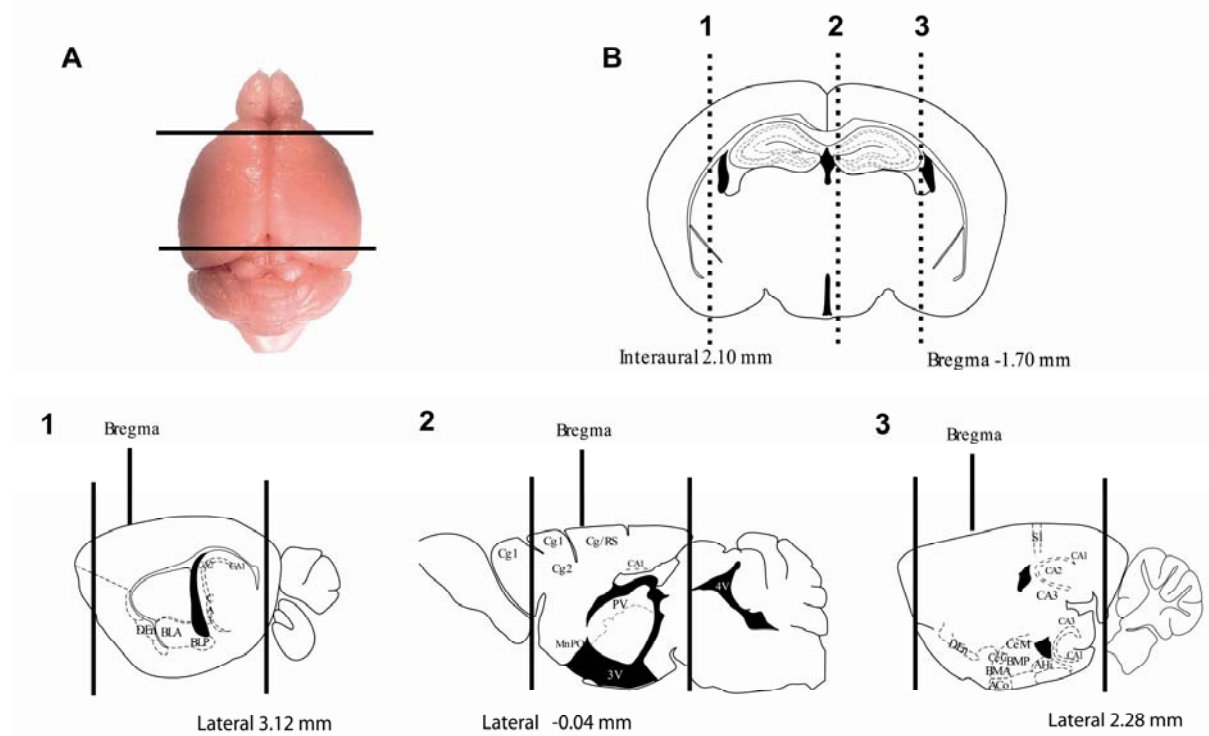


Figure 5. Isolated murine brain regions for isolation of total mRNA. **A** Overview of murine brain. Solid black lines indicate cutting points for brain region isolation. **B** Sagittal brain section where dotted black lines indicate selected lateral overview plates (adapted from (Franklin and Paxinos, 2007)). **1** DE_n: dorsal endopiriform cortex; BLA: basolateral amygdala, anterior part; BLP: basolateral amygdala, posterior part; CA1-3 regions of the hippocampus. **2** Cg1,2: cingulate cortex; PV: paraventricular hypothalamic nucleus; MnPO: median preoptic nucleus; 3V: third ventricle. **3** S1: somatosensory cortex; ACo: cortical amygdala; CeC: central amygdala, cortical part; CeM: central amygdala, medial part; BMA, BMP: basomedial amygdala, anterior and posterior part; AHi: amygdalohippocampal region.

2.1.1.2. Reverse transcription of total mRNA into cDNA

Reverse transcription was performed using the Omniscript Reverse Transcription Kit according to the manufacturer's instructions. In brief, 0.1 µg/µl total mRNA were added to a master mix containing a final concentration of 1x RT buffer, dNTP mix at

0.5 mM each dNTP, 1 μ M Oligo-dT primers, 0.5 unit/ μ l RNase inhibitor, 0.2 units/ μ l Omniscript Reverse Transcriptase and RNase-free water to the desired volume. The solution was incubated for 1 hour at 37 °C in a PCR thermocycler to allow for reverse transcription and the resulting cDNA was stored at -20 °C thereafter.

2.1.1.3. Amplification of NPSR cDNA from total cDNA

The NPSR cDNA sequence for amplification was selected to include only the translatable sequence based on the complete NPSR cDNA sequence shown below (NCBI Reference Sequence: NM_175678). The sequence of interest is highlighted in yellow and contains a start and a stop codon.

```

61 gagacagtga gacctgacct tgccctgagcc atgccagcca acctcacaga gggcagcttt
121 catgcccaacc agactgtgccc gatgctagat tcttccccag tagcttgccac tgaattgtg
181 acgttcactg aagcactggg ggctgaggag tggggctcct tctactcctc cttaagaca
241 gaacagctga taaccctgtg ggtcctggtt gtcgtcacta ttgtgggaaa ctctgtttgtg
301 ctgttctcca cgtgcagaag aaaaagaaag tccagaatga ccttctttgt gacacaattg
361 gccatcacag actccttcac gggcctgatc aacatcttga cagacattat ttggcgattc
421 acaggagact tcatggcccc tgacctgggt tgcagagtcg tccgctactt gcaggttgtc
481 ctgctgtatg cctctaccta cgtcctgggt tccctcagca tagacagata ccatgccatc
541 gtttacccca tgaagtttct tcaaggagag aagcaagcca aagtcctcat cggaatagcg
601 tggagcctct cgttcctggt ctccattccc acgctgatca tatttgggaa aaggacactt
661 tccaatgggtg aggtgcagtg ctgggcactg tggccggatg actcctactg gaccccgtac
721 atgaccatcg tcgcctttct ggtgtacttc attcccttgg caattatcag cgttatctat
781 ggccttgtga tccgaactat ttggatgaaa agcaaaaacc atgagacggt gatttccaac
841 tgctcagatg gcaaaactat ctgcagctac aaccgagggc tcatctctaa ggcaaaaatc
901 aaggccatca agtatagcat cgtcataatc cttgctttca tctgctgctg gagccatac
961 ttctctttg acatattaga caacttcaac gtccctccag acaccaagga gcgtttctat
1021 gcctctgtga ttatccagaa cctgcccgcc ttgaacagtg ccattaacct cctcatctac
1081 tgcattctca gcagctccat ctgctcccc tgcaagatgc aaagatcaca ggattccaga
1141 atgacatacc gagagagaag cgagagacac gagatgcaga ttctctccaa gccggaattc
1201 atctaaacct tgaggcagta gtgctaggct gaacttagtc agctctcctg gatctttacc

```

NPSR was amplified from total cDNA using specific primers for cloning into pEGFP-C1 and pcDNA3.1 (-) plasmids (see Table 1). For tagging NPSR with FLAG, the FLAG-tag sequence (shown here in blue) was inserted into the reverse primer and the stop codon of the NPSR cDNA sequence was replaced by a stop codon within the reverse primer. The primers contained inserted restriction sites. The primer sequences are listed in Table 2 (restriction sites shown in red).

Table 1. Plasmids used for cloning EGFP-NPSR and NPSR-FLAG constructs.

Plasmid	Manufacturer
pEGFP-C1	Clontech, Mountain View, CA, USA
pcDNA3.1 (-)	Invitrogen, Darmstadt, Germany

Table 2. Primer sequences used for amplification of murine NPSR from murine cDNA for cloning into pEGFP-C1 and pcDNA3.1 (-).

Plasmid	Primer	Primer sequence	Restriction enzyme	Insert size
pEGFP-C1 and pcDNA3.1 (-)	forward	5'-AATGCCTCGAGTTATGC CAGCCAACCTCACAGAG-3'	XhoI	1150 bp
	reverse	5'-GCCGCGGATCCTCAGCCT AGCACTACTGCCTC-3'	BamHI	
pcDNA3.1 (-) with FLAG-tag	forward	5'-CTAGCTCGAGATGCCAGC CAACCTCACAGA-3'	XhoI	1146 bp
	reverse	5'-CTAGGGATCCCTACTTG TCGTCATCGTCTTTGTAGTC GATGAATTCCGGCTTGGGA GA-3'	BamHI	

The PCR master mix contained 1 µg template cDNA per reaction volume of 100 µl, which included a final concentration of 1x PCR Buffer, dNTPs at 0.2 mM each dNTP, 1.5 mM MgCl₂, forward and reverse primer at 0.5 µM each primer, 2.5 units *Taq* polymerase and autoclaved distilled H₂O (dH₂O) as needed.

The PCR program used for amplification was as follows:

1. initial denaturation: 94 °C – 3 min
 2. denaturation: 94 °C – 45 seconds
 3. annealing: 56 °C – 30 seconds
 4. elongation: 72 °C – 1.5 min
 5. final elongation: 72 °C – 10 min
 6. pause at 4 °C
- } 40 cycles

Products were stored at -20 °C until further use.

2.1.1.4. Cloning insert into plasmid

Insertion of the PCR product into the corresponding vector occurred according to the “sticky end” principle. Inserts and plasmids were digested with the respective enzymes in a 50 µl volume for 2 hours in a water bath at 37 °C. The restriction digest

solution contained 1 µg of plasmid added to 5 µl 10x NEBuffer 3 + 5 µl 10x bovine serum albumin (BSA), 4 units restriction enzyme and dH₂O.

Products of the restriction digest were loaded on a Tris/Borate/Ethylenediaminetetraacetic acid (EDTA) (TBE) agarose gel containing 0.01 % ethidium bromide (EtBr) and separated by gel electrophoresis. As EtBr intercalates in the DNA strands and glows upon UV stimulation, the DNA bands could be visualized under UV light and cut from the gel with a scalpel. DNA was eluted from the gel with the QIAquick Gel Extraction Kit using a microcentrifuge according to the manufacturer's instructions. In brief, the excised bands were weighed in 2 ml tubes and 3 volumes Buffer QG were added to 1 volume of gel (100 mg ~ 100 µl) and subsequently incubated for 10 min at 50 °C, vortexing every 2-3 min to speed up agarose solubilization. Afterwards, 1 gel volume isopropanol was added to the solution to increase yield and mixed. The mixture was then pipetted into a QIAquick spin column and DNA was bound to the column membrane by centrifugation at 13.2 krpm for 1 min. The centrifugation was repeated after addition of 1 ml Buffer QG to remove all traces of agarose. DNA was washed by addition of 0.75 ml Buffer PE followed by two centrifugation steps to completely remove all ethanol traces. DNA was eluted into a clean 2 ml tube by addition of 30 µl dH₂O, incubation at RT for 1 min and subsequent centrifugation. Products were stored at -20 °C.

To ligate the insert into the vector, insert and vector were added in a 6:1 ratio for 10 ng vector to 2 µl Reaction Buffer for T4 ligase, 1 µl of T4 ligase and water up to 20 µl total volume. The mixture was incubated at room temperature for 10 min and the reaction was then stopped by inactivating the enzyme at 65 °C for 15 min (otherwise the transformation efficiency would be significantly decreased). Products were stored at -20 °C.

For amplifying the DNA, competent bacteria (*E. coli* DH5α) were transformed with the vectors containing the inserts. Around 10 ng DNA were added to 50 µl solution of competent bacteria and incubated on ice for 30 min. The heat-shock was performed at 42 °C for 45 seconds, then 900 µl SOC-medium (Super Optimal Broth (SOB) medium with 20 mM glucose) were added and followed by incubation for 60 min on a thermomixer at 37 °C and 600-700 rpm to initiate ampicillin resistance. The bacterial

suspension was plated on lysogeny broth (LB) (containing 1x ampicillin and kanamycin) agar plates and incubated overnight at 37 °C. Since the plasmids contain an ampicillin resistance gene, only bacteria that have taken up the construct and express this gene are expected to grow and form colonies in the presence of ampicillin. The next day, colonies were picked with a pipette tip and transferred to an Erlenmeyer flask containing 500 ml lysogeny broth (LB) medium with 1x ampicillin and then incubated for 14-16 hours at 37 °C on a mixer at 200 rpm to allow for bacterial growth.

DNA was isolated from the bacterial suspension using the PureYield Plasmid Midiprep System according to the manufacturer's instructions. In brief, a lysate was prepared by centrifuging cells at 5000 g and resuspending the pellet in Cell Resuspension Solution. For DNA purification, the suspension was mixed with Cell Lysis Solution (avoiding precipitate formation) and subsequently with Neutralization Solution. Cellular debris was cleared by centrifugation at 15000 g for 15 min and by vacuum passage through a Clearing Column, which filtered out the lysate and where DNA bound to the binding membrane of the Binding Column. Afterwards, the column was washed with Column Wash Solution. After drying, DNA was eluted in 600 µl Nuclease-Free Water. DNA concentrations were measured with the Nanophotometer. Products were stored at -20 °C. Correct insert integration was checked by sequencing of the product (outsourced to GATC Biotech AG, Konstanz, Germany).

2.1.2. Transfection of HEK cells with the NPSR constructs

In order to characterize the behavior of the NPSR constructs on a cellular level, the constructs were used to transfect human embryonic kidney (HEK) cells, an immortalized cell line that has previously been used to study NPSR distribution (Bernier et al., 2006). Cells were cultured in 10 cm dishes in an incubator at 37 °C and 5 % CO₂, using Dulbecco's modified Eagle's medium (DMEM) with 10 % fetal calf serum (FCS), 1 % sodium pyruvate and 1 % antibiotic-antimycotic solution. Cells were split 1:10 twice a week. For splitting, medium was removed and cells washed with phosphate buffered saline (PBS) to remove all traces of FCS which inhibits the trypsin used for detaching cells. PBS was removed and trypsin-EDTA solution was added. The cells were then incubated for 1 min in the incubator to increase enzyme

activity, followed by medium addition, and the cells were taken up in suspension and then passaged to another culture vessel.

For seeding, cells were taken up in suspension, diluted with trypan blue which stains dead cells and counted using the Neubauer counting chamber. From the result, the number of live cells per ml can be extrapolated according to the following formula:

$$\text{number of cells / ml} = (\text{number of live cells in all quadrants} / 4) \times \text{dilution factor} \times 10^4$$

2.5×10^6 HEK cells per well were seeded in 24-well plates and allowed to grow in the incubator until they had reached 50-60 % confluence (ca. 24 hours). The transfections were performed using the ExGen 500 *in vitro* Transfection Reagent. 2 μg DNA in 100 μl 150 mM NaCl were vortexed gently and spun down briefly, then 6 equivalents ExGen (3.3 μl) were added, the solution was vortexed for 10 seconds and incubated at RT for 10 min to allow formation of DNA/ExGen-complexes. Then 100 μl solution were pipetted per well and the culture plate was centrifuged for 5 min at 280 g at RT. Cells were incubated for 48 hours to allow for expression of construct.

Correct construct expression was checked on two levels: mRNA and protein level.

2.1.2.1. Expression of NPSR constructs on mRNA level

Total mRNA was isolated from transfected cells using the NucleoSpin RNA II Kit according to the manufacturer's instructions. In brief, medium was removed and cells washed with PBS, then 350 μl Buffer RA1 containing 1 % β -mercaptoethanol were added to lyse the cells. The cells were taken up in suspension and pipetted up and down vigorously to improve the lysis process, then the lysate was filtered by passing through a NucleoSpin Filter in a centrifugation step of 1 min at 13.2 krpm. The supernatant was adjusted for RNA binding by mixing with 350 μl ethanol and the RNA was bound to the silica membrane of a NucleoSpin RNA II Column in a centrifugation step. The silica membrane was then desalted by addition of 350 μl Membrane Desalting Buffer (MDB) and centrifugation for drying. DNA was digested by addition of 95 μl DNase reaction mixture (consisting of 10 μl reconstituted DNase (rDNase) and 90 μl Reaction Buffer for rDNase) and incubation for 15 min at RT. The silica membrane was washed in three steps separated by centrifugation steps of 30 seconds: 1) 200 μl Buffer RA2 to inactivate the DNase; 2) 600 μl Buffer RA3; and 3)

250 µl Buffer RA3. The final centrifugation step lasted 2 min to completely dry the membrane. Highly pure, DNA-free RNA was eluted in 40 µl RNase-free H₂O. Products were stored at -80 °C.

The total mRNA was reversely transcribed into cDNA as described above (2.1.1.2.) and NPSR was amplified specifically via PCR (2.1.1.3.). To check if the isolated mRNA amount was similar in both transfected and control samples, actin-beta amplification was performed in parallel as described above (2.1.1.3.) with the following changes: annealing temperature = 62 °C; and used primers: forward: 5'-CTACAATGAGCTGCGTGTGGC-3'; reverse: 5'-CAGGTCCAGACGCAGGATGGC-3'. PCR products were checked for length and intensity by separation via gel electrophoresis (2.1.1.4.).

2.1.2.2. Immunofluorescence of NPSR constructs

For checking NPSR expression on the protein level, cells were seeded on cover slips coated with 0.1 % gelatin. For coating, the cover slips were incubated in a Petri dish in the gelatin solution for up to 3 hours at RT. The gelatin was then removed and the cover slips were washed three times in PBS and were then stored in PBS at 4 °C in a Petri dish sealed with parafilm.

36 hours after transfection, medium was removed, cover slips were washed three times with ice-cold PBS and then fixed in 4 % paraformaldehyde (PFA) solution overnight at 4 °C. The next day, cover slips were placed on parafilm, washed three times with PBS and then permeabilized by incubation with 0.1 % triton in PBS for 20 min. All steps were performed at RT; after addition of fluorescent compounds, all steps were performed in the dark. After washing, unspecific binding sites were blocked by incubation with 10 % BSA in PBS for 60 min in the dark. The blocking solution was then removed and the antibody dilution in 1 % BSA in PBS was added and incubated for 60 min in the dark. After washing, the secondary fluorophore-coupled antibody was added followed by an identical incubation step as previously. Finally, the cells were washed and counterstained for 10 min with a 1:5000 dilution of 4',6-diamidino-2-phenylindole (DAPI) from a stock solution of 1 mg/ml in PBS. DAPI intercalates in the DNA and can be stimulated with fluorescent light to emit a blue signal, thereby creating a nuclear counterstain. After a last washing step, the cover

slips were then mounted with a fluorescence-preserving medium, Shandon Immu-Mount.

For the NPSR-FLAG construct, a primary FLAG-antibody was used and detected with a secondary antibody coupled to Alexa488 (green). For the EGFP-NPSR construct, no staining except the nuclear staining was used, since EGFP already emits a green signal that allows for localization of the fusion protein. Primary antibodies are listed in Table 3, secondary antibodies are listed in Table 4.

Table 3. Primary antibodies for immunofluorescence.

Antibody	Dilution	Species	Manufacturer
Anti-FLAG	1:100	rabbit	Sigma-Aldrich, St Louis, MA, USA

Table 4. Secondary antibodies for immunofluorescence.

Antibody	Dilution	Species	Manufacturer
Anti-rabbit Alexa488	1:300	donkey	Invitrogen, Darmstadt, Germany

Image acquisition was performed using either an epifluorescence or a confocal microscope.

2.1.3. Stimulation with Cy3-NPS

In order to examine receptor behavior upon ligand stimulation, transfected HEK cells were stimulated with a fluorescent NPS conjugate, Cy3-NPS, which emits a red signal upon stimulation with light of a certain wavelength. This method allowed for tracking of receptor-ligand complex via fluorescent signals.

To visualize the receptor-ligand complex, a protocol from (Grady et al., 1995) was adapted. In brief, 100 nM Cy3-NPS in PBS was added to the cell medium and the cells (previously seeded on coated cover slips) were incubated at 4 °C for 60 min to allow for binding of the ligand to the membranary receptor and to inhibit cell metabolism. Medium was then removed and cells were washed three times with ice-

cold PBS to remove all traces of unbound ligand. Cells were then either fixed immediately in ice-cold PFA as described above (2.1.2.2.), or warm medium was added and the cells were incubated in the incubator to allow for receptor-ligand internalization and processing, since at 37 °C, the cellular metabolism is again upscaled. In cells expressing FLAG-NPSR, immunofluorescent stainings were performed (2.1.2.2.); cells expressing EGFP-NPSR were only stained for nuclear visualization.

Image acquisition was performed using either an epifluorescence or a confocal microscope.

2.2. ICV and intranasal application of fluorescent NPS conjugates in mice

2.2.1. Animals

For visualization of Cy3-NPS uptake *in vivo*, 10 weeks old male C56BL/6N mice bred in the animal facility of the Max Planck Institute (MPI) of Biochemistry, Martinsried, were used.

2.2.2. Stereotactic surgery and ICV injection

For stereotactic surgery, the mice were fixed in a stereotactic frame and kept under forene (100 %, V/V) anesthesia (active substance: isofluran; induction: 2.5 %; maintenance: 1.5 %; in O₂; flow rate: 1 l/min) for the entire duration of the surgery (ca. 30 min). The mice received acute analgetic treatment with Metacam subcutaneously (s.c.) during surgery (0.5 mg/kg; in NaCl). 23 gage stainless-steel guide cannulas were implanted unilaterally at the following coordinates: 0.3 mm caudal and 1.1 mm lateral from the bregma; and 1.3 mm ventral from the skull surface (Figure 6). The guide cannulas were fixed with the aid of two screws and a two-component adhesive. The mice were allowed to recover for 7 days after surgery to restore system homeostasis. Substance infusions were performed manually on mice anesthetized by brief inhalation of isoflurane using a 30 gage injection cannula connected to a Tygon tube and a 10 µl Hamilton syringe. After infusion, the injection cannula was kept in place for an additional 30 s to prevent substance outflow. Mice were injected with 2 µl of either Cy3-NPS or rhodamine-NPS (10 µM) or unconjugated rhodamine (1 g/ml) in PBS and sacrificed 30 min after injection. To

additionally check the uptake specificity of fluorescent NPS conjugates, 2 μ l of native rat NPS at 50 or 100 μ M in Ringer solution were pre-injected 10 min before injection of Cy3-NPS.

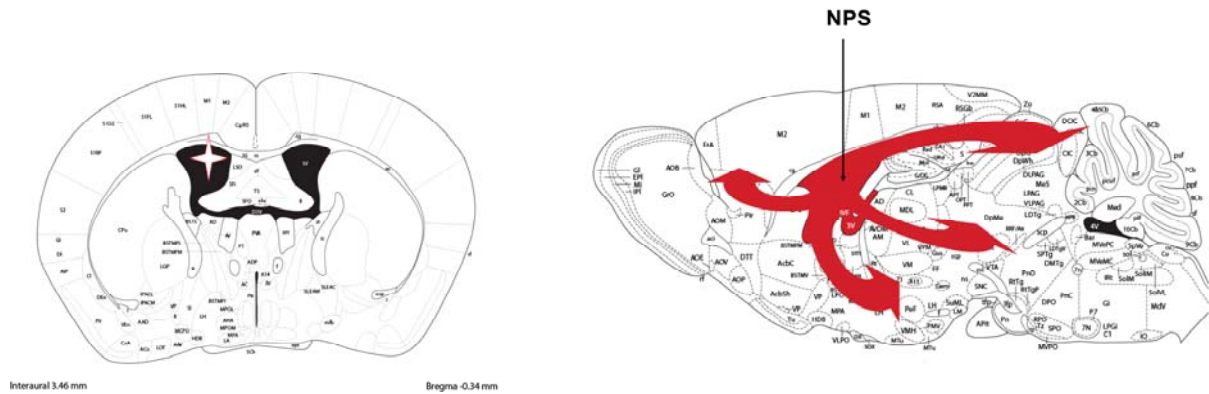


Figure 6. Injection site and distribution pattern of Cy3-NPS. Injection site shown on the left as a red star. The hypothesis stated that Cy3-NPS would enter the cerebrospinal fluid (CSF) upon ICV delivery and from there distribute throughout the entire brain (shown here on the right as red arrows) and be internalized specifically into cells expressing active NPSR at the membrane. Brain overview adapted from (Franklin and Paxinos, 2007).

In order to determine whether the internalization of the fluorescent NPS conjugates was dependent upon NPSR or upon other mechanisms, these were co-injected with specific NPSR antagonists: either [D-Cys(tBu)5]NPS (Camarda et al., 2009) or the active enantiomer of 3-oxo-1,1-diphenyl-tetrahydrooxazolo-[3,4-a]pyrazine-7-carboxylic acid 4-fluoro-benzylamide (SHA 68), (R)-SHA 68, both 1.5 mM (= 150 fold concentration of Cy3-NPS) (Okamura et al., 2008; Trapella et al., 2011). Animals were sacrificed by cervical dislocation 30 min after injection.

2.2.3. Intranasal application of fluorescent NPS conjugates

To determine whether NPS can reach its specific cerebral target cells after intranasal delivery, Cy3-NPS was applied intranasally in mice anesthetized with ketamine-rompun at 0.1 ml/10 g and placed in a supine position, with the head supported at a 45 degree angle to the body. This has been determined by others to be the optimal position in which least substance loss to the sinuses occurs (van den Berg et al., 2002). Cy3-NPS (10 μ M) or unconjugated rhodamine (10 g/ml) in a volume of 7 μ l were applied alternatingly to each nostril using a 10 μ l pipette; after 5 min, the procedure was repeated. This break was designed to avoid overfilling of the nostrils

and substance loss by exhalation. The mice were sacrificed by cervical dislocation 30 min after application.

2.2.4. Brain removal and immunohistochemistry

After sacrifice, the whole brains were removed immediately and post-fixed in 4 % PFA overnight at 4°C, then shock-frozen in methylbutane and stored at -80°C. Cryosections of 40 µm were then cut from the olfactory bulb until the first third of the cerebellum.

For observation of the distribution pattern of Cy3-NPS, the sections were thaw-mounted and counterstained with DAPI for 15 min, then washed by immersion into PBS. After mounting with Shandon Immu-Mount, the sections were stored at 4°C.

To quantify Cy3-NPS uptake between ICV and intranasal administration, a four-point scale was used to score both signal intensity and number of labeled cells as follows: very strong, +++; strong, ++; moderate, +; weak/scattered, -/+; and no signal, -.

For characterization of the cells that took up Cy3-NPS on the basis of specific markers for various cell types, stainings against these markers were performed on free-floating brain sections. The markers selected were as follows: 1) neurofilament as a neuronal marker; 2) glial fibrillary acidic protein (GFAP) as an astrocytic marker; and 3) ionized calcium binding adaptor molecule 1 (Iba-1) as a marker for macrophages and microglia. Primary antibodies are listed in Table 5, secondary antibodies in Table 6.

Table 5. Primary antibodies for immunohistochemistry on brain sections.

Antibody	Dilution	Species	Manufacturer
Neurofilament	1:1000	mouse	Abcam, Cambridge, UK
GFAP	1:250	rabbit	DAKO, Glostrup, Denmark
Iba-1	1:1000	rabbit	Wako, Richmond, VA, USA

Table 6. Secondary antibodies for immunohistochemistry on brain sections.

Antibody	Dilution	Species	Manufacturer
Anti-rabbit Alexa488	1:300	donkey	Invitrogen, Darmstadt, Germany
Anti-mouse Alexa488	1:300	donkey	Invitrogen, Darmstadt, Germany

Brain sections were taken up during cutting in a freezing buffer and then stored at -20 °C in the dark. For immunohistochemistry, all incubation steps were performed in a 6-well plate on a shaker to ensure optimal distribution of the reagents over the entire surface and among all brain sections. The minimal required volume was 0.5 ml per well. All steps were performed in the dark and after wrapping the vessel in aluminium foil. Brain sections were washed three times for 10 min in PBS and then blocked in 10 % goat serum and 1 % triton in PBS for 1 hour at RT. Then sections were incubated with primary antibodies in 1 % goat serum and 0.3 % triton in PBS overnight at RT or for 2 days at 4 °C. After three washing steps of 10 min each in PBS, the sections were incubated with the secondary antibody coupled to Alexa488 (green, so as to not overlap with the red signal from the fluorophore-coupled NPS) diluted in the same solution as for the primary antibody. The sections were then washed six times with PBS for 15 min per washing step; DAPI was included in the fourth washing step. For mounting, the sections were transferred to a box filled with double distilled H₂O (ddH₂O) and mounted on the slides using a thin brush.

Image acquisition was performed using either an epifluorescence or a confocal microscope.

2.3. Analysis of behavioral and molecular effects of intranasal NPS application

2.3.1. Animals

For behavioral experiments after intranasal NPS application and for the mouse model of PTSD, 6 weeks old male C57BL/6N mice were purchased from Charles River and allowed to habituate until they were 10 weeks old, at which time-point the experiments started. Male 10 weeks old HAB mice were obtained from the breeding facility of the MPI of Biochemistry, Martinsried. The mice that underwent the PTSD

paradigm were housed in groups of 4 mice per cage; all other mice were housed singly. All experiments were approved by the Government of Upper Bavaria and were in accordance with European Union Directive 86/609/EEC.

2.3.2. Intranasal NPS application in C57BL/6N and HAB mice

Two mouse groups were used for each experiment. A control group was mock-treated with the NPS solvent (vehicle treatment) and a treatment group received the active substance.

Native rat NPS diluted in Ringer solution was applied intranasally in the alert mice which were restrained manually during application in a supine position with the head fixed in a position of approximately 45 degrees to the body (see Figure 7). The application was performed as in the case of Cy3-NPS (2.2.3.), allowing a 5 min break to avoid exhalation and overfilling of the nostrils, as well as reduced or delayed absorption. Mice were held immobile for 10 seconds after substance application until all the substance had been absorbed. Substance exhalation was carefully monitored during and after application and was found to be minimal to non-occurring.



Figure 7. Intranasal treatment in alert mice restrained manually.

To determine the optimal NPS dose for eliciting behavioral effects after intranasal application, the C57BL/6N mice received 7, 14 and 28 nmol of substance per mouse. The HAB mice then received the dose that had been determined to be optimal in this first assay, which was 14 nmol per mouse.

2.3.2.1. Behavioral assays

The mice were tested 4 hours after application. The question of interest was whether intranasal application of NPS has the same anxiolytic effects as described by others for ICV injection. However, since it is very difficult to distinguish between increased locomotion and reduced anxiety, parameters that relate to both these aspects were examined in each test.

The mice were tested in three different assays performed in the following order: open field, dark-light box and EPM (for an overview of the experimental timeline see Figure 22). Each test lasted for 5 min, with a 5 min interval between single tests. The open field, which consists of an open round arena, was performed first to obtain a baseline of locomotion as measured by the total distance traveled. If there are no differences in locomotion in the open field, it can be safely assumed that the treatment had no effect on locomotion. To double-check, locomotion-related indices were also investigated in the subsequent anxiety tests. The principle of the dark-light box, which consists of two chambers (a small black and dark one and a white, brightly lit larger one, connected by a single passage), relies on the fact that mice naturally prefer darker environments where they feel more protected from potential predators. On the other hand, mice also like to explore new environments, an aspect which is taken into account by making the “risky” light chamber larger. Reduced anxiety will be mirrored by an increased percentage of time spent in the light chamber. To characterize possible changes in locomotion, the percent distance traveled in the light chamber was also compared between vehicle and NPS treatment. Finally, in the EPM, a plus-shaped platform elevated at ca. 1 m above the floor and consisting of two open and two closed arms (described in detail in 1.6.2.), the percent time spent on the open arm served as a measure of anxiety, while the number of entries into the closed arms was taken as a reliable indicator of locomotion. The animals’ behavior during testing was videotaped and relevant parameters were analyzed with the tracking software ANY-maze version 4.30.

2.3.2.1.1. Statistical analysis

The data was analyzed using one-way analysis of variance (ANOVA) with Bonferroni’s *post hoc* test in the case of the C57BL/6N mice and two-tailed unpaired

t-test for the HAB mice. Outliers were excluded using Grubbs' test. p -values between 0.1 and 0.05 were considered to represent a trend, p -values below 0.05 were considered significant.

2.3.2.2. Analysis of molecular changes after NPS treatment

2.3.2.2.1. Preparation of single brain regions and selection of candidates

To better characterize the changes elicited by NPS treatment in protein expression (which had not been described until now), especially such changes as might shed light on the anxiolytic mechanisms of NPS, two brain regions that have been strongly linked to anxiety and fear formation and extinction were chosen: the hippocampus (Hc) and the prefrontal cortex (Pfc). In these brain regions, candidates involved in the glutamatergic system and in synaptic plasticity were selected for investigation following a hypothesis-driven approach, since both NPS effects and the pathological processes of anxiety disorders have been associated with these systems. These candidates were: subunits 1 and 2 of the AMPA receptor (GluR1 and GluR2); the astrocytic glutamate transporter (Glt-1); and isoforms I and II of synapsin. Changes in expression levels of these candidates were examined on the mRNA as well as on the protein level. The single brain regions were prepared on ice from the freshly isolated brain. For subsequent total mRNA isolation, the brain regions were isolated 4 hours after treatment, since changes on the transcriptional level are very fast, preserved in RNase-free 2 ml tubes and shock-frozen in liquid nitrogen. For protein isolation, the brain regions were isolated 24 hours after treatment, to allow time for effects on the protein level to materialize, shock-frozen in methylbutane (pre-cooled and stored on dry ice) and then kept in 2 ml tubes. All samples were stored at -80 °C.

2.3.2.2.2. mRNA isolation and real-time PCR

mRNA was isolated as described in detail in 2.1.1.1. and then reverse transcribed into cDNA as described in 2.1.1.2.. For evaluation of candidate mRNA expression, real-time PCR was performed. The QuantiFast SYBR Green PCR Kit was used according to the manufacturer's instructions. In brief, 5 μ l QuantiFast Mix were mixed with 1 μ l forward and 1 μ l reverse primer from a stock of 5 pmol/ μ l and with 1 μ l H₂O, the master mix was pipetted into glass capillaries and then 2 μ l cDNA were added.

Before real-time PCR, the samples were centrifuged briefly. The real-time PCR settings used were as follows:

1. initial denaturation: 95 °C – 10 min
 2. denaturation: 95 °C – 10 seconds
 3. annealing + elongation: 60 °C – 30 seconds
- } 40 cycles

A melting curve was generated at the end of every run to ensure the quality of the PCR product. Crossing points (C_p) were calculated automatically using the absolute quantification fit points method. Relative gene expression was determined by the $2^{-\Delta\Delta C_T}$ method (Livak and Schmittgen, 2001). C_p values were normalized to expression levels of the housekeeping gene glyceraldehyde 3-phosphate dehydrogenase *Gapdh*. Primers designed by others were used for *Glut-1* (Perisic et al., 2010), *GluR1* and *GluR2* (Blanco et al., 2011). Self-designed primers are shown in Table 7.

Table 7. Real-time PCR primers for synapsin I and II and *Gapdh*.

Gene of interest	Forward primer	Reverse primer
<i>Synapsin I</i>	5'-CACCGACTGGGCAAA ATACT-3'	5'-TCCGAAGAACTTC CATGTCC-3'
<i>Synapsin II</i>	5'-CCTTCATCGACGCCA AGTAT-3'	5'-GAGCAGGCATCTAC CCAGAG-3'
<i>Gapdh</i>	5'-CCATCACCATCTTC CAGGAGCGAG-3'	5'-GATGGCATGGACTGT GGTCATGAG-3'

2.3.2.2.2. Protein isolation and immunoblotting

A protease inhibitor cocktail was freshly added at 1x final concentration to homogenization and extraction buffer before use. 100 µl homogenization buffer were added to each brain tissue sample and the tissue was homogenized thoroughly with the turrax. An equal amount of extraction buffer was added and the lysate subsequently sonicated thirty times. The samples were then centrifuged at 13 krpm for 5 min at RT to spin down the debris and the supernatant was transferred into a new tube. This lysis method does not open the nucleus; the lysate therefore contains exclusively cytosolic and membranary protein fractions.

Protein concentration was determined using the BCA Protein Assay Reagent (bicinchoninic acid) according to the manufacturer's instructions. In brief, a BSA

standard in water was prepared with descending protein concentrations: 2 mg/μl, 1.5 mg/μl, 1 mg/μl, 0.75 mg/μl, 0.5 mg/μl, 0.25 mg/μl, 0.125 mg/μl, 0.025 mg/μl and 0 mg/μl. The BCA working reagent was made by mixing BCA Reagent A with Reagent B at a ratio of 50:1. 200 μl working reagent were pipetted per well of a 96-well plate and 25 μl of the standards and subsequently of the samples were added. The plate was incubated in the dark at 37 °C for 1 hour to allow for development of the colorimetric reaction. In an alkaline medium, proteins reduce Cu^{2+} to Cu^{1+} ; BCA forms a complex with Cu^{1+} , which leads to development of a violet-colored compound, the intensity of which is proportional to the protein concentration in the sample. Absorbance was then measured at 562 nm in a plate reader. Protein samples were then adjusted to a concentration of 2 μg/μl for loading on the gel. The dilutions were made with dH_2O containing protease inhibitor cocktail at 1x concentration and with Laemmli buffer and then inactivated for 10 min at 95 °C.

For immunoblotting, proteins were loaded on gels and separated by sodium dodecyl sulfate polyacrylamide gel electrophoresis (SDS-PAGE). Each gel consisted of a separation gel (lower part) and a stacking gel containing the wells (upper part). For the stacking gel the solution contained 25 % lower Tris buffer, 1 % of 20 % SDS, 30 % acrylamide at the desired concentration for the needed gel percentage, dH_2O up to the desired volume (25 ml solution sufficient for 4 gels), and initializing factors for the polymerization: 0.26 % of 10 % ammonium persulfate (APS) and 0.26 % tetraethylmethylenediamine (TEMED). The gel was cast between two glass plates and the solution was covered with isopropanol in order to avoid bubble formation and unevenness. After the gel had solidified, all traces of isopropanol were discarded and the stacking gel was cast. The stacking gel consisted of 23 % upper Tris buffer, 1 % of 20 % SDS, 13 % of 30 % acrylamide, dH_2O up to the desired volume (10 ml solution sufficient for 4 gels), and initializing factors for the polymerization: 0.25 % of 10 % APS and 0.25 % TEMED. The stacking gel was then cast on top of the separation gel and the comb was inserted to create the wells (15 wells per gel, maximal volume per well: 20 μl). After the stacking gel had polymerized, the gels were either used immediately or stored at 4 °C wrapped in wet towels for up to one week. For loading, gels were placed in Laemmli running buffer and loaded with equal amounts of the samples, including a protein marker ranging between 170 kDa and 25 kDa. The electrophoresis was performed first at 80 V, until the proteins had passed

the edge between stacking gel and separation gel (ca. 20 min) and then at 120 V for as long as deemed necessary for optimal separation (ca. 90 min). During the blotting process, proteins were transferred from the gel to a nitrocellulose membrane. Gel and membrane overlapped and were wrapped in two layers of filter paper and two layers of sponge on each side. Blotting was performed in WetBlot Buffer at 400 mA for 1 hour. To check for adequate protein transfer, the membranes were stained in Ponceau solution to unspecifically stain all proteins. Excess Ponceau was washed off in dH₂O and the membranes were then blocked in 5 % milk solution in Tris-buffered saline with Tween 20 (TBST) for 1 hour at RT on a shaker at 30 rpm. Membranes were then incubated with the primary antibody diluted in 2.5 % milk in TBST for up to 48 hours at 4 °C on a shaker at 30 rpm. Excess antibody was washed off in three washing steps of 10 min each in TBST on a shaker at 70 rpm and membranes were then incubated in secondary antibody coupled to horseradish peroxidase (HRP), diluted as described for the primary antibody, for 1 hour at RT on a shaker at 30 rpm. After three more washing steps, membranes were incubated in a self-made HRP substrate solution for 1 min on a shaker at 30 rpm to initiate the luminescence reaction, which was then detected on X-ray films in a dark room using an automated developing machine. Primary antibodies are listed in Table 8, secondary antibodies in Table 9.

Quantification of protein expression was performed by quantification of the pixel density of the protein bands on digitalized films using ImageJ software. Protein expression was normalized to the housekeeping protein GAPDH.

Table 8. Primary antibodies for immunoblotting.

Antibody	Dilution	Species	Manufacturer
GluR1	1:100	goat	Santa Cruz Biotechnologies, Santa Cruz, CA, USA
GluR2	1:100	goat	Santa Cruz Biotechnologies, Santa Cruz, CA, USA
Glt-1	1:100	goat	Santa Cruz Biotechnologies, Santa Cruz, CA, USA
synapsin	1:2000	rabbit	Synaptic Systems, Göttingen, Germany
GAPDH	1:2000	mouse	Santa Cruz Biotechnologies, Santa Cruz, CA, USA

Table 9. Secondary antibodies for immunoblotting.

Antibody	Dilution	Species	Manufacturer
Anti-goat	1:10000	donkey	Santa Cruz Biotechnologies, Santa Cruz, CA, USA
Anti-mouse	1:25000	goat	Sigma-Aldrich, St Louis, MA, USA
Anti-rabbit	1:7500	goat	Sigma-Aldrich, St Louis, MA, USA

2.3.2.2.3. Statistical analysis

Normalized data from real-time PCR and immunoblotting were analyzed using the two-tailed unpaired t-test. *p*-values between 0.1 and 0.05 were considered to represent a trend, *p*-values below 0.05 were considered significant.

2.3.3. Intranasal NPS application in a mouse model of PTSD

2.3.3.1. Behavioral assays

The PTSD mouse model is based on administration of a strong electrical foot-shock (1.5 mA) considered equivalent to trauma in humans. This shock is administered in a rectangular shock context containing a grid. As shown previously, the development of the PTSD-like phenotype reaches a maximum at day 28 post-shock and persists in the long-term until at least as late as day 60 (Siegmund and Wotjak, 2007; Golub et al., 2011). To investigate the curative effects of intranasal NPS treatment on the full-blown PTSD pathology, shocked mice were divided into two groups: mock-treatment with Ringer solution (vehicle) and treatment with 8 nmol NPS in Ringer solution as described above (2.3.2.). Treatment was performed 2 hours before behavioral testing. This time-point was chosen earlier than the previously used one (4 hours, 2.3.2.1.) in the hope that the behavioral effects would be even more marked earlier on. Three behavioral tests were performed on three consecutive days to test for specific symptoms of the PTSD-like phenotype and acute NPS treatment was performed 2 hours before each test. First, the freezing behavior in the shock context was measured to check for fear expression to trauma-specific cues. For this purpose, mice were placed in the conditioning context (described above) and their freezing behavior was scored for 3 min, freezing being defined as no further movement of the mouse (Siegmund and Wotjak, 2007). Second, to test for social interaction, which has been shown to be strongly decreased in PTSD patients, mice were kept in their

home cage (placed in a sound-isolated cubicle), allowed to habituate for 3 min and then exposed to a similarly treated interaction partner, who represented the control (vehicle was always paired off with vehicle and NPS treatment was always paired off with NPS treatment). Social interaction was described as sniffing, licking, close following and allogrooming (cleaning the control partner's body), whereas avoidance of social interaction was defined as escaping to the other end of the cage and keeping the approaching interaction partner at bay in an upright position with lifted paws (Siegmund and Wotjak, 2007). These two parameters were scored for 4 min. Finally, to test for hyperarousal, the startle reflex, which is highly increased in PTSD patients, was quantified. In this case, the acoustic startle reflex was measured: mice were exposed to 4 different startle stimuli (white noise, duration: 20 ms) of growing intensity (75 dB, 90 dB, 105 dB and 115 dB), 15 seconds apart, and the startle response was measured (Golub et al., 2011).

2.3.3.2. Protein and mRNA expression in Hc and Pfc

Brain regions (Pfc and Hc) were isolated as described above (2.3.2.3.1.) 24 hours after the last treatment. The same candidates were examined on mRNA and protein levels by real-time PCR and immunoblotting, respectively (2.3.2.3.1.-3.).

2.3.3.3. Measurement of corticosterone plasma levels

Trunk blood was isolated from the decapitated mice 24 hours after the last treatment, between 09:00 a.m. and 12:00 a.m., and collected in tubes containing EDTA to prevent clotting. The samples were then centrifuged at RT, 8000 rpm, for 10 min, to separate plasma from cell pellet. The plasma was then transferred into a new tube and stored at -20 °C.

Corticosterone plasma levels were measured using the Corticosterone (Rat/Mouse) solid phase enzyme-linked immunoabsorbent assay (ELISA) kit according to the manufacturer's instructions. The ELISA was based on the principle of competitive binding. In brief, after all reagents had reached RT, 10 µl of calibrator solutions C0-C5 containing increasing corticosterone concentrations (0 – 15 – 50 – 185 – 640 – 2250 ng/ml) and of each sample were pipetted into separate wells into a microtiterplate containing wells coated with polyclonal rabbit anti-corticosterone antibody; measurements were performed in duplicates. 100 µl incubation buffer per

well were then added, followed by 50 μ l per well of enzyme conjugate containing HRP-coupled corticosterone. After 2 hours incubation at RT on a microplate mixer, the content of the wells was discarded and the wells were rinsed 4 times with 300 μ l 1x washing solution per well. 200 μ l of substrate solution containing tetramethylbenzidine (TMB) and H_2O_2 were added to each well and the plate was incubated for 30 min in the dark; the reaction was subsequently stopped by addition of 50 μ l stop solution to each well. The absorbances of the wells' content were then measured at 450 nm in a microplate reader.

2.3.3.4. Statistical evaluation

All statistical evaluations were performed using GraphPad Prism 5.03.

2.3.3.4.1. Behavioral assays

The % freezing for context-specific fear was compared between the two groups using the two-tailed unpaired t-test. The % social interaction was similarly compared between the two groups using the two-tailed unpaired t-test. For evaluation of the acoustic startle response (ASR), the response intensity was compared between the two groups using a two-way ANOVA with group (vehicle vs. NPS) as one factor and tone-pitch (75 dB, 90 dB, 105 dB and 115 dB) as the second factor, followed by Bonferroni's *post hoc* test.

2.3.3.4.2. Protein and mRNA data

Expression levels of protein and mRNA were compared between the two groups using the two-tailed unpaired t-test (see 2.3.2.3.3.).

2.3.3.4.3. Corticosterone plasma levels

A standard curve was plotted on a semi-log plot using the calibrator concentrations in ng/ml (X values) and the corresponding assay results (the measured absorbances, Y values) as reference points. As the value 0 cannot be plotted on a semi-log plot, the zero-concentration X value was approximated using 1.0e-003, which is two log units below the lowest non-zero X value, in order to plot the top of the curve as accurately as possible. All X values were subsequently log transformed. The curve was then fit according to a nonlinear regression and sigmoidal dose-response with variable slope.

The unknown X values corresponding to the corticosterone concentrations in the samples were then interpolated from the fitted curve and reverse-transformed from the log values to obtain the corticosterone concentrations in ng/ml. The mean corticosterone concentration values were compared between vehicle and treatment groups using the two-tailed unpaired t-test.

2.4. Behavioral effects of NPS treatment via injection into the ventral CA1 region (vCA1)

2.4.1. Stereotactic surgery

Stereotactic surgery was performed as described above (2.2.2.). Guide cannulas were implanted at the following coordinates: 3.1 mm posterior and \pm 3 mm lateral from the bregma, and 2 mm ventral from the skull surface. For behavioral experiments, animals were implanted bilaterally; for injection of Cy3-NPS implantation was performed unilaterally.

2.4.2. Injection of Cy3-NPS into vCA1

Cy3-NPS was administered unilaterally at a concentration of 0.01 nmol/ μ l and in a total volume of 0.7 μ l (solvent: Ringer solution) as described above (2.3.2.). Brains were removed and cryosections were collected and counterstained with DAPI as described above (2.2.4.).

2.4.3. Behavioral assays

Mice were injected bilaterally either with 0.1 nmol native rat NPS in a total volume of 0.5 μ l for each side (solvent: Ringer solution) (treatment group) or with 0.5 μ l of Ringer solution for each side (vehicle group). 30 min after injection, three behavioral assays (open field, dark-light test and EPM) were performed sequentially in the order mentioned, as described previously (2.3.2.1.). 24 hours after the behavioral assays, mice were injected bilaterally with fluorescein, which emits a green signal upon stimulation and can therefore be seen very well in brain sections. Mice were immediately sacrificed afterwards and the locations of the guide cannulas were checked in histological cryosections of 40 μ m counterstained with DAPI (see above). Mice with deviating injection sites were excluded from all further analysis.

2.4.3.1. Statistical analysis

Statistical analysis was performed using the two-tailed unpaired t-test.

3. Results

3.1. Cloning of NPSR and *in vitro* analysis of NPSR-NPS interaction

In order to characterize the behavior of NPSR upon NPS binding, constructs of the murine NPSR were generated that allow tracking of the receptor upon expression in cell culture. The experiments were performed with two different constructs, i.e. EGFP-NPSR and NPSR-FLAG (see Figure 8).

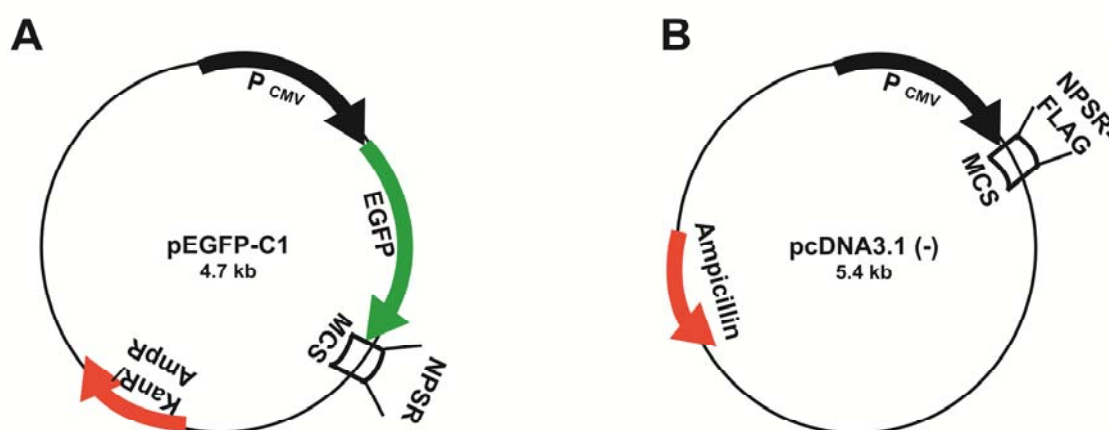


Figure 8. Cloning strategy of tagged NPSR constructs. **A** In pEGFP-C1, NPSR was inserted after the EGFP-sequence. **B** In pcDNA 3.1 (-), the FLAG-tagged NPSR sequence was inserted. P_{CMV}: cytomegalovirus promoter. KanR/AmpR: kanamycin/ampicillin resistance gene. MCS: multiple cloning site.

In the EGFP-NPSR construct, NPSR was coupled N-terminally to enhanced green fluorescent protein (EGFP) to allow for direct tracking by microscopy imaging without additional stainings. In the NPSR-FLAG construct, the FLAG tag was attached C-terminally to NPSR, in order to rule out that the interaction between NPSR and EGFP may influence the behavior of the receptor. NPSR-FLAG was visualized by immunofluorescent stainings against the FLAG tag. A fluorescent NPS conjugate (Cy3-NPS) was used for stimulation of cells transfected with the receptor constructs to allow for visualization of their interaction. All experiments were performed in HEK cells, since they are the most commonly used cell line for initial characterization of constructs and have been previously used for investigation of human and murine NPSR distribution (Bernier et al., 2006).

3.1.1. Visualization of EGFP-NPSR and FLAG-NPSR in HEK cells

Gel electrophoresis of NPSR amplification products with specific primers in cDNA from HEK cells showed that NPSR mRNA is expressed specifically in HEK cells transiently transfected with plasmids containing EGFP-NPSR and NPSR-FLAG (Figure 9A, B). No NPSR expression was detected by this method in HEK cells either transfected with the empty cloning vector or untransfected (Figure 9A, B). Control actin amplification confirmed that similar amounts of cDNA were present in all investigated samples (Figure 9A).

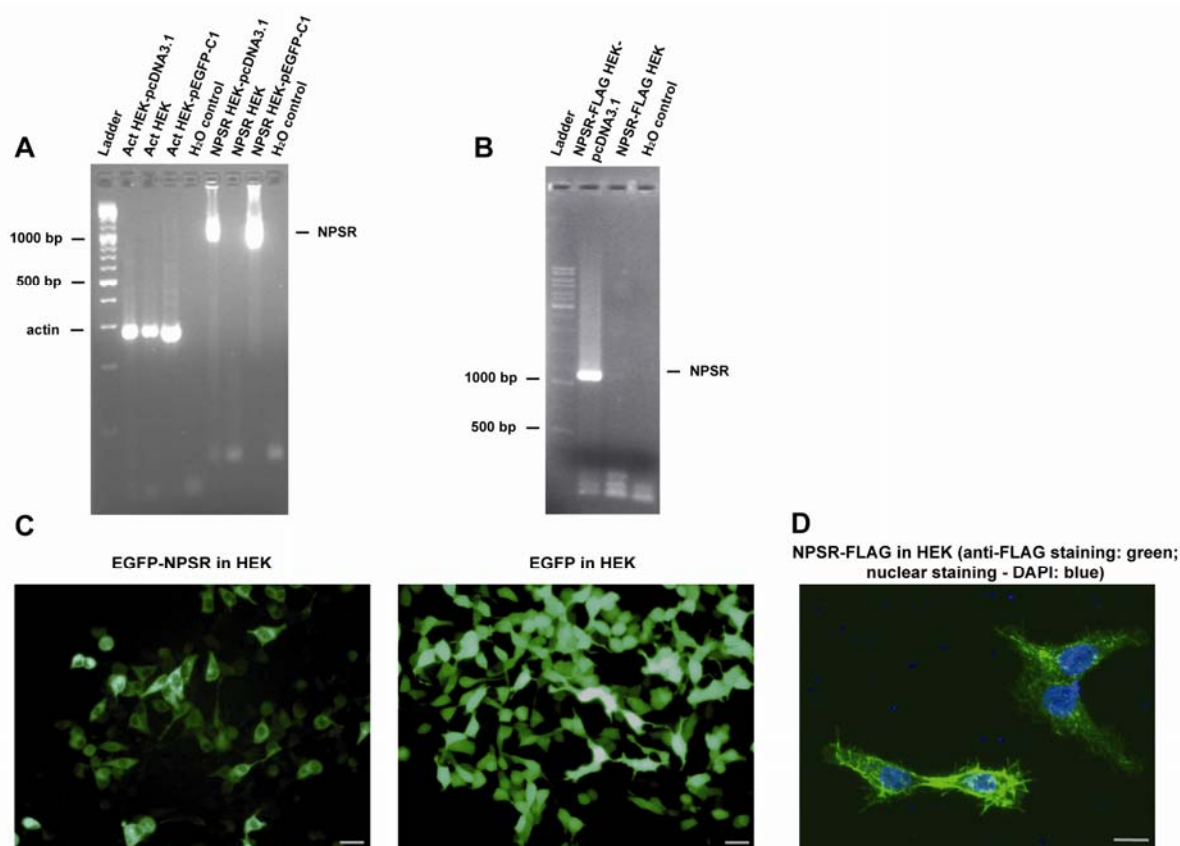


Figure 9. Cloning and expression of NPSR constructs. **A** 3 % TBE agarose gel showing PCR products actin and NPSR from cDNA of HEK cells transfected with NPSR in pcDNA3.1 (-) and untransfected. Predicted band weight: NPSR = 1125 bp; actin = 270 bp. **B** 3 % TBE agarose gel showing PCR product NPSR amplified from cDNA of HEK cells transfected with NPSR-FLAG in pcDNA3.1 (-) and untransfected. Predicted band weight: NPSR = 1125 bp. **C** EGFP-NPSR (green) expression in HEK cells as compared to EGFP expression in HEK cells transfected with pEGFP-C1. Image taken with an epifluorescence microscope in live cells at 20x magnification. Scale bars, 40 μ m. **D** Immunostaining against FLAG (green) in HEK cells expressing NPSR-FLAG. Nuclear staining: DAPI (blue). Image taken with a confocal microscope at 60x magnification. Scale bar, 20 μ m.

Epifluorescence and confocal microscopy of living and fixed cells revealed that the tagged NPSR constructs are also well expressed at the protein level (Figure 9C, D). Both constructs were expressed cytosolically as well as at the membrane, which coincides with results obtained by others after immunostaining of HEK cells expressing hemagglutinin (HA)-tagged NPSR in permeabilized and non-permeabilized cells (Bernier et al., 2006). There were significant differences in the amount of expressed protein between HEK cells transfected with EGFP-NPSR and those transfected with the empty pEGFP-C1 vector (Figure 9C). While EGFP was very strongly expressed throughout the cell with no significant differences between compartments, EGFP-NPSR had a lower expression intensity and was comparably more highly expressed at the cell membrane. NPSR-FLAG, visualized by immunostaining of FLAG on PFA-fixed cells, showed the membranary distribution of the receptor even more clearly (Figure 9D).

3.1.2. Stimulation of NPSR-expressing HEK cells with Cy3-NPS

To investigate the behavior of receptor-ligand complex after ligand stimulation, Cy3-NPS was added to HEK cells expressing EGFP-NPSR. 10 min after ligand addition, Cy3-NPS had already bound to its receptor in a highly specific manner, as revealed by colocalization of red and green signals, and the receptor-ligand complex was internalized into the cells (Figure 10). There, it accumulated into cytoplasmic and perinuclear vesicles, as shown previously for other neuropeptides upon binding to their GPCRs (Grady et al., 1995).

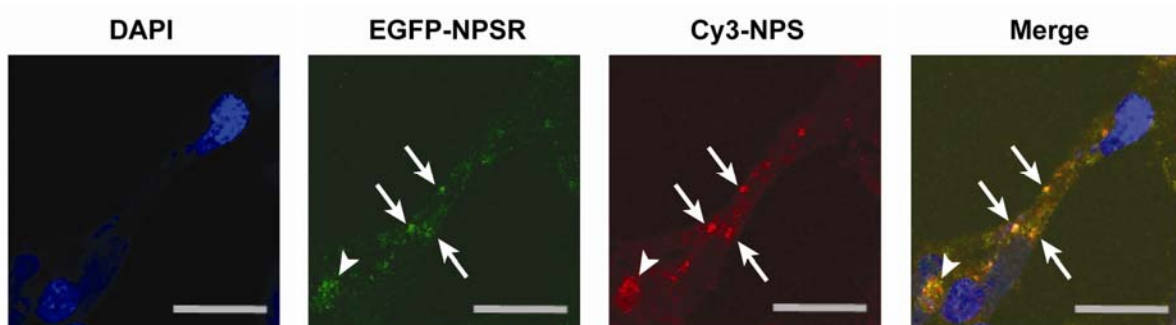


Figure 10. HEK cells transiently transfected with EGFP-NPSR (green) after 10 min of incubation with Cy3-NPS (red) (adapted from (Ionescu et al., 2012)). Nuclear staining: DAPI (blue). Rightmost panel depicts an overlay of all three channels and shows colocalization of Cy3-NPS and EGFP-NPSR (yellow) in cytoplasmic (arrows) and perinuclear (arrowheads) vesicular structures. All images were taken with a confocal microscope. Scale bars, 20 μm .

These results were confirmed also for FLAG-NPSR (Figure 11), confirming that the specific behavior observed here is not due to any interaction of the receptor with the quite large EGFP.

In order to better characterize the rough dynamics of this process, HEK cells expressing FLAG-NPSR were stimulated with Cy3-NPS (Figure 11). A timeline of receptor-ligand internalization showed that immediately after ligand addition (0 min), Cy3-NPS bound to the receptor at the cell membrane and created an overlapping outline of the cell surface. At 10 min, the receptor-ligand complex had for the most part been internalized into the cell in small cytoplasmic vesicles, and the receptor fraction at the membrane was depleted in comparison with the previous time-point. At 30 min, Cy3-NPS and some of the receptor to which it had bound had mostly accumulated in a large perinuclear vesicle, with only a few smaller vesicles still present in the rest of the cytoplasm; the receptor presence at the membrane had been restored almost completely to the initial state.

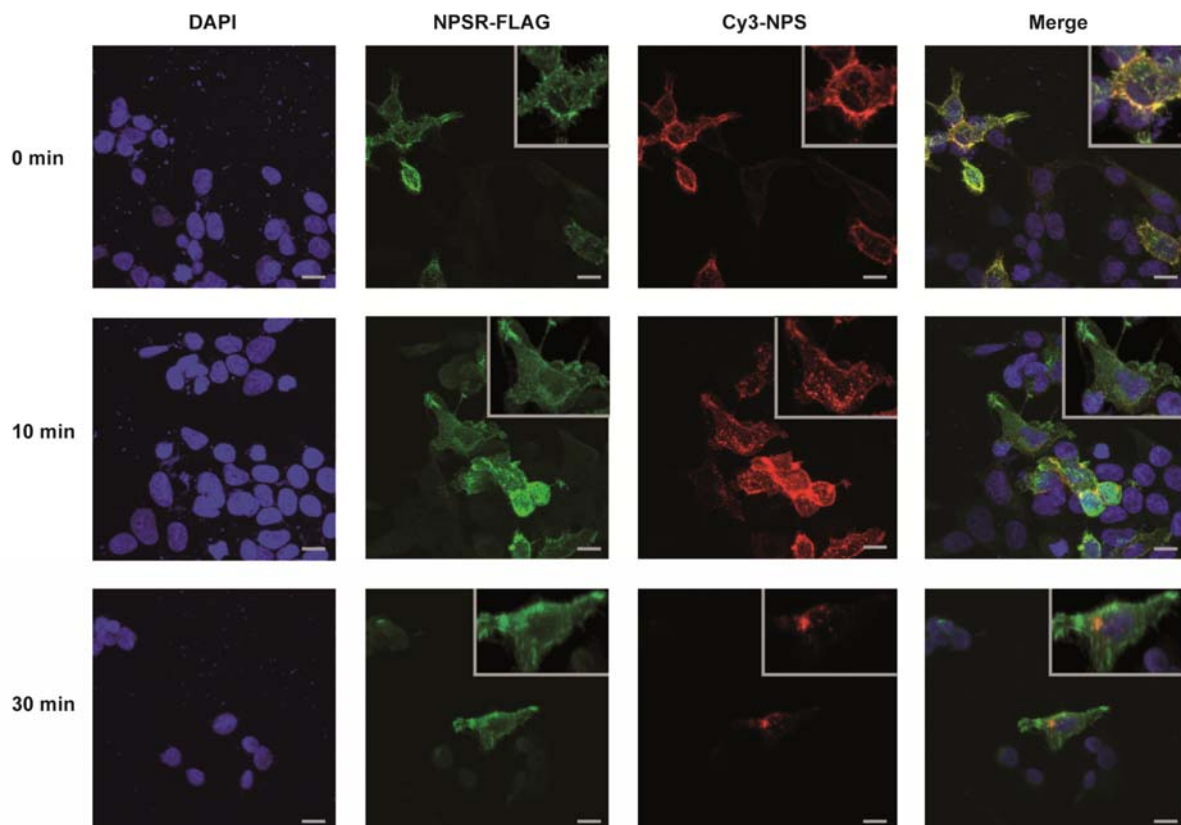


Figure 11. Timeline of Cy3-NPS internalization in HEK cells expressing NPSR-FLAG at 3 different time-points: 0 min, 10 min and 30 min after Cy3-NPS addition. Nuclear staining: DAPI (blue). Immunostaining against FLAG: green. Cy3-NPS: red. All images were taken with a confocal microscope. Scale bars, 20 μ m.

These results showed fluorescently labeled NPS to be appropriate for tracking at single-cell resolution interactions with the receptor and intracellular internalization in cell culture.

3.2. Brain target regions and target neurons of NPS

Therefore, relying upon the above results obtained in cell culture, Cy3-NPS was used here for investigating the intracerebral distribution pattern *in vivo* after intranasal delivery. Since, as described previously in detail (see 1.5.), targeting the CNS after intranasal administration is dependent upon many factors, such as size and polarity of the molecule under investigation, this approach served to establish for the first time the feasibility of intranasal delivery in the case of NPS. Fluorophore-conjugated NPS was used because the radioactively labeled ligands employed so far for intra-CNS tracking after intranasal administration have a very low spatial resolution that enables localization only to brain regions and not to single cells or subcellular compartments (Thorne et al., 2004).

First, *in vivo* tracking of this substance was investigated using intracerebroventricular (ICV) injection, an established method for brain delivery into mice; this experiment was then reproduced for intranasal application. The hypothesis underlying these experiments was that Cy3-NPS will become distributed evenly throughout all cerebral structures upon reaching the brain and will accumulate specifically in cells expressing NPSR via internalization of the receptor-ligand complex.

3.2.1. Identification of brain target regions and cells of NPS by intracerebroventricular (ICV) administration of Cy3-NPS

In order to check whether the NPSR-dependent intracellular internalization of Cy3-NPS observed in cell culture also works *in vivo*, Cy3-NPS was delivered to the brain first by ICV injection.

At 30 min after unilateral ICV administration of Cy3-NPS, the substance had distributed throughout the brain and uptake within single cells in specific brain regions had occurred. A complete overview of brain regions where cells took up Cy3-NPS is available in Table 10.

Table 10. Overview of brain regions targeted by Cy3-NPS.

<p>Forebrain</p> <ul style="list-style-type: none"> Accumbens nucleus Anterior olfactory area, ventral part Anterior olfactory area, external part <p>Basal ganglia</p> <ul style="list-style-type: none"> Globus pallidus <p>Cerebral cortex</p> <ul style="list-style-type: none"> Primary motor cortex Secondary motor cortex Somatosensory cortex Cingulate cortex, area 1 Endopiriform cortex <p>Amygdala</p> <ul style="list-style-type: none"> Medial amygdaloid nuclei Anterior cortical amygdaloid nuclei Posterior cortical amygdaloid nuclei Basolateral amygdala Central amygdala Lateral amygdala Bed nucleus of the stria terminalis (intraamygdaloid division) Amygdalohippocampal area <p>Hippocampus</p> <ul style="list-style-type: none"> Dentate gyrus CA1 CA2 CA3 Ventral hippocampus, granular layer of dentate gyrus 	<p>Thalamus</p> <ul style="list-style-type: none"> Medial habenula Lateral habenula Paraventricular thalamic nucleus Mediodorsal thalamic nucleus <p>Hypothalamus</p> <ul style="list-style-type: none"> Arcuate nucleus Paraventricular nucleus Dorsomedial nucleus Ventromedial nucleus Periventricular nucleus Suprachiasmatic nucleus <p>Preoptic area</p> <ul style="list-style-type: none"> Median preoptic nucleus Ventromedial preoptic nucleus Vascular organ of the lamina terminalis <p>Midbrain and brainstem areas</p> <ul style="list-style-type: none"> Dorsal raphe Posterodorsal tegmental nucleus Periaqueductal gray Central gray of the pons Red nucleus Locus coeruleus Barrington's nucleus Medial parabrachial nucleus Medial vestibular nucleus <p>Cerebellum</p> <ul style="list-style-type: none"> Purkinje cells
---	--

Cell populations containing Cy3-NPS were identified in regions associated with stress-response and learning such as the lateral habenula and the mediodorsal thalamic nuclei, respectively (Figure 12B), as well as in regions with neuroendocrine function, such as the arcuate and ventromedial hypothalamic nuclei (Figure 12C).

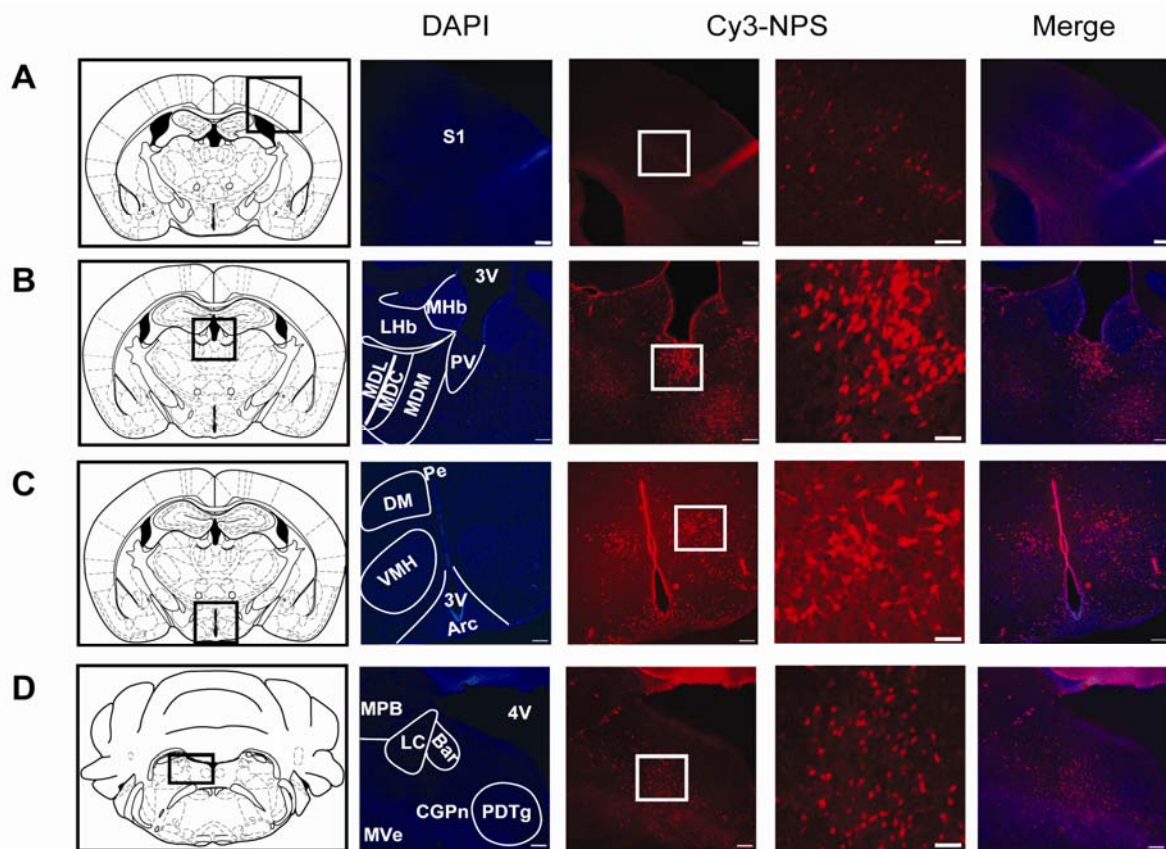


Figure 12. Representative selection of mouse brain regions targeted by ICV-administered fluorescent Cy3-NPS (Ionescu et al., 2012). **A-D** Leftmost panels show a schematic overview of murine brain regions (Franklin and Paxinos, 2007). Middle panels show nuclear counterstain DAPI (blue) (scale bar, 100 μ m) and cell populations having taken up Cy3-NPS (red). The images in the red channel are presented in two different magnifications (scale bars, 100 μ m and 10 μ m) – white rectangles indicate area of magnification. Rightmost panels show an overlay of the blue and red channels (scale bar, 100 μ m). **A** Cortical structures: primary somatosensory cortex (S1). **B** Thalamic structures: paraventricular thalamic nucleus (PV), sporadically in medial habenula (MHb), lateral habenula (LHb), mediodorsal thalamic nucleus (MD): medial (MDM), central (MDC) and lateral (MDL). Third ventricle (3V). **C** Hypothalamic structures: periventricular hypothalamic nucleus (Pe), dorsomedial hypothalamic nucleus (DM), ventromedial hypothalamic nucleus (VMH), arcuate hypothalamic nucleus (Arc). Third ventricle (3V). **D** Brainstem structures: central gray of the pons (CGPn), medial vestibular nucleus (MVe), sporadically in posterodorsal tegmental nucleus (PDTg), Barrington’s nucleus (Bar), sporadically in locus coeruleus (LC) and in medial parabrachial nucleus (MPB). Fourth ventricle (4V). All images were acquired with a confocal microscope and are representative for a total of 10 mice. See Table 10 for a complete list of brain regions where uptake of Cy3-NPS was detected.

Most interestingly, Cy3-NPS uptake was detected also in regions farther away from the cerebroventricular system, for instance in cortical regions (Figure 12A), and in very caudal brain regions like the locus coeruleus, the tegmental nucleus, Barrington’s nucleus and the parabrachial nucleus (Figure 12D). Even in the

cerebellum, which is distant from both the ventricular system and the injection site, single cells were found to contain Cy3-NPS (Figure 13). This data proves that ICV administration of Cy3-NPS is capable of targeting the entire murine brain, not only regions close to the ventricular system.

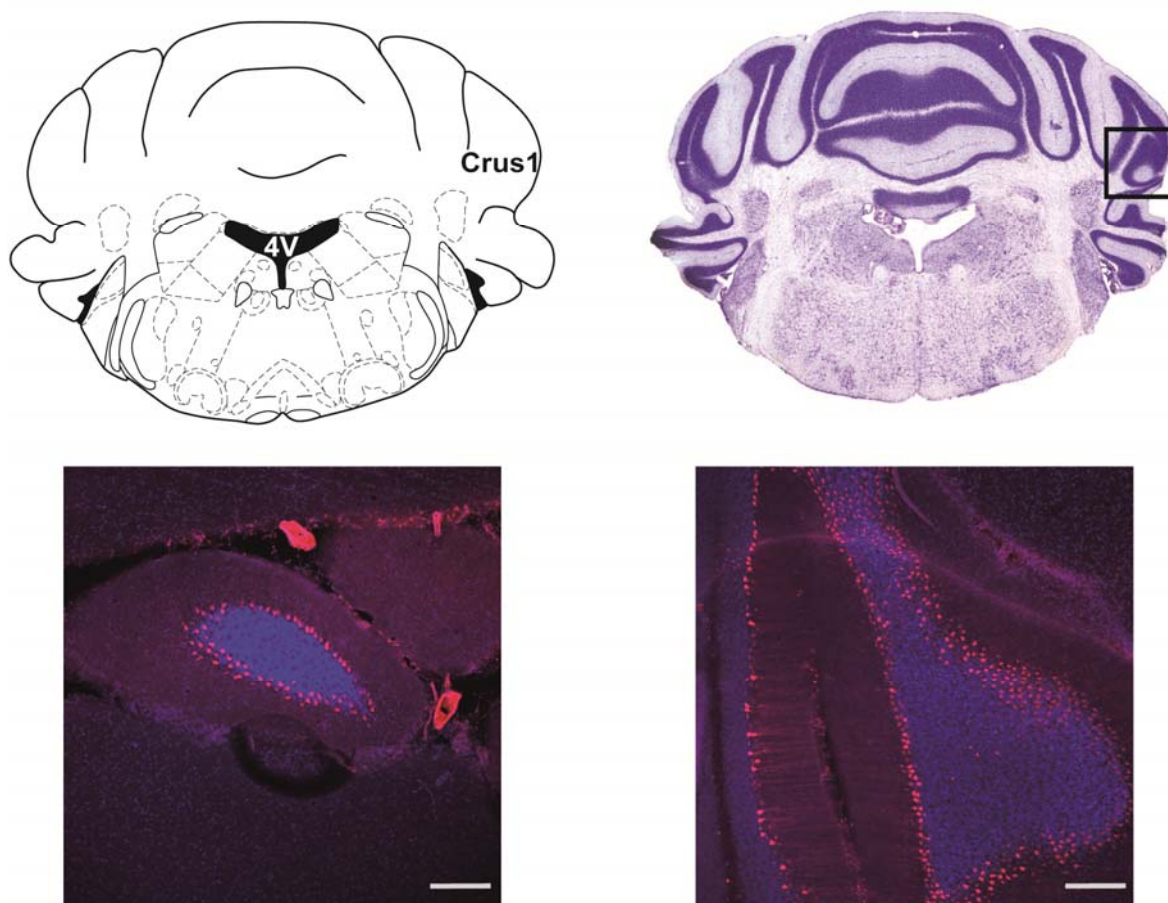


Figure 13. Representative image of Cy3-NPS uptake in neurons of the cerebellum after ICV injection. Upper panel shows schematic overview and Nissl staining of the brain section (Franklin and Paxinos, 2007). Crus1: crus 1 of the ansiform lobule. 4V: fourth ventricle. Images were taken with a confocal microscope at 10x magnification. Scale bars, 100 μ m.

3.2.2. Specificity of Cy3-NPS uptake

In order to ascertain that the observed Cy3-NPS uptake is specific for the unlabeled neuropeptide and dependent upon NPSR expression at the cell membrane, various control experiments were performed.

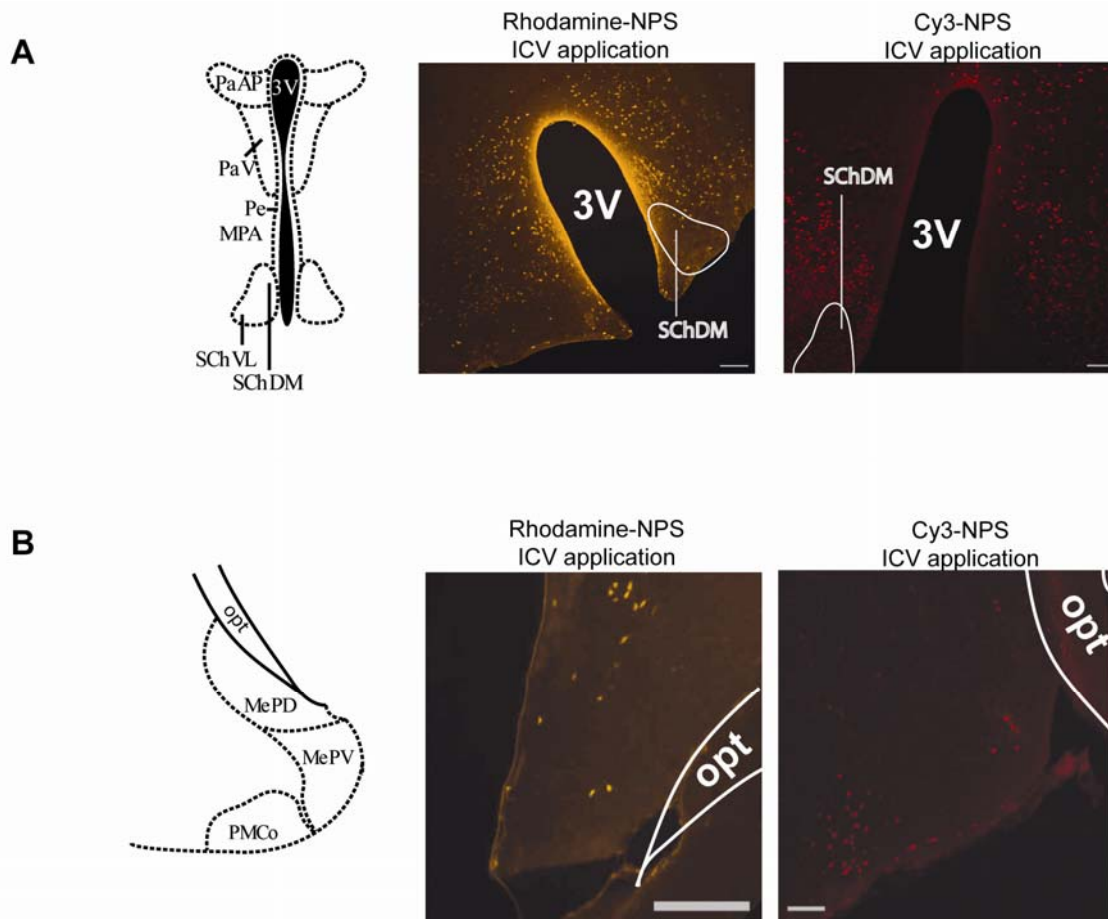


Figure 14. Intracerebral distribution of Cy3-NPS and rhodamine-NPS shown here exemplarily in two brain regions 30 min after ICV delivery of substance (leftmost panels: overview images, Franklin and Paxinos, 2007) (Ionescu et al., 2012). Left panel: rhodamine-NPS (images taken with an epifluorescence microscope, representative for a total of 5 mice). Right panel: Cy3-NPS (images taken with a confocal microscope). **A** Third ventricle (3V). Hypothalamic structures: anterior parvicellular paraventricular hypothalamic nucleus (PaAP), ventral paraventricular hypothalamic nucleus (PaV), dorsolateral and ventromedial suprachiasmatic nucleus (SchDL, SchVM). **B** Optical tract (opt). Amygdaloid structures: medial posteroventral and posterodorsal amygdaloid nuclei (MePV, MePD), posteromedial cortical amygdaloid nucleus (PMCo). Scale bars, 100 μ m.

First, the distribution patterns of two different fluorescent NPS conjugates (Cy3-NPS and rhodamine-NPS) upon ICV injection were examined (Figure 14). Comparison of substance uptake in various brain regions, such as hypothalamic structures (Figure 14A) and amygdaloid nuclei (Figure 14B), revealed identical distribution and internalization patterns for Cy3-NPS and rhodamine-NPS. In addition, the same experiment was performed to compare the distributions of Cy3-NPS and unconjugated rhodamine, respectively (Figure 15). As visible in an example from the olfactory region, Cy3-NPS is specifically internalized into certain cells, while pure

rhodamine distributes evenly in the brain parenchyma, forming aggregates that do not correspond to any cellular structure. These results prove that the uptake observed is dependent only upon NPS and not upon the fluorescent tag, nor upon the combination of NPS and fluorescent tag.

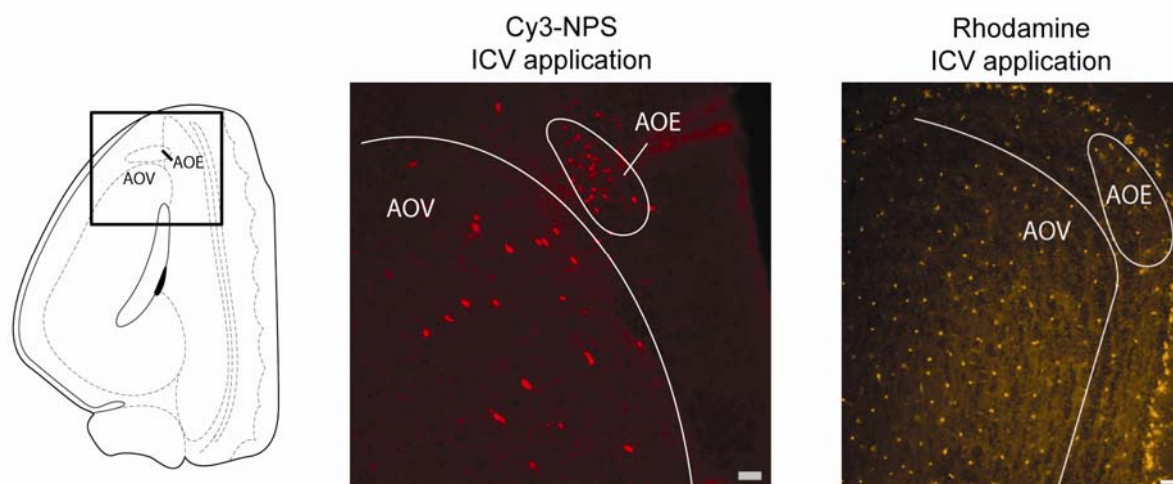


Figure 15. Intracerebral distribution of unconjugated rhodamine shown exemplarily in a region from the olfactory bulb 30 min after ICV administration (Ionescu et al., 2012). Images were taken with an epifluorescence microscope. Image from the same area 30 min after ICV administration of Cy3-NPS (left panel). Image was taken with a confocal microscope. Ventral and external part of the anterior olfactory area (AOV, AOE) (overview image, Franklin and Paxinos, 2007). Scale bars, 20 μ m.

Second, to prove that NPS uptake occurs via interaction with an NPS-specific binding partner expressed at the cell membrane, unlabeled NPS was pre-injected at fivefold concentration of Cy3-NPS 10 min before ICV administration of Cy3-NPS. The assumption was that the unlabeled NPS would saturate the binding partners and therefore inhibit Cy3-NPS uptake 10 min later. Since this approach does not exclude the existence of an additional binding partner besides the already known NPSR, two competitive NPSR-antagonists, the peptidergic antagonist [D-Cys(tBu)5]Neuropeptide S (Camarda et al., 2009) and (R)-SHA68, the active enantiomer of SHA 68 (Okamura et al., 2008; Trapella et al., 2011), were co-injected with Cy3-NPS in a parallel experiment. Uptake and distribution of the fluorescent substance were subsequently examined. As expected, pre-injection of unlabeled NPS as well as co-injection with the competitive NPSR-antagonists strongly reduced Cy3-NPS uptake throughout the brain (Figures 16 and 17). Therefore, it can be

concluded that intracellular Cy3-NPS uptake is dependent upon expression of active NPSR at the cell membrane.

To sum up, these control experiments indicate that by this method, it was possible to identify the hitherto unknown physiological target cells and target brain regions of NPS.

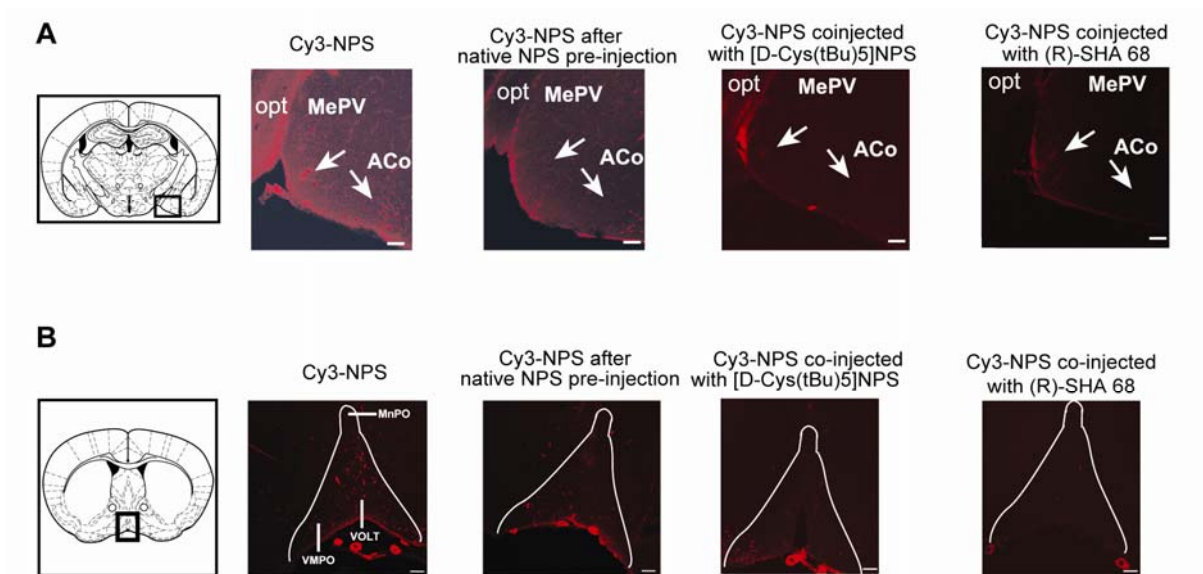


Figure 16. Analysis of NPSR-dependence of Cy3-NPS uptake *in vivo* (adapted from (Ionescu et al., 2012)). From left to right: Coronal sections through mouse brain (overview (Franklin and Paxinos, 2007)) without and after pre-injection of native NPS at 5fold concentration 10 min before ICV administration of Cy3-NPS, and after co-injection with the NPSR antagonists [D-Cys(tBu)5]Neuropeptide S and (R)-SHA68 at 150fold concentration. **A** Posteroventral nucleus of the medial amygdala (MePV), cortical amygdala (ACo). Scale bars, 20 μ m. **B** Exemplary image from the preoptic area comparing uptake of Cy3-NPS. Median preoptic nucleus (MnPO), the vascular organ of the lamina terminalis (VOLT) and the ventromedial preoptic nucleus (VMPO). Optic tract (opt). All images are representative for a total of 4 mice pre-treated with native NPS before ICV administration of Cy3-NPS and a total of 3 mice co-treated with the antagonists. Scale bars, 100 μ m. All images were taken with a confocal microscope.

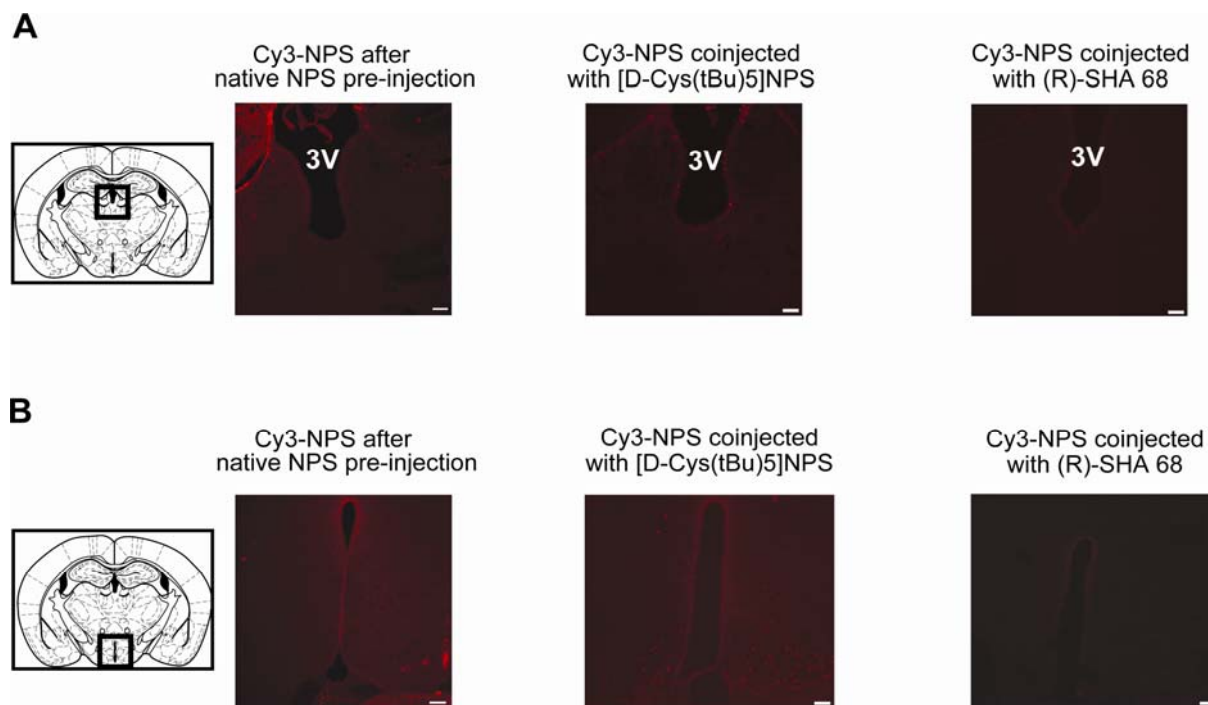


Figure 17. Uptake of Cy3-NPS after pre-injection of native NPS or NPSR antagonists (adapted from (Ionescu et al., 2012)). Leftmost panels show overview images of the respective brain regions (Franklin and Paxinos, 2007). Exemplary images of brain areas from murine brains having received pre-injection of native NPS at 5fold concentration before ICV administration of Cy3-NPS or after coinjection of Cy3-NPS and NPSR antagonists [D-Cys(tBu)5]NPS and (R)-SHA 68 at 150fold concentration. **A** Thalamic structures (compare Figure 12B); and **B** hypothalamic structures (compare Figure 12C). Third ventricle: 3V. All images were taken with a confocal microscope. Scale bars, 100 μ m.

3.2.3. Characterization of cell types taking up Cy3-NPS

As shown above, intracerebral Cy3-NPS administration is not only a valid method to track NPS delivery into the brain at the cellular level, but also led to identification of NPS target brain regions and cells. Therefore, in a next step, these cells were characterized with regard to their subtype.

Cells that had internalized Cy3-NPS appeared, from a morphological point of view, very similar to neurons: they were larger and had fewer processes when compared to either astroglia or microglia. In addition, immunostainings with antibodies against neuronal markers (neurofilament – NF, Figure 18A) as well as against astroglial (GFAP, Figure 18B) and microglial markers (Iba-1, Figure 18C) revealed that the Cy3-NPS signal colocalizes only with the neuronal marker.

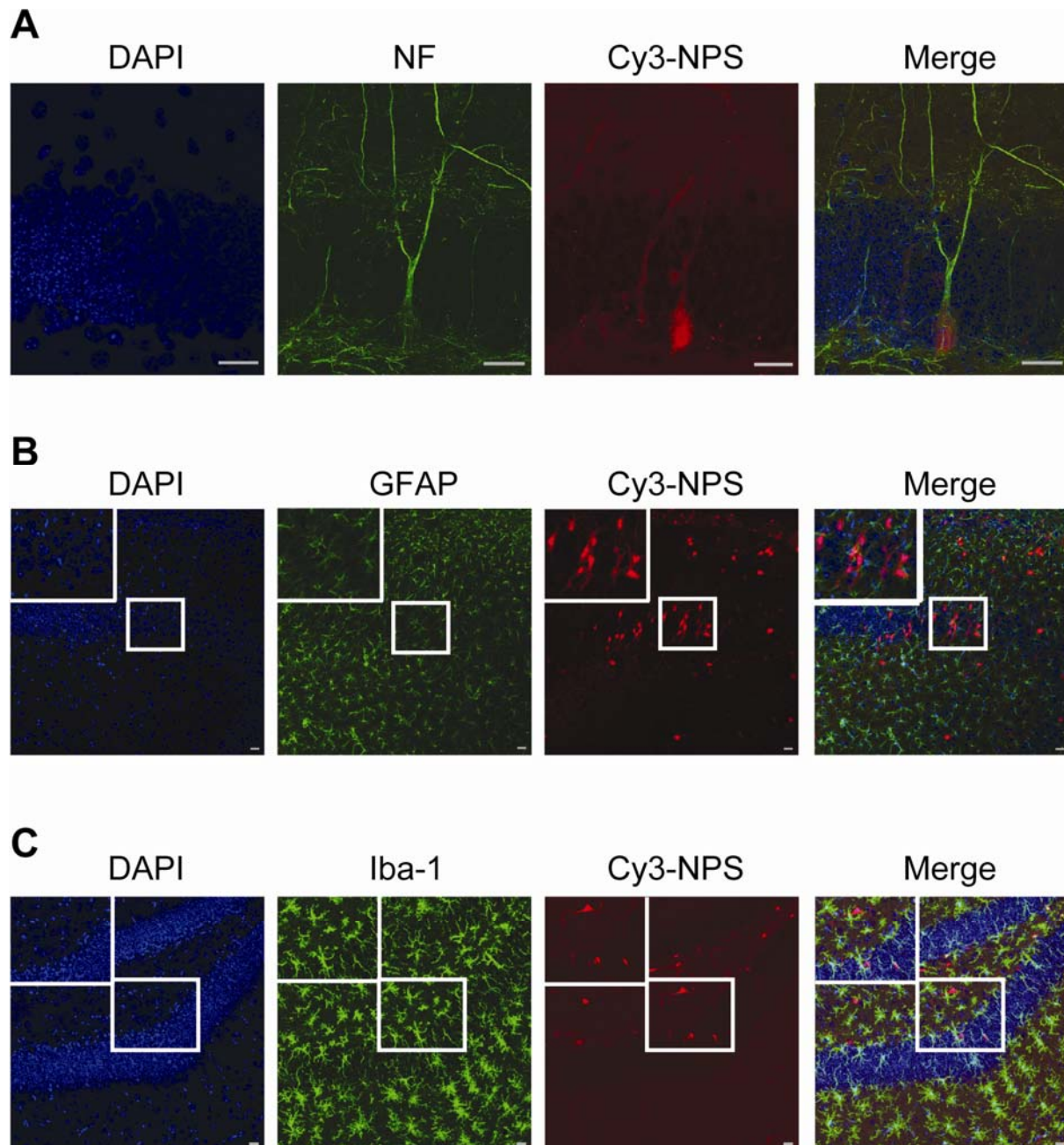


Figure 18. Analysis of cell types targeted by Cy3-NPS (Ionescu et al., 2012). **A** Co-staining with the neuronal marker neurofilament (NF) (green). This representative image was taken from the dentate gyrus. Scale bar, 20 μm . Z-stack of 10 images in 1 μm intervals. **B** Hippocampal CA3 region after co-staining with glial fibrillary acidic protein (GFAP) (green), an astroglial marker. Z-stack of 18 images in 1 μm intervals. Scale bar, 20 μm . **C** Dentate gyrus after co-staining with the microglial marker Iba-1 (green). Z-stack of 19 slices in 1 μm intervals. Scale bar, 20 μm . Cy3-NPS: red; nuclear counterstain DAPI: blue. All images were acquired with a confocal microscope and are representative for a total of 10 mice.

These results strongly suggest that the cells taking up Cy3-NPS in a highly specific NPSR-dependent manner are most likely neurons. Therefore, the assumption is obvious that these target neurons of NPS are also the ones responsible for mediating NPS-elicited behavioral effects.

3.2.4. Intranasal administration of Cy3-NPS

Relying on this data, the next step consisted in applying Cy3-NPS intranasally and examining the distribution pattern in comparison to the one observed after ICV injection of the labeled substance. Intranasal administration of Cy3-NPS led to substance distribution and intracellular uptake following a pattern highly similar to ICV injection. Although the targeted brain regions were largely identical to the ones observed after ICV injection, the intensity of the Cy3-NPS signal in the single cells was significantly lower after intranasal instillation than after injection of Cy3-NPS directly into the cerebral ventricles. A comparison of the targeted brain regions and of the Cy3-NPS signal intensities throughout the entire brain after ICV and intranasal administration can be found in Table 11.

Table 11. Overview of brain regions targeted by Cy3-NPS comparing ICV and intranasal administration as regards intensity and number of cells having taken up Cy3-NPS (adapted from (Ionescu et al., 2012)).

	ICV	IN		ICV	IN
Forebrain			Thalamus		
Accumbens nucleus	++	++	Medial habenula	+++	+++
Anterior olfactory area, ventral part	++	++	Lateral habenula	+++	+++
Anterior olfactory area, external part	++	++	Paraventricular thalamic nucleus	+++	+++
Basal ganglia			Mediodorsal thalamic nucleus	+++	+++
Globus pallidus	+++	-/+	Hypothalamus		
Cerebral cortex			Arcuate nucleus	++	++
Primary motor cortex	+++	-/+	Paraventricular nucleus	++	++
Secondary motor cortex	+++	-/+	Dorsomedial nucleus	++	++
Somatosensory cortex	+++	-/+	Ventromedial nucleus	++	++
Cingulate cortex, area 1	++	-/+	Periventricular nucleus	++	++
Endopiriform cortex	++	-/+	Suprachiasmatic nucleus	++	++
Amygdala			Preoptic area		
Medial amygdaloid nuclei	++	-/+	Median preoptic nucleus	+	+
Anterior cortical amygdaloid nuclei	++	-/+	Ventromedial preoptic nucleus	+	+
Posterior cortical amygdaloid nuclei	++	-/+	Vascular organ of the lamina terminalis	+	+
Basolateral amygdala	+	+	Midbrain and brainstem areas		
Central amygdala	+	-/+	Dorsal raphe	+	+
Lateral amygdala	+	-/+	Posterodorsal tegmental nucleus	+	+
Bed nucleus of the stria terminalis (intraamygdaloid division)	+	+	Periaqueductal gray	+	+
Amygdalohippocampal area	+	+	Central gray of the pons	+	+
Hippocampus			Red nucleus	+	+
Dentate gyrus	+	+	Locus coeruleus	++	+
CA1	+++	+++	Barrington's nucleus	++	+
CA2	+++	+++	Medial parabrachial nucleus	+	+
CA3	+++	+++	Medial vestibular nucleus	+	+
Ventral hippocampus, granular layer of dentate gyrus	+++	+++	Cerebellum		
			Purkinje cells	+++	+

The Cy3-NPS uptake pattern in single cells largely corresponded to the one observed in cell culture upon stimulation with Cy3-NPS, especially with regard to the

vesicular internalization pattern (Figure 19A). Furthermore, the Cy3-NPS signal colocalized as expected exclusively with the neurofilament signal, showing that intranasal NPS application also targets only neurons (Figure 19B). Control experiments with intranasal rhodamine application showed a different distribution pattern than intranasally applied Cy3-NPS, confirming the specificity of the uptake after intranasal application (Figure 19C).

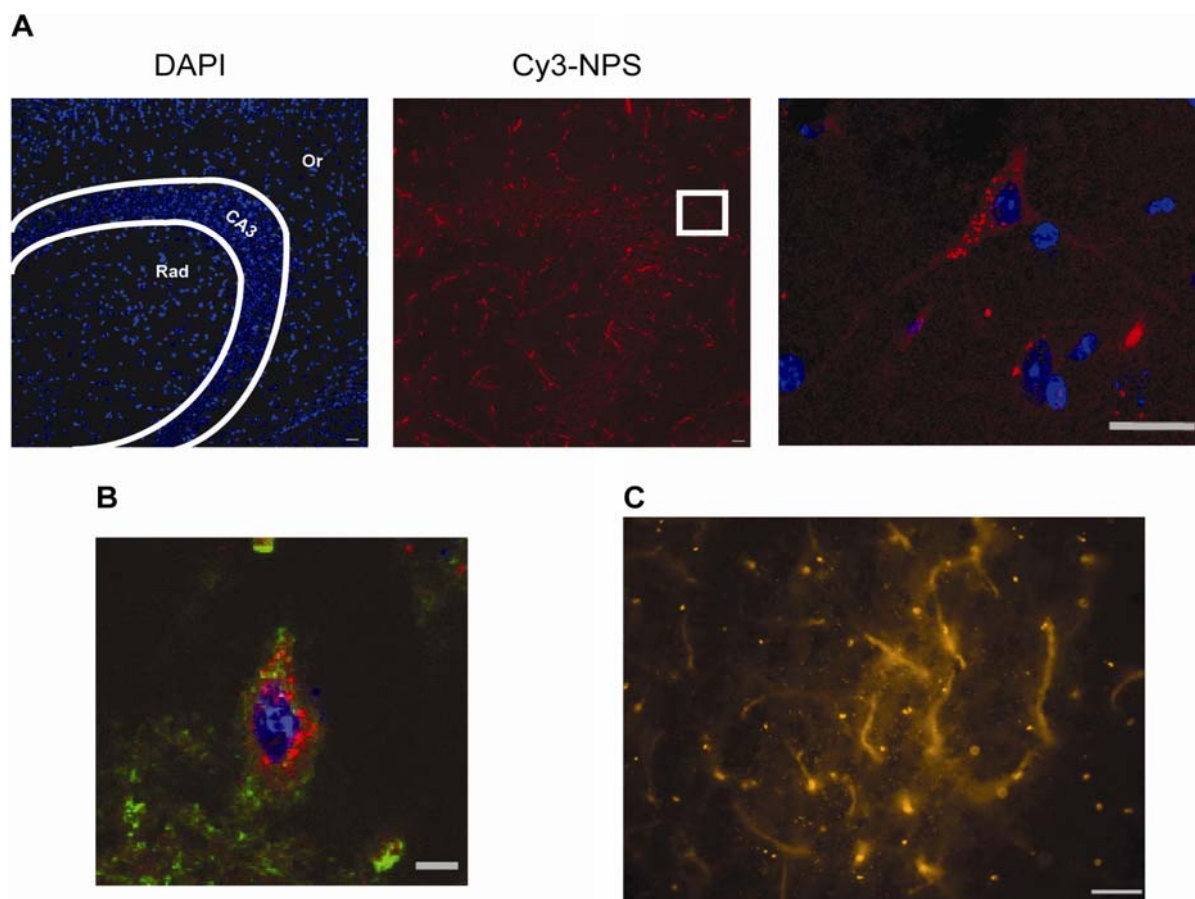


Figure 19. Intracerebral distribution of Cy3-NPS after intranasal administration. Intraneuronal uptake of Cy3-NPS (red) 30 minutes after intranasal delivery shown exemplarily in the hippocampus. Nuclear staining: DAPI (blue). **A** Overview of the hippocampus after intranasal Cy3-NPS application. Rad: radiate layer of the hippocampus; Or: oriens layer of the hippocampus. White inset: Hippocampal neuron from the oriens layer (CA3 region), Z-stack of 10 images in 1 μm intervals. **B** Hippocampal neuron from the pyramidal layer (CA3 region) after NF staining (green). All images were taken with a confocal microscope and are representative for a total of 3 mice. **C** Intracerebral distribution of unconjugated rhodamine shown exemplarily in a region from the olfactory bulb 30 min after intranasal administration. Image taken with an epifluorescence microscope. Scale bars, 20 μm .

In conclusion, intranasal application of Cy3-NPS demonstrates that NPS can reach the brain following this administration method and is internalized specifically into its target neurons in brain regions identified previously by ICV administration.

3.2.5. Identification of the hippocampus as a novel target brain region of NPS

The findings from this study also shed light on the brain regions involved in the anxiolytic effects of NPS. Cy3-NPS uptake was detected in the dorsal endopiriform cortex, as well as in the basal ganglia and in amygdaloid nuclei, most important among which is the basolateral amygdala, a brain region closely linked to anxiety regulation and associated with NPS effects in mice (Jüngling et al., 2008; Meis et al., 2008; Fendt et al., 2010) (Figure 20).

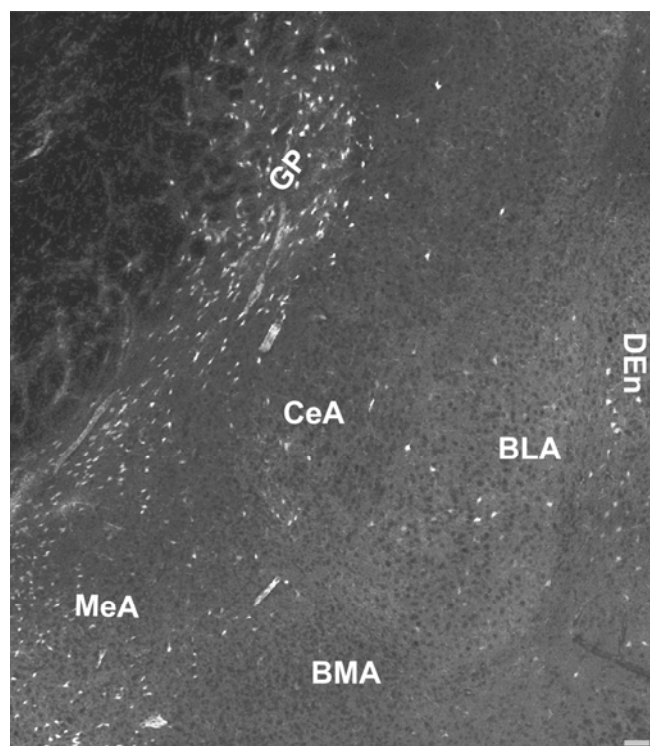


Figure 20. Amygdaloid structures targeted by Cy3-NPS (bright white): central amygdala (CeA), medial amygdala (MeA), basolateral amygdala (BLA), basomedial amygdala (BMA). Cortical structures: dorsal endopiriform cortex (DEn). Basal ganglia: globus pallidus (GP). Image taken with a confocal microscope. Scale bar, 200 μ m. Adapted from (Ionescu et al., 2012).

Most fascinating however was the identification of the hippocampus as a novel target brain region of NPS. Both ICV and intranasal administration of Cy3-NPS led to uptake of the labeled substance in the CA1, CA2 and CA3 regions as well as in the dentate gyrus (Tables 10 and 11, Figure 19A and Figure 21A). Cy3-NPS was

internalized with high specificity into the cell bodies and throughout the processes of certain neuronal populations of the hippocampus (Figure 21B, C). This new finding immediately raises questions concerning the mechanistic role of the hippocampus in the NPS-dependent regulation of fear and anxiety.

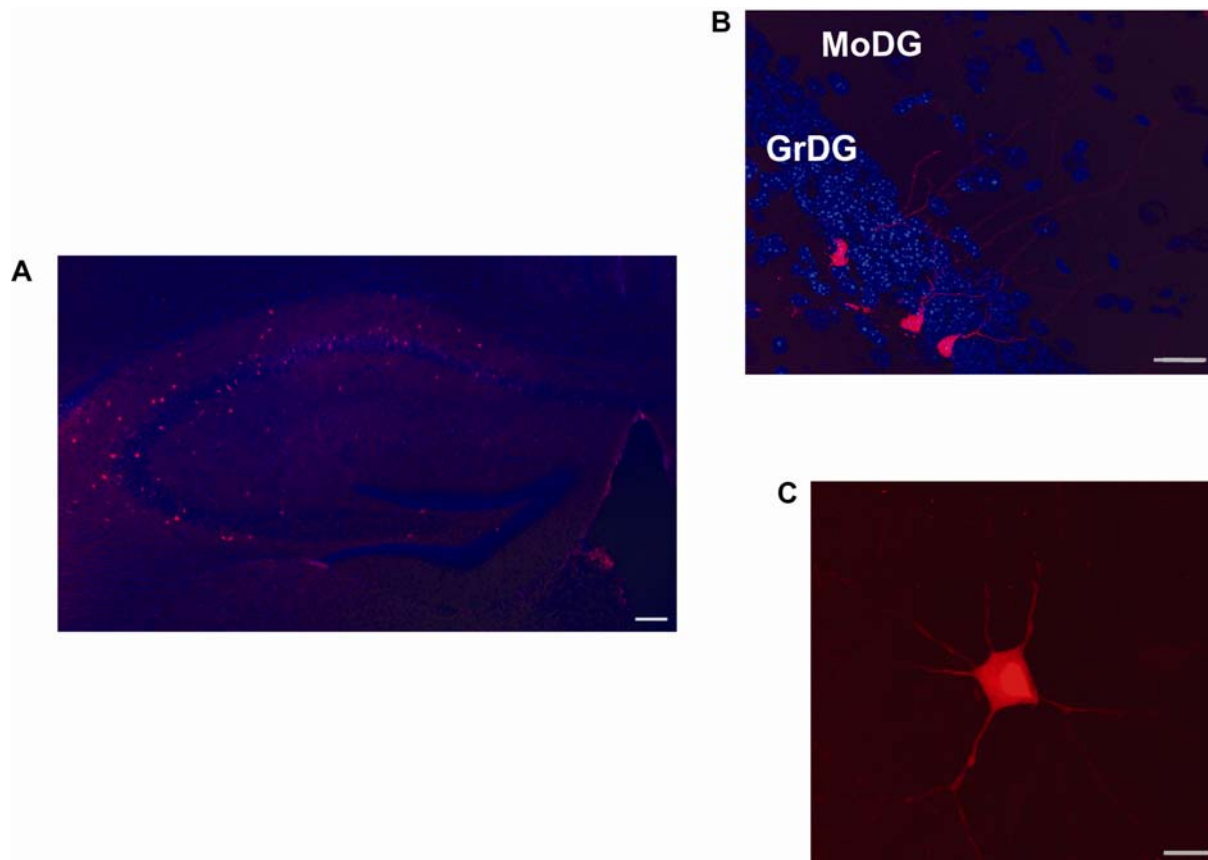


Figure 21. The hippocampus as a novel target region of NPS. **A** Representative overview image of the hippocampus after ICV injection of Cy3-NPS. Scale bar, 100 μm . **B** Morphologically representative cells from the granular dentate gyrus. Granular dentate gyrus (GrDG), molecular dentate gyrus (MoDG). Scale bar, 20 μm . Z-stack of 15 images in 0.59 μm intervals. **C** Morphologically representative cell from the CA3 region. Scale bar, 20 μm . Z-stack of 13 images in 0.59 μm intervals. All images were taken with a confocal microscope.

3.3. Behavioral and molecular effects of intranasally applied NPS

After having ascertained that intranasally applied NPS reaches and distributes through the mouse brain, the next step was to reproduce the anxiolytic effects seen after ICV administration. An additional aspect under investigation was the regulatory effect of NPS on protein and mRNA expression levels of selected candidates.

3.3.1. Behavioral phenotype after intranasal NPS application

Since the pharmacodynamics of intranasal application are known to be very different from those of ICV injection (Thorne et al., 1995; Thorne and Frey, 2001), the optimal dosis for observing behavioral effects would most likely differ. In order to establish the optimal NPS dose for eliciting behavioral effects after intranasal treatment, three different NPS doses (7, 14 and 28 nmol) were applied intranasally in C57BL/6N mice and their effects were compared in three different behavioral tests: open field, dark-light test and elevated plus maze (EPM). In view of these differences between ICV and intranasal administration, animals were tested at 4 hrs after intranasal application rather than at 30 min, as for ICV treatment (see Figure 22 for an overview of the experimental schedule). The time-point for behavioral testing after intranasal treatment was chosen according to data from literature which show that effective concentrations of intranasally applied substances can be detected in the CNS up to 4 hrs after application (Thorne et al., 1995; Jansson and Björk, 2002).

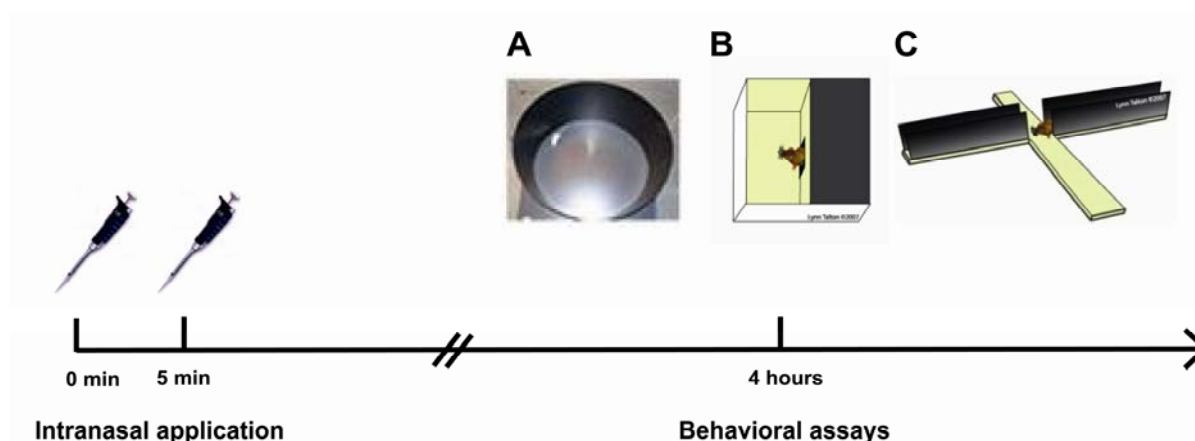


Figure 22. Experimental timeline: intranasal NPS application at 0 and at 5 min in alert C57BL/6N and HAB mice restrained manually. Behavioral testing 4 hours after first application: **A** open field, **B** dark-light box, and **C** EPM.

The open field, performed first to obtain a baseline of locomotion, showed no differences in locomotion for any of the three doses between controls and treated mice ($F_{2, 26} = 1.364$; $p = 0.2733$) (Figure 23A). However, in the dark-light test, a trend towards decreased latency to the first entry into the light compartment (a parameter for measuring anxiety) was observed for animals treated with 14 and 28 nmol NPS ($F_{2, 24} = 3.382$; $p = 0.0508$) (Figure 23B). This was especially meaningful since the locomotion as measured in percent distance traveled in the light chamber did not

change ($F_{2, 24} = 0.2080$; $p = 0.8136$), hinting at locomotion-independent anxiolytic effects. Most important, clear-cut anxiolytic effects were observed in the EPM, where animals treated with 14 nmol NPS significantly increased their percent time spent on the open arm ($F_{2, 24} = 4.127$; $p = 0.0288$) (Figure 23C). Here again, the observed anxiolytic effects were locomotion-independent, as the number of entries into the closed arm (a reliable indicator of locomotion in the EPM) did not differ between groups ($F_{2, 24} = 0.5957$; $p = 0.5591$).

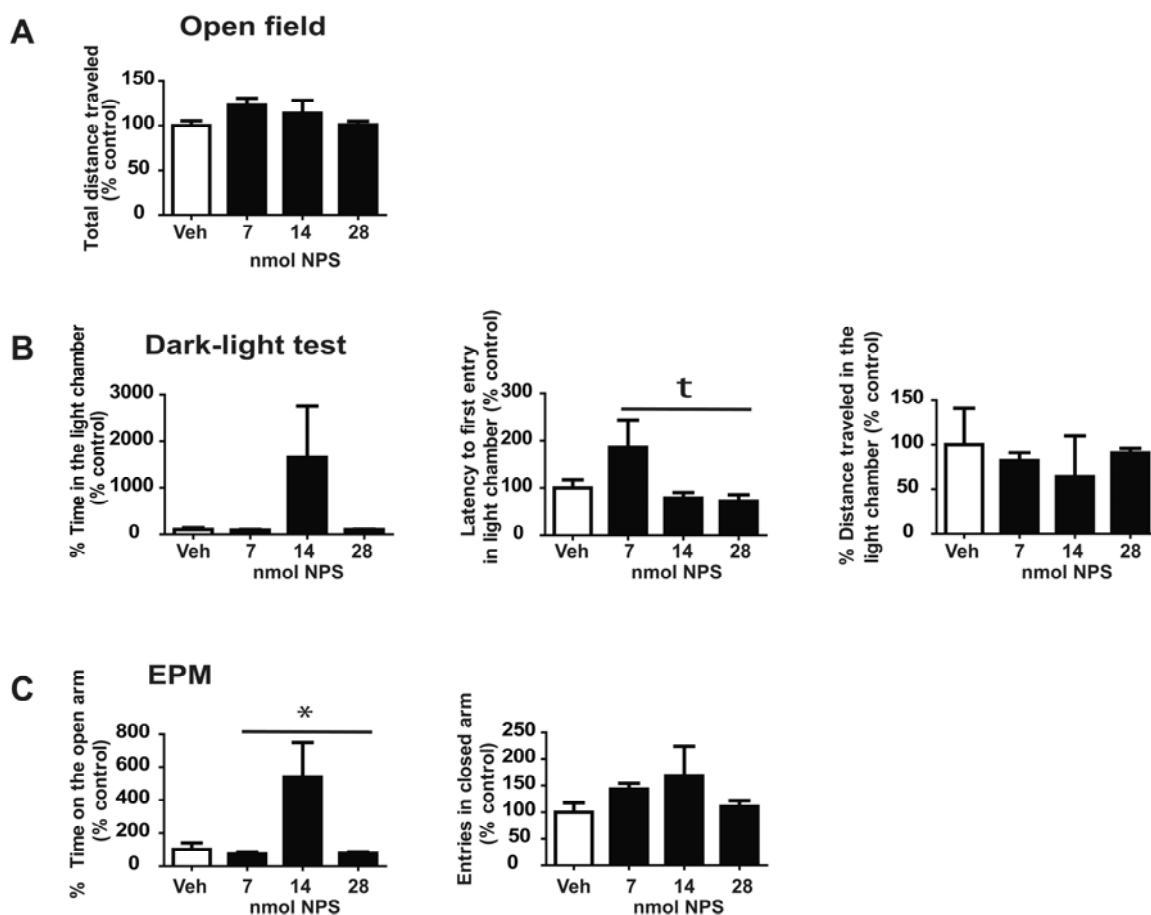


Figure 23. Behavioral effects of transnasally delivered NPS in C57BL/6N mice. C57BL/6N mice were tested 4 hrs after intranasal NPS treatment (7 nmol, 14 nmol and 28 nmol) in **A** open field, **B** dark-light test (% time in the light chamber: $F_{2, 24} = 1.666$; $p = 0.2102$) and **C** EPM. $n = 10$. Statistical analysis: one-way ANOVA with Bonferroni's *post hoc* test. The data is shown as % change relative to control. t $p < 0.1$; * $p < 0.05$. All data are shown as mean \pm s.e.m.

These results showed 14 nmol NPS to be the optimal dose for intranasal application with the goal of eliciting anxiolytic effects in mice. These anxiolytic effects were locomotion-independent and became most evident when animals were tested 4 hours after application.

3.3.2. Regulatory effects of NPS on protein and mRNA expression of proteins involved in the glutamatergic system and synaptic plasticity

Until now, there was no data in literature examining the regulatory effects of NPS on cerebral protein and mRNA expression *in vivo*. Therefore, candidates representing likely targets for NPS-mediated regulation were selected relying on publications that link NPS to the glutamatergic system (Han et al., 2009) and to synaptic function (Jüngling et al., 2008; Raiteri et al., 2009). These candidates included subunits 1 and 2 of the α -amino-3-hydroxy-5-methyl-4-isoxazolepropionic acid (AMPA) receptor (GluR1 and GluR2) and the astrocytic glutamate transporter (Glt-1), as well as isoforms I and II of synapsin. The expression of these candidates was examined on both mRNA and protein levels after intranasal NPS treatment (for a complete overview of the experimental schedule please see Figure 24). These investigations were performed after treatment with 14 nmol NPS in brain regions that have been associated with anxiety regulation, such as the hippocampus (moreover newly identified in this work as a target brain region of NPS) and the prefrontal cortex. Furthermore, analyses were performed at two different time-points. mRNA expression levels were investigated 4 hours after treatment, since regulation of mRNA expression is usually a fast process. Protein expression levels were examined both 4 hours after treatment (the time-point where behavioral effects are most pronounced) and 24 hours after treatment, since usually, the cellular protein synthesis machinery is too slow to produce detectable changes in protein expression levels within 4 hours.

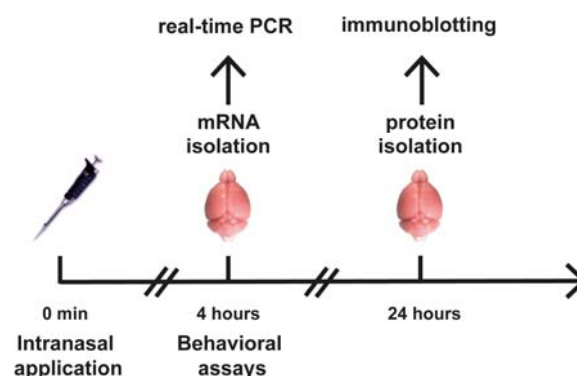


Figure 24. Overview of the experimental schedule for isolation of brain regions at 4 hours after treatment for mRNA isolation (subsequently analyzed by real-time PCR) and at 24 hours after treatment for protein isolation (subsequently analyzed by immunoblotting).

In mRNA expression, there was a trend towards decrease of Glt-1 expression in the hippocampus of NPS-treated mice as compared to controls ($t = 1.865$, $df = 8$, $p = 0.0992$) (Figure 25A), accompanied by an increase in the prefrontal cortex ($t = 4.562$, $df = 7$, $p = 0.0026$) (Figure 25B).

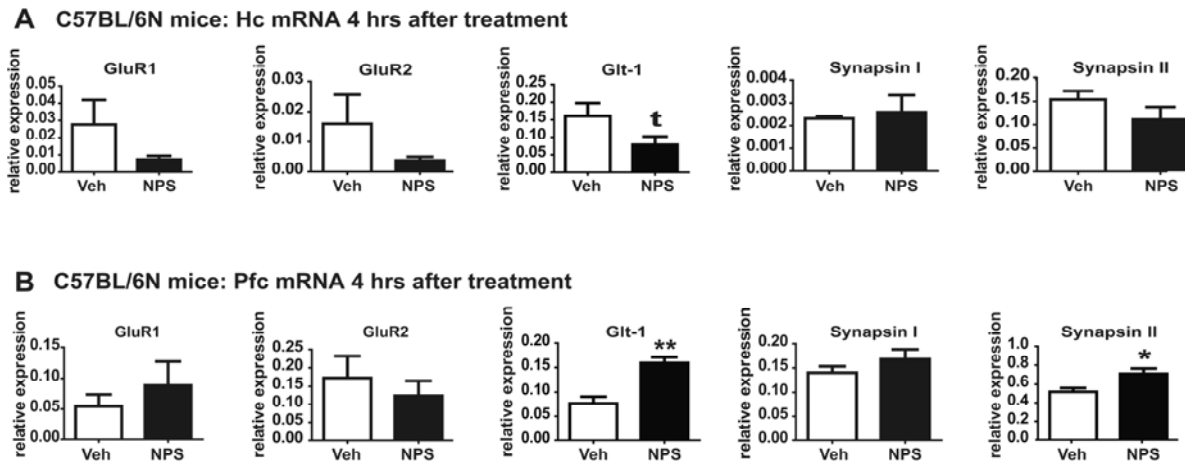


Figure 25. Effects of transnasally delivered NPS (14 nmol) 4 hours after application on mRNA levels in hippocampus (Hc) and prefrontal cortex (Pfc) of C57BL/6N mice. **A** Real-time PCR analysis of Hc lysate from C57BL/6N mice 4 hours after intranasal NPS treatment. GluR1: $t = 1.236$, $df = 7$, $p = 0.2562$; GluR2: $t = 1.242$, $df = 8$, $p = 0.2493$; Synapsin I: $t = 0.3580$, $df = 4$, $p = 0.7385$; Synapsin II: $t = 1.243$, $df = 7$, $p = 0.2540$. **B** Real-time PCR analysis of Pfc lysate from C57BL/6N mice 4 hours after intranasal NPS treatment. GluR1: $t = 0.7166$, $df = 5$, $p = 0.5057$; GluR2: $t = 0.6839$, $df = 8$, $p = 0.5133$; Synapsin I: $t = 1.063$, $df = 7$, $p = 0.3230$. Internal expression control: GAPDH. C57BL/6N: $n = 5$ for each group. Statistical analysis: two-tailed unpaired t-test. t $p < 0.1$; * $p < 0.05$; ** $p < 0.01$. All data are shown as mean \pm s.e.m.

As expected, there were no changes in protein levels at 4 hours after treatment in either the hippocampus or the prefrontal cortex (Figure 26).

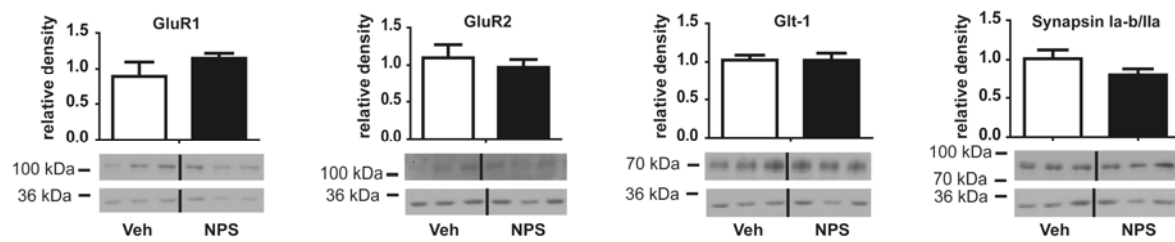
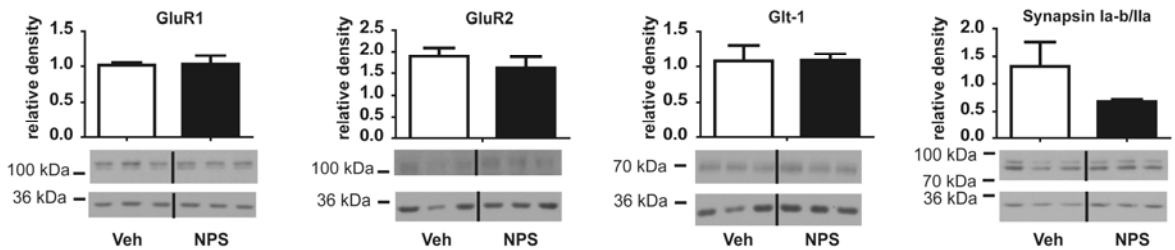
A C57BL/6N mice: Hc protein 4 hrs after treatment**B** C57BL/6N mice: Pfc protein 4 hrs after treatment

Figure 26. Effects of transnasally delivered NPS (14 nmol) 4 hours after application on protein levels in hippocampus (Hc) and prefrontal cortex (Pfc) of C57BL/6N mice. **A** Immunoblot analysis of Hc lysate from C57BL/6N mice 4 hours after intranasal NPS treatment. GluR1: $t = 1.192$, $df = 8$, $p = 0.2675$; GluR2: $t = 0.657$, $df = 8$, $p = 0.5552$; Glt-1: $t = 0.02711$, $df = 8$, $p = 0.9790$; Synapsin Ia-b/IIa: $t = 1.506$, $df = 6$, $p = 0.1828$. **B** Immunoblot analysis of Pfc lysate from C57BL/6N mice 4 hours after intranasal NPS treatment. GluR1: $t = 0.1030$, $df = 8$, $p = 0.9205$; GluR2: $t = 0.8469$, $df = 8$, $p = 0.4217$; Glt-1: $t = 0.03901$, $df = 8$, $p = 0.9698$; Synapsin Ia-b/IIa: $t = 1.384$, $df = 6$, $p = 0.2038$. Internal expression control: GAPDH (35 kDa in immunoblot excerpts). Blot excerpts show three representative adjacent bands of each group. The immunoblot data represent cumulated data from at least three independent experiments. C57BL/6N: $n = 5$ for each group. Statistical analysis: two-tailed unpaired t-test. All data are shown as mean \pm s.e.m.

24 hours after treatment, synapsin Ia-b/IIa protein expression significantly increased in the hippocampus ($t = 2.561$, $df = 8$, $p = 0.0336$) (Figure 27A). Additionally, in the prefrontal cortex, NPS treatment significantly increased protein expression of GluR1 ($t = 3.219$, $df = 8$, $p = 0.0123$) and Glt-1 ($t = 2.561$, $df = 8$, $p = 0.0336$) (Figure 27B).

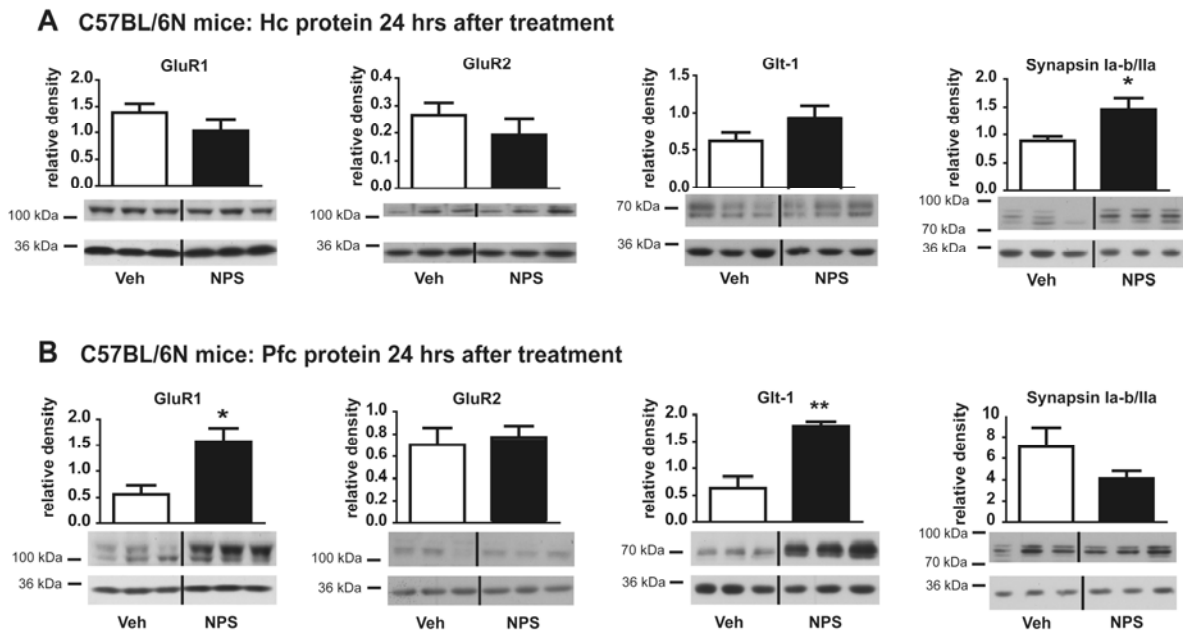


Figure 27. Effects of transnasally delivered NPS (14 nmol) 24 hours after application on protein levels in hippocampus (Hc) and prefrontal cortex (Pfc) of C57BL/6N mice. **A** Immunoblot analysis of Pfc lysate from C57BL/6N mice 24 hours after intranasal NPS treatment. GluR2: $t = 0.2798$, $df = 8$, $p = 0.7868$; Synapsin Ia-b/IIa: $t = 1.549$, $df = 6$, $p = 0.1601$. **B** Immunoblot analysis of Hc lysate from C57BL/6N mice 24 hours after intranasal NPS treatment. GluR1: $t = 1.271$, $df = 8$, $p = 0.2396$; GluR2: $t = 0.9666$, $df = 8$, $p = 0.3621$; Glit-1: $t = 1.628$, $df = 8$, $p = 0.1421$. Internal expression control: GAPDH (35 kDa in immunoblot excerpts). Blot excerpts show three representative adjacent bands of each group. The immunoblot data represent cumulated data from at least three independent experiments. C57BL/6N: $n = 5$ for each group. Statistical analysis: two-tailed unpaired t-test. * $p < 0.05$; ** $p < 0.01$. All data are shown as mean \pm s.e.m.

To sum up, behavioral effects of NPS treatment were accompanied by changes in mRNA expression levels; long-term NPS-elicited changes were found in protein expression levels. These findings demonstrate the ability of NPS to regulate expression of proteins associated with the glutamatergic circuit and with synaptic plasticity in brain regions involved in anxiety such as the hippocampus and the prefrontal cortex. These regulatory effects are dependent on the examined candidate, the brain region and the time-point after treatment and occur differentially on protein and mRNA levels.

3.4. The role of the ventral hippocampus in NPS-elicited anxiolytic effects

As described previously in this work, the hippocampus was identified as a novel NPS target region by ICV and intranasal administration of Cy3-NPS (see Figures 19 and 21). Additionally, electrophysiological recordings have confirmed that NPS affects

basal synaptic transmission and plasticity at CA3-CA1 synapses (Ionescu et al., 2012). Therefore, the next step consisted in characterizing the role of the hippocampus in mediating the anxiolytic effects of NPS at the behavioral level by local injection of NPS into the ventral CA1 region, a method widely used hitherto for characterization of the amygdala in NPS-elicited behavior (Jüngling et al., 2008; Fendt et al., 2010).

3.4.1. Cy3-NPS distribution is restricted to the ventral CA1 region (vCA1) after local injection

In order to ascertain that NPS, after injection into vCA1, will not spread to other brain regions and thereby result in hippocampus-independent effects, Cy3-NPS was injected into vCA1 and its distribution was subsequently analyzed. Already a small amount of Cy3-NPS (0.01 nmol) resulted in intracellular uptake close to the injection site (Figure 28).

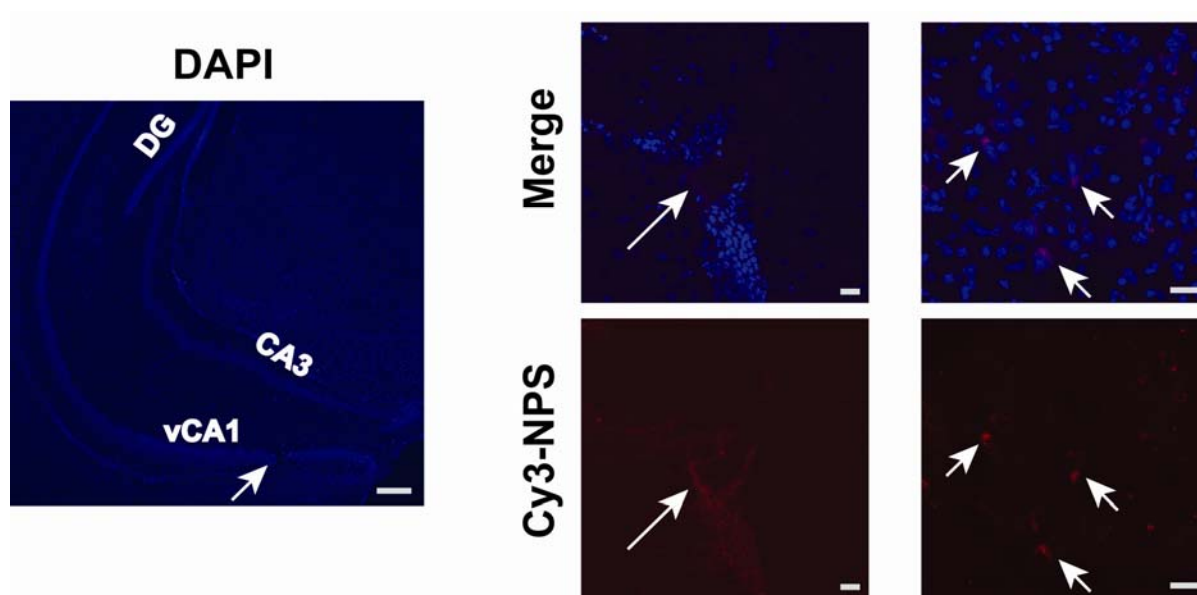


Figure 28. Cy3-NPS (0.01 nmol) is locally confined to the injection site after injection into vCA1. Injection site on sagittal brain section (4x magnification), followed by 20x magnification. Nuclear staining: DAPI (blue). Cy3-NPS: red. Long arrows indicate injection site. Short arrows indicate cells having taken up Cy3-NPS. All images were taken with a confocal microscope. DG: dentate gyrus; vCA1: ventral CA1 region; CA3 region. Scale bars 4x: 200 μm ; scale bars 20x: 40 μm .

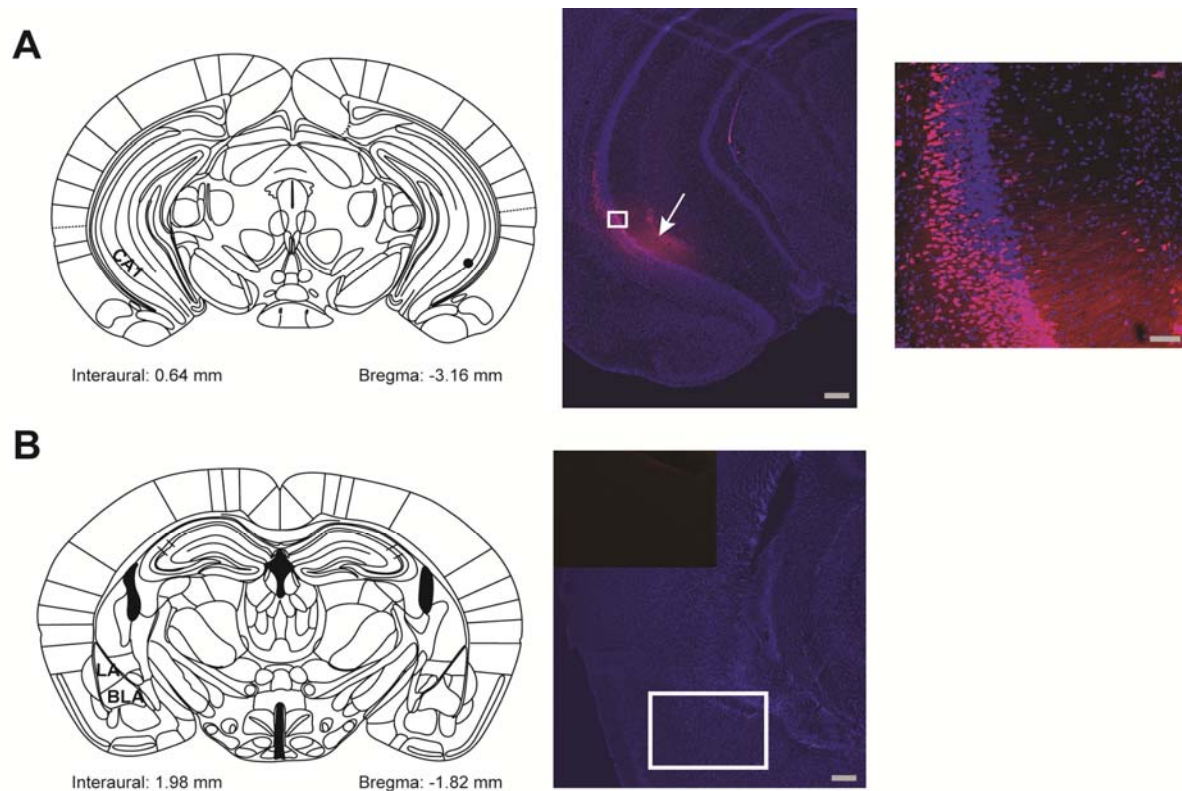


Figure 29. Cy3-NPS (0.07 nmol) is locally confined to the injection site after injection into vCA1. **A** Leftmost: Injection site on anatomical plate (Franklin and Paxinos, 2007). Middle and right: Overlay of DAPI (nuclear staining, blue) and Cy3 (red) signals at 4x (left) and 20x (right) magnification. Arrow indicates injections site on brain section. **B** Left: Anatomical plate showing lateral amygdala (LA) and basolateral amygdala (BLA) (Franklin and Paxinos, 2007), and (right) overview of amygdala in brain section after injection of vCA1 at 4x magnification (overlay: DAPI and Cy3 channels; inset: Cy3 channel). All images were taken with a confocal microscope. Scale bars 4x: 200 μ m; scale bars 20x: 20 μ m.

3.4.2. NPS injection into vCA1 leads to anxiolytic locomotion-independent effects

Having proved that NPS does not spread outside the injection site, the next question was whether injection of NPS into vCA1 is sufficient to produce similar anxiolytic effects as the already published intra-amygdala (Jüngling et al., 2008) and ICV injection (Xu et al., 2004; Jüngling et al., 2008; Leonard et al., 2008; Rizzi et al., 2008). Since locomotory changes may influence anxiety-related read-out in behavioral assays, basal locomotion was examined in the open field and anxiety- and locomotion-related parameters in the dark-light test and in the EPM, which have been shown to highlight different aspects of anxiety-related behavior (Gonzalez et al., 1996; van Gaalen and Steckler, 2000; Bailey et al., 2007) (for a complete overview of

the experimental schedule please see Figure 30). Injection sites into vCA1 are shown in Figure 31A.

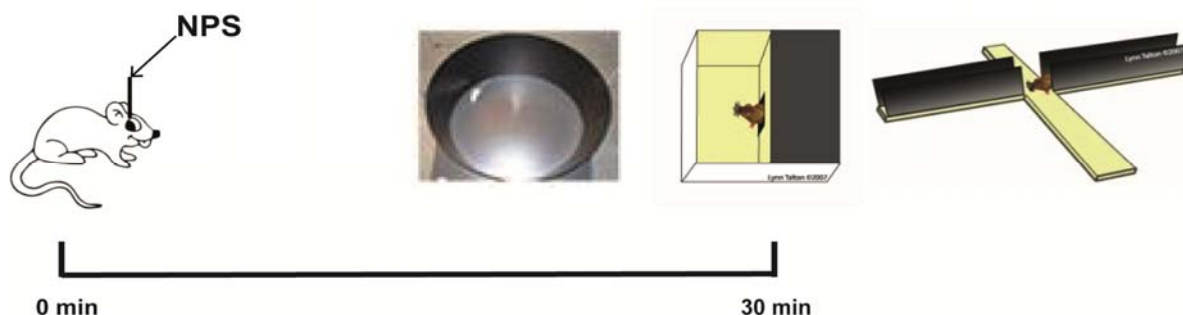


Figure 30. Overview of experimental timeline of NPS injection into vCA1. Injection was performed at 0 min, and 30 min later, mice underwent the behavioral assays open field, dark-light box and EPM in this sequence.

Intrahippocampal NPS treatment did not affect locomotion in any of the three tests (Figure 22B-D). Most important, however, NPS elicited anxiolytic effects in the EPM, as shown by a significant increase in the percent time spent on the open arm ($t = 2.227$, $df = 14$, $p = 0.0429$) (Figure 31D). These anxiolytic effects were locomotion-independent, since the total number of entries in the closed arm remained unchanged ($t = 0.2035$, $df = 14$, $p = 0.8416$) (Figure 31D). These test-specific effects coincide well with our previous findings that intranasally applied NPS elicits the strongest anxiolytic effects in the EPM (Ionescu et al., 2012).

Taken together, these results not only confirm our previous report of NPS target neurons in the hippocampus (Ionescu et al., 2012), but also show that intrahippocampal injection of NPS is sufficient to produce anxiolytic behavioral effects.

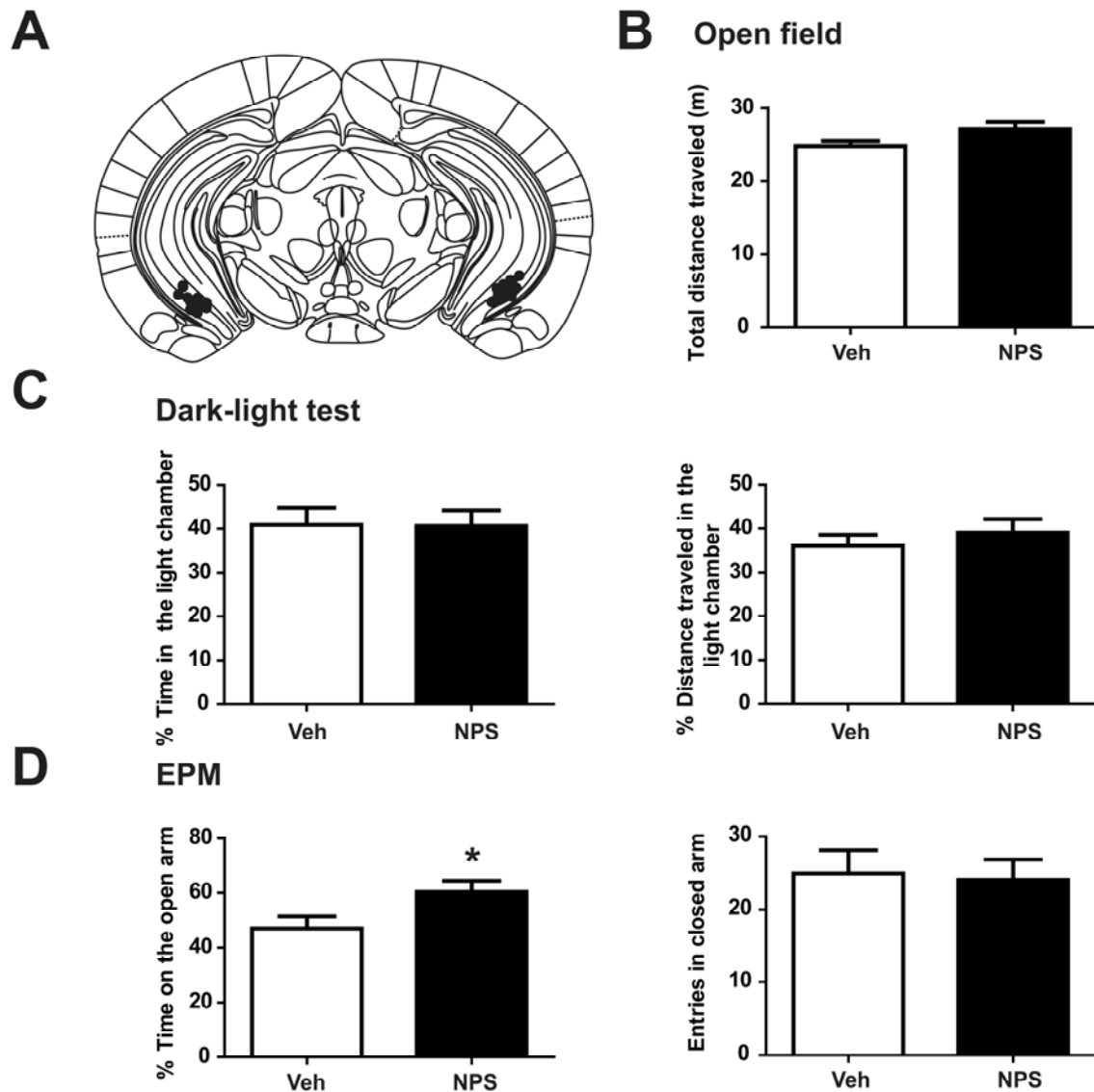


Figure 31. NPS injection into the ventral CA1 region (vCA1) produces anxiolytic, locomotion-independent effects in the EPM. **A** Overview of injection sites on anatomical plate (Franklin and Paxinos, 2007). **B** Basal locomotion in open field test ($t = 1.928$, $df = 14$, $p = 0.0744$). **C** Anxiety- and locomotion-related parameters in the dark-light test (% time in light chamber: $t = 0.04641$, $df = 14$, $p = 0.9636$; % distance in light chamber: $t = 0.7346$, $df = 14$, $p = 0.4747$). **D** Anxiety- and locomotion-related parameters in the EPM. Data are shown \pm s.e.m. Statistical analysis: two-tailed unpaired t-test. * $p < 0.05$.

3.5. Acute intranasal NPS treatment in high anxiety behavior (HAB) mice, a mouse model for pathological anxiety

Intranasal NPS treatment was shown here to elicit anxiolytic effects in C57BL/6N mice. The next step was to examine the therapeutic effects of NPS in a mouse model of pathological anxiety. The HAB mice that have been inbred for over 40 generations

for pathologically high trait anxiety (Landgraf et al., 2007) (see 1.6.1.) were selected for this purpose. NPS was applied intranasally at 14 nmol/animal, the dose that was found to have optimal anxiolytic effects in the EPM in C57BL/6N mice (see 3.3.1.). The mice were then exposed to the same behavioral testing paradigm as used for C57BL/6N mice (open field, dark-light test and EPM) 4 hours after application (see Figure 22).

3.5.1. Behavioral phenotype after intranasal NPS application

In the open field, NPS had no effects on basal locomotion ($t = 0.8610$, $df = 19$, $p = 0.2000$) (Figure 32A). In the dark-light test, however, the percent time spent in the light chamber was significantly increased ($t = 2.316$, $df = 18$, $p = 0.0163$) and moreover, there was also a trend towards decreased latency to the first entry in the light chamber, as observed in C57BL/6N mice ($t = 1.451$, $df = 18$, $p = 0.0820$) (Figure 32B). These results were locomotion-independent, as the percent distance traveled in the light chamber remained unchanged between NPS-treated and control animals ($t = 0.8146$, $df = 18$, $p = 0.2130$). NPS treatment did not induce any changes in the EPM, either in the percent time spent on the open arm ($t = 0.6839$, $df = 18$, $p = 0.2514$) or in the number of entries into the closed arm ($t = 0.07032$, $df = 18$, $p = 0.4724$) (Figure 32C).

In conclusion, NPS treatment can induce anxiolytic effects even in the case of pathologically high anxiety, an aspect which had hitherto not been investigated. This is evidenced in the case of the HAB mice by locomotion-independent reduction of anxiety in the dark-light test.

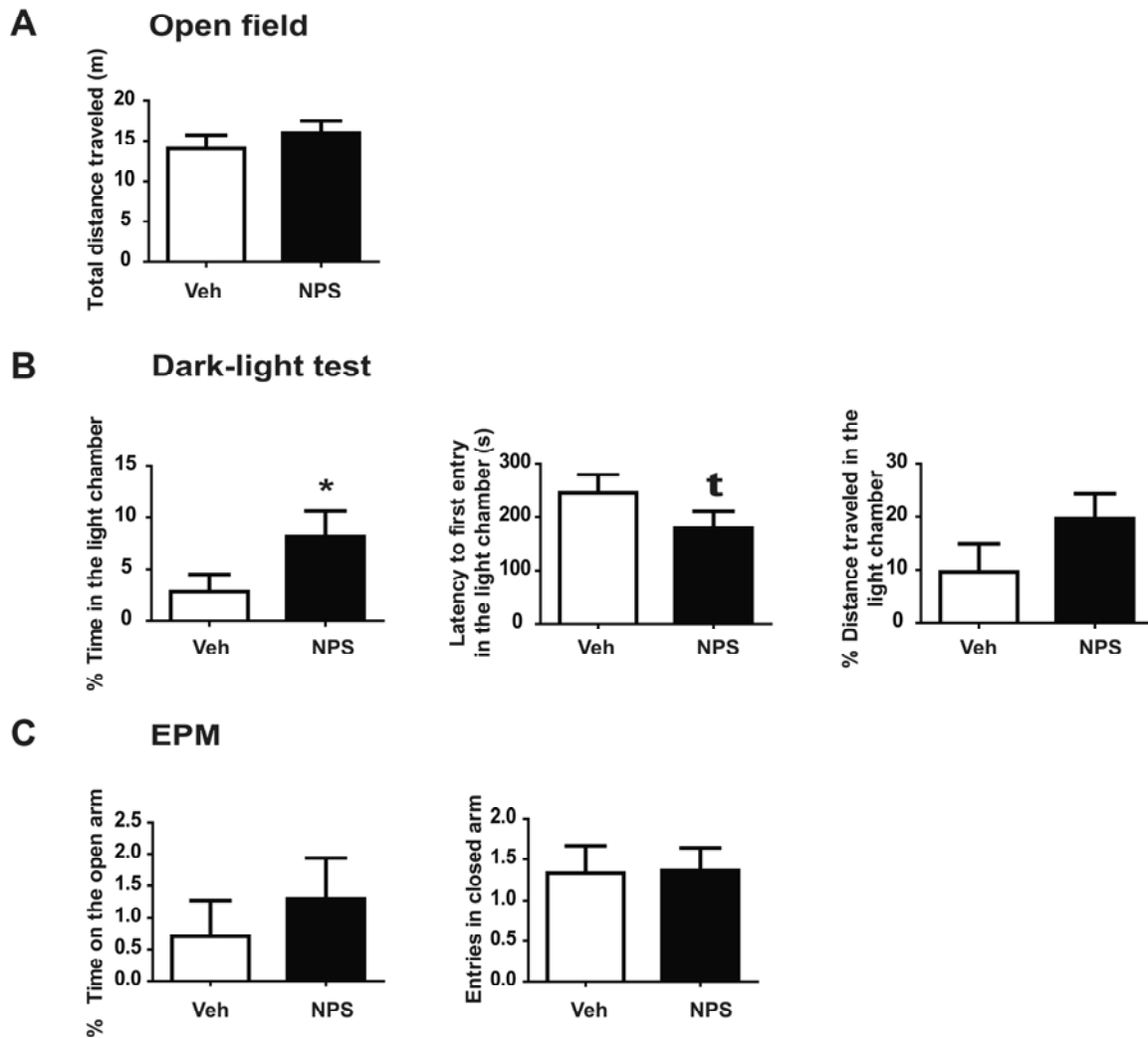


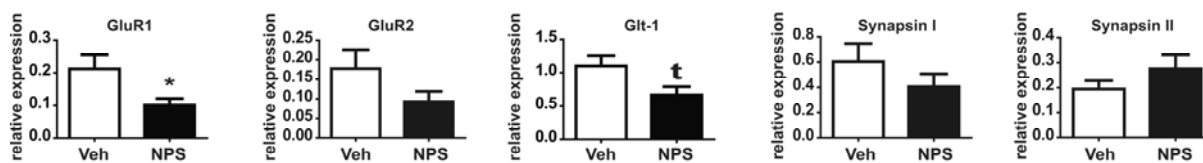
Figure 32. Behavioral effects of transnasally delivered NPS in HAB mice. HAB mice were tested 4 hours after intranasal NPS treatment (14 nmol) in **A** open field, **B** dark-light test and **C** EPM. $n = 10$. Statistical analysis: one-sided unpaired t-test. t $p < 0.1$; * $p < 0.05$. All data are shown as mean \pm s.e.m.

3.5.2. Regulatory effects of NPS on protein and mRNA expression of proteins involved in the glutamatergic system and synaptic plasticity

Since it has been established previously in this work that NPS has regulatory effects on protein expression in C57BL/6N mice, it was interesting to examine this aspect in the HAB mice as well. For this purpose, the same candidates that had been examined in C57BL/6N mice (GluR1, GluR2, Glt-1 and synapsin isoforms I and II) were now investigated at the mRNA level 4 hours after treatment and at the protein level 24 hours after treatment in hippocampus and prefrontal cortex.

4 hours after treatment, NPS treatment led to significantly decreased mRNA expression of GluR1 ($t = 2.361$, $df = 8$, $p = 0.0459$) as well as to a trend towards decreased mRNA expression of Glt-1 ($t = 2.198$, $df = 8$, $p = 0.0591$) in the hippocampus (Figure 33A). The last finding corresponds to the observations in the hippocampus of NPS-treated C57BL/6N mice. In the prefrontal cortex, NPS had no effects on mRNA expression of the examined candidates (Figure 33B).

A HAB mice: Hc mRNA 4 hrs after treatment



B HAB mice: Pfc mRNA 4 hrs after treatment

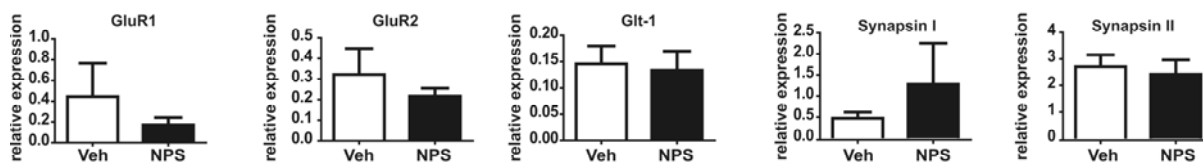


Figure 33. Effects of transnasally delivered NPS (14 nmol) 4 hours after application on mRNA levels in hippocampus (Hc) and prefrontal cortex (Pfc) of HAB mice. **A** Real-time PCR analysis of Hc lysate from HAB mice 4 hours after intranasal NPS treatment. GluR2: $t = 1.540$, $df = 8$, $p = 0.1620$; Synapsin I: $t = 1.123$, $df = 8$, $p = 0.2940$; Synapsin II: $t = 1.339$, $df = 5$, $p = 0.2383$. **B** Real-time PCR analysis of Pfc lysate from HAB mice 4 hours after intranasal NPS treatment. GluR1: $t = 0.7371$, $df = 7$, $p = 0.4850$; GluR2: $t = 0.7957$, $df = 8$, $p = 0.4492$; Glt-1: $t = 0.2440$, $df = 7$, $p = 0.8143$; Synapsin I: $t = 0.8174$, $df = 8$, $p = 0.4373$; Synapsin II: $t = 0.4126$, $df = 8$, $p = 0.6907$. HAB: $n = 5$ for each group. Statistical analysis: two-tailed unpaired t-test. $t < 0.1$; * $p < 0.05$. All data are shown as mean \pm s.e.m.

24 hours after treatment, there were no differences in protein expression levels of the examined candidates in the hippocampus (Figure 34A). However, in the prefrontal cortex, NPS-treated HAB mice displayed a trend towards increased protein expression of GluR1 ($t = 2.228$, $df = 10$, $p = 0.0500$), as well as significantly increased GluR2 protein expression ($t = 2.832$, $df = 10$, $p = 0.0178$) (Figure 34B).

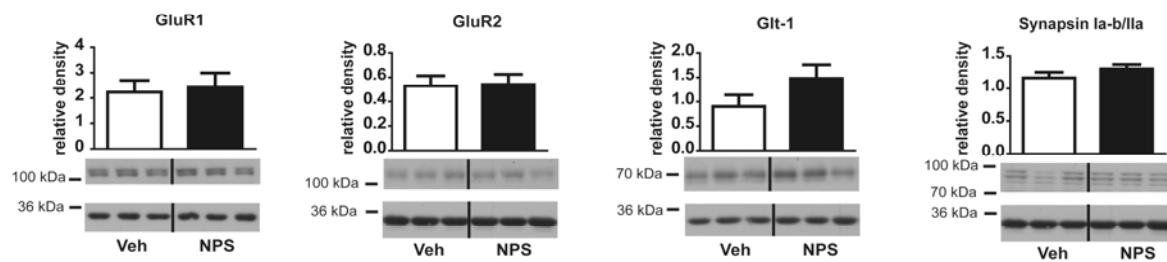
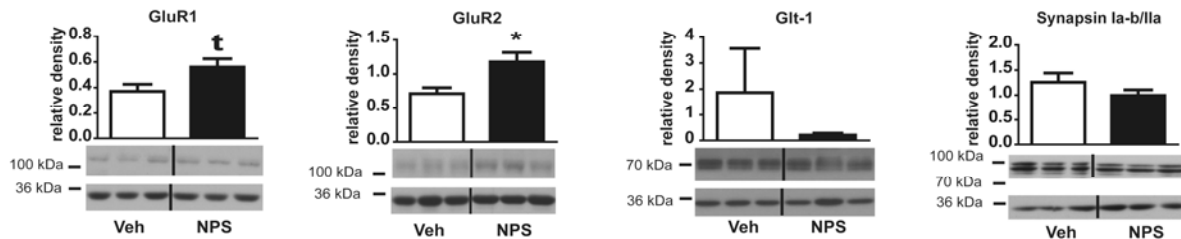
A HAB mice: Hc protein 24 hrs after treatment**B** HAB mice: Pfc protein 24 hrs after treatment

Figure 34. Effects of transnasally delivered NPS (14 nmol) 24 hours after application on protein levels in hippocampus (Hc) and prefrontal cortex (Pfc) of HAB mice. **A** Immunoblot analysis of Hc lysate from HAB mice 24 hours after intranasal NPS treatment. GluR1: $t = 0.2502$, $df = 9$, $p = 0.8081$; GluR2: $t = 0.1124$, $df = 10$, $p = 0.9127$; Glit-1: $t = 1.582$, $df = 10$, $p = 0.1447$; Synapsin Ia-b/IIa: $t = 1.197$, $df = 9$, $p = 0.2619$. **B** Immunoblot analysis of Pfc lysate from HAB mice 24 hours after intranasal NPS treatment. Glit-1: $t = 0.8817$, $df = 9$, $p = 0.4009$; Synapsin Ia-b/IIa: $t = 0.9739$, $df = 10$, $p = 0.3531$. Internal expression control: GAPDH (35 kDa in immunoblot excerpts). Blot excerpts show three representative adjacent bands of each group. The immunoblot data represent cumulated data from at least three independent experiments. HAB: $n = 5$ for each group. Statistical analysis: two-tailed unpaired t-test. $t p < 0.1$; * $p < 0.05$. All data are shown as mean \pm s.e.m.

In conclusion, NPS exerts regulatory effects on mRNA and protein expression of candidates involved in the glutamatergic circuit also in a mouse model of pathological anxiety. These regulatory effects of intranasally applied NPS in HAB mice overlap in part with those observed in C57BL/6N mice, i.e. in the case of Glit-1 mRNA expression in the hippocampus and GluR1 protein expression in the prefrontal cortex.

3.6. Acute intranasal NPS treatment in a mouse model of PTSD

In order to test whether NPS treatment can improve PTSD-related symptoms, shocked mice were treated intranasally with either NPS or vehicle daily on three consecutive days starting at day 28 post-shock, a time-point at which a full-blown PTSD-like pathology has been described in this mouse model (Siegmund and

Wotjak, 2007). Behavioral and molecular analyses were then performed to examine the influence of NPS on the phenotype of these mice.

3.6.1. Behavioral results

The behavioral phenotype of the mice was evaluated in three tests performed on three consecutive days (for an overview of the experimental schedule see Figure 35).

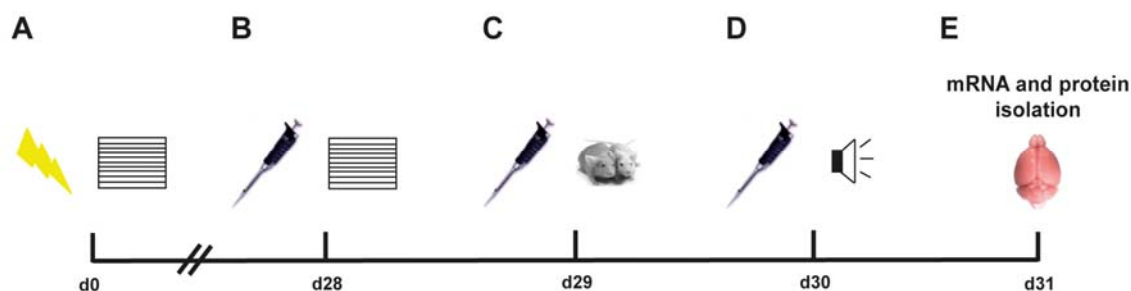


Figure 35. Overview of the experimental timeline in intranasal NPS application in a mouse model of PTSD. **A** At day 0 (d0), mice received the electric shock. **B** At day 28 (d28), mice were treated intranasally with either vehicle or NPS and 2 hours later tested for conditioned fear in the shock context. **C** At day 29 (d29), mice were treated with either vehicle or NPS and 2 hours later tested for social interaction. **D** At day 30 (d30), mice were treated with either vehicle or NPS and 2 hours later tested for their acoustic startle response. **E** At day 31 (d31), mice were sacrificed for brain removal, from which protein and mRNA were subsequently isolated.

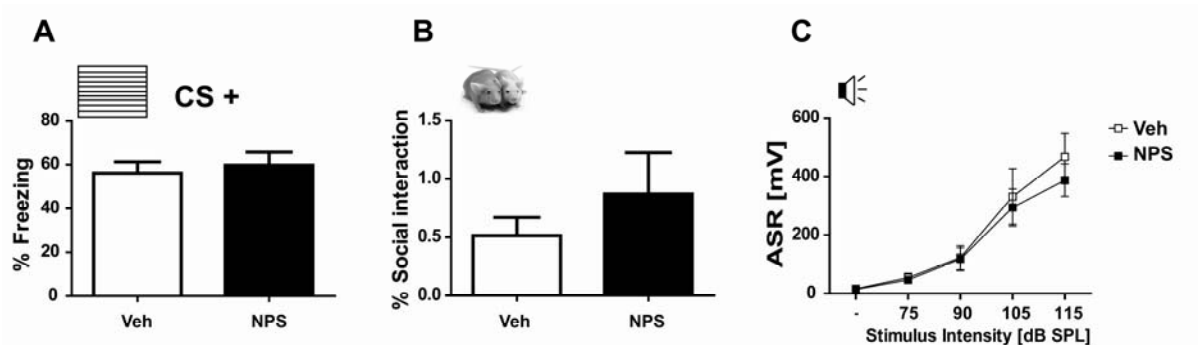


Figure 36. Behavioral effects of NPS treatment in the mouse model of PTSD. **A** Response to reexposure to conditioning context (CS +) measured in % freezing. **B** Measure of social interaction. **C** Intensity of acoustic startle response (ASR) to a tone of increasing sound level. The data represents mean peak startle amplitude in response to 30 stimuli of each intensity value.

The parameters measured were: percent freezing in the shock context (CS +), percent social interaction and intensity of acoustic startle response (ASR) depending

on noise intensity. No differences were observed in these parameters between NPS-treated and vehicle-treated shocked mice (Figure 36).

3.6.2. Analyses of mRNA and protein expression in hippocampus and prefrontal cortex in the PTSD mouse model

The molecular effects of NPS treatment were examined in this mouse model in addition to the behavioral read-out of NPS-treated shocked mice, in order to fully characterize the potential therapeutic effects of this substance. Therefore, in addition to behavioral testing, changes in mRNA and protein levels of selected candidates that had been found to be regulated by NPS treatment in non-shocked C57BL/6N and HAB mice (see 3.3.2. and 3.5.2.) were examined in the hippocampus and prefrontal cortex, two brain regions that have been described as affected in PTSD (Shin et al., 2004, 2006; Golub et al., 2011). Again, these candidates were GluR1, GluR2, Glt-1, and synapsin (isoforms I and II).

In the hippocampus of shocked mice, NPS treatment led to increased synapsin I ($t = 2.408$, $df = 7$, $p = 0.0469$) and II ($t = 2.525$, $df = 8$, $p = 0.0355$) mRNA levels, as well as to an upward trend in synapsin Ia-b/IIa protein expression ($t = 2.140$, $df = 7$, $p = 0.0696$) compared to vehicle-treated controls 24 hours after the last application (Figure 37D).

In addition, a trend towards increased expression of GluR1 ($t = 2.049$, $df = 8$, $p = 0.0746$) and GluR2 ($t = 2.016$, $df = 7$, $p = 0.0836$) mRNA was observed (Figure 37A). On the protein level, these changes did not materialize in the case of GluR1, whereas GluR2 protein expression decreased significantly ($t = 4.341$, $df = 7$, $p = 0.034$) (Figure 37B). On the other hand, Glt-1 mRNA and protein expression remained unaffected (Figure 37C).

In the prefrontal cortex, NPS treatment resulted in an upward trend in GluR2 mRNA expression ($t = 2.2028$, $df = 8$, $p = 0.0770$), while GluR2 protein expression remained unchanged ($t = 1.591$, $df = 8$, $p = 0.1504$) (Figure 38A). There were no other changes in mRNA or protein expression of any of the observed candidates (Figure 38B, C and D).

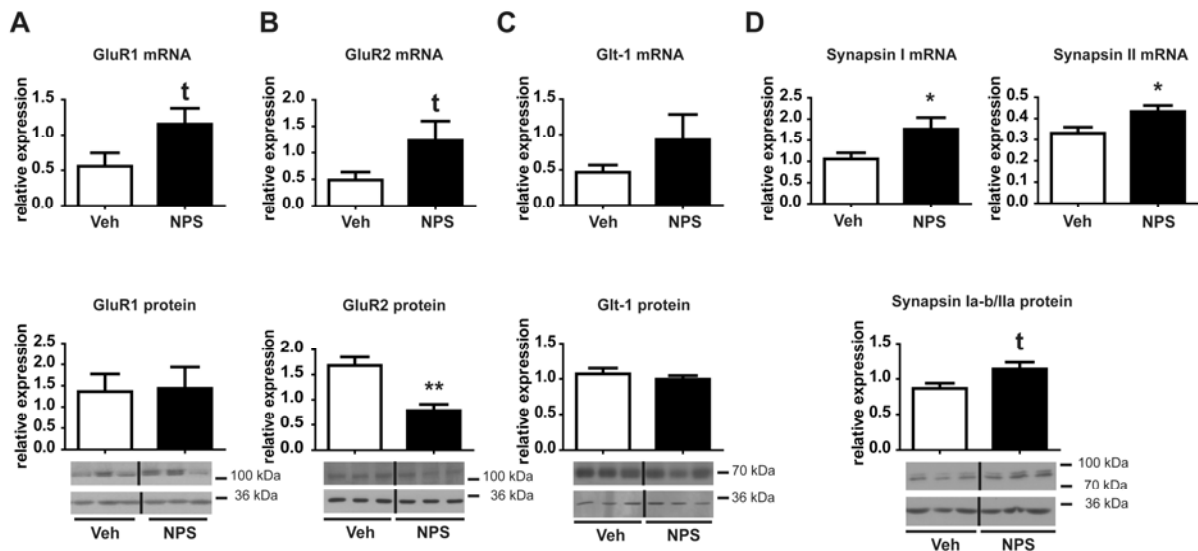


Figure 37. Effects of NPS treatment in the hippocampus on mRNA and protein expression of proteins involved in the glutamatergic circuit and in synaptic plasticity in shocked mice. **A** GluR1 mRNA and protein ($t = 0.2528$, $df = 8$, $p = 0.8068$) expression. **B** GluR2 mRNA and protein expression. **C** Glit-1 mRNA ($t = 1.219$, $df = 8$, $p = 0.2575$) and protein ($t = 0.7859$, $df = 8$, $p = 0.4546$) expression. **D** Synapsin I and II mRNA and synapsin Ia-b/IIa protein expression. Internal expression control: GAPDH (35 kDa in immunoblot excerpts). Blot excerpts show three representative adjacent bands of each group. The immunoblot data represent cumulated data from at least three independent experiments. $n = 5$. Statistical analysis: two-tailed unpaired t-test. t $p < 0.1$; * $p < 0.05$. All data are shown as mean \pm s.e.m.

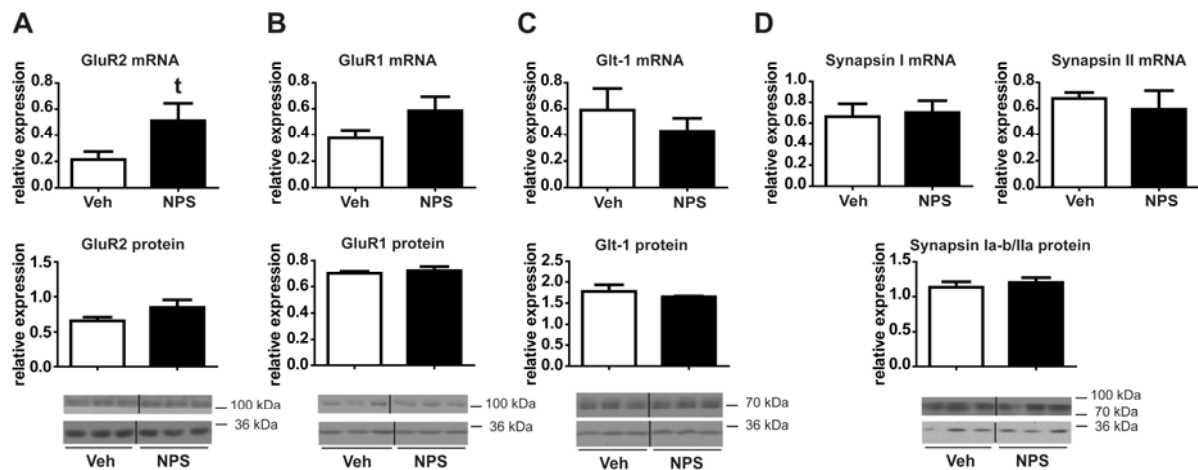


Figure 38. Effects of NPS treatment in the prefrontal cortex on mRNA and protein expression of proteins involved in the glutamatergic circuit and in synaptic plasticity in shocked mice. **A** GluR2 mRNA and protein ($t = 1.591$, $df = 8$, $p = 0.1504$) expression. **B** GluR1 mRNA ($t = 1.719$, $df = 8$, $p = 0.1239$) and protein ($t = 1.591$, $df = 8$, $p = 0.5467$) expression. **C** Glit-1 mRNA ($t = 0.8482$, $df = 8$, $p = 0.4210$) and protein ($t = 0.7889$, $df = 8$, $p = 0.4529$) expression. **D** Synapsin I and II mRNA expression ($t = 0.2337$, $df = 7$, $p = 0.8219$) and synapsin Ia-b/IIa protein expression ($t = 0.6485$, $df = 8$, $p = 0.5348$). Internal expression control: GAPDH (35 kDa in immunoblot excerpts). Blot excerpts show three representative adjacent bands of each group. The immunoblot data represent cumulated data from at least three independent experiments. $n = 5$. Statistical analysis: two-tailed unpaired t-test. t $p < 0.1$. All data are shown as mean \pm s.e.m.

3.6.3. Corticosterone plasma levels

Given that NPS has been shown to influence the HPA axis (Smith et al., 2006), which is known to be affected in PTSD (Ehlert et al., 2001; Shea et al., 2005; de Kloet et al., 2006), corticosterone levels were investigated by corticosterone ELISA in plasma samples of shocked mice. Acute NPS treatment at day 28 after shock led to a trend towards increased plasma corticosterone levels compared to vehicle treatment ($t = 1.802$, $df = 14$, $p = 0.0932$) (Figure 39B).

In conclusion, NPS treatment in the PTSD mouse model did not affect the behavioral phenotype. At the molecular level on the other hand, NPS regulated expression levels of examined candidates both on mRNA and on protein level and, most importantly, led to an increase in synapsin levels that had also been observed in non-shocked C57BL/6N mice (see 3.3.2.). Moreover, NPS increased circulating corticosterone plasma levels up to 24 hours after treatment.

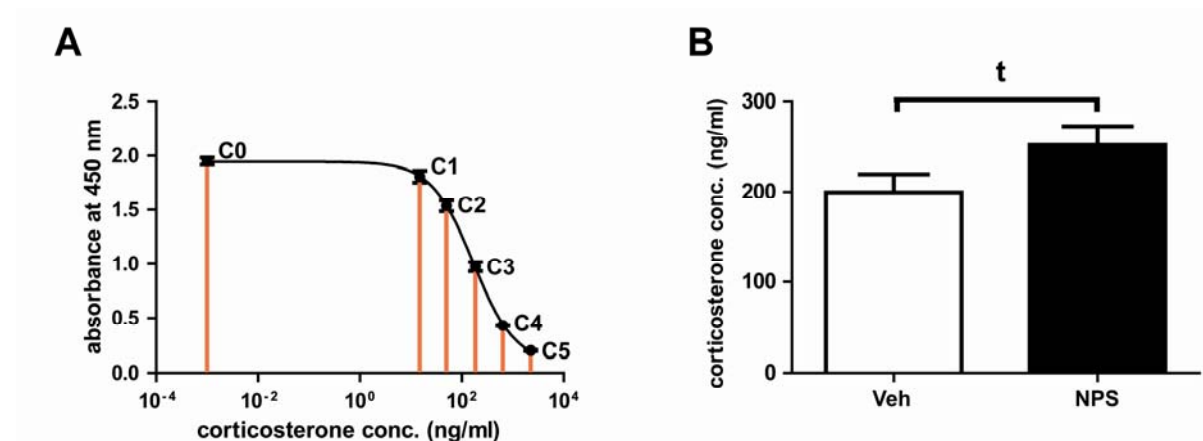


Figure 39. Corticosterone levels in plasma obtained from trunk blood of shocked mice after NPS treatment. **A** Fitted curve in a semi-log plot showing known corticosterone concentrations in ng/ml at the power of 10 from the calibrator samples C0-C5 and the corresponding absorbance values. **B** Graph showing mean corticosterone concentrations (extrapolated from fitted curve) of the two groups. Statistical analysis: two-tailed unpaired t-test. $t p < 0.1$. All data are shown as mean \pm s.e.m.

4. Discussion

4.1. Anxiolytic effects of intranasally applied NPS in C57BL/6N and HAB mice

The main focus of this study was the characterization of NPS-elicited anxiolytic effects in view of the potential of NPS as a novel therapeutic for anxiety disorders, including PTSD. NPS represents a prime candidate for this purpose, since, although it has been reported to have reward-like effects (Cao et al., 2011), it does not act via the GABA_A receptor like benzodiazepines and therefore will most likely not have their undesirable side-effects, especially as regards sedation, a common secondary action of benzodiazepine treatment (Cloos and Ferreira, 2009).

Most important for the implementation of an NPS-based therapy in patients was establishing a non-invasive application procedure appropriate for use in humans, as opposed to the ICV administration that was hitherto used in rodents. The results presented here show for the first time that intranasally applied NPS can successfully target the mouse brain. Although work done by others has already revealed that intranasally applied substances, among them neuropeptides, can target the CNS (Born et al., 2002; Dufes et al., 2003; Thorne et al., 2004, 2008; Dhuria et al., 2009), this was until now not proven in the case of NPS. Testing the feasibility of intranasal NPS delivery was crucial, since only the molecular structure of a substance is generally not sufficient to predict whether and to what extent the substance of interest will reach the brain after intranasal delivery (Ozsoy et al., 2009; Dhuria et al., 2010). In addition, even if the substance is able to bypass the nose-brain barrier and reach the brain, it is still a considerable challenge to identify the correct dosis for eliciting the desired therapeutic effects, since the nasal bioavailability of hydrophilic peptides and proteins is usually below 1 % (Ozsoy et al., 2009), in part as a consequence of the neuropeptide-degrading enzymes of the nasal mucosa (Ohkubo et al., 1994).

It is therefore remarkable that here, NPS could not only be tracked within the murine brain after intranasal application, but also induced locomotion-independent anxiolytic effects in mice. The data on successful transnasal delivery of NPS to alert mice presented here strongly encourage the development of NPS-based anxiolytics by providing the basis for intranasal NPS administration in patients.

The behavioral results obtained in C57BL/6N mice treated intranasally with NPS are very similar to the ones described previously by others after ICV injection of NPS (Jüngling et al., 2008; Leonard et al., 2008). The effects of NPS on both anxiety and locomotion were examined in two different standardized behavioral assays: the dark-light test and the EPM. This was done to improve the characterization of the NPS-induced behavioral phenotype, since both tests have been shown to cover different facets of anxiety (van Gaalen and Steckler, 2000; Bailey et al., 2007). The first test performed was the open field, which may be considered a fairly stressful experience for the animals. While it cannot be excluded with absolute certainty that the sequence of the tests might affect the behavioral readout, it is unlikely to assume that the control and treatment group were affected differently by this experience, as they did not show any difference in locomotion in the open field. The only possible way to circumvent the potential inter-test effects would have been to perform the assays on different days, so as to allow sufficient time for the influence of the single tests to disappear. However, this would have led to the additional difficulty of repeated NPS treatment, which would also have biased the results due to potential effects of chronic versus acute treatment. Although the behavioral effects of intranasal NPS treatment become apparent at a later time-point than described for ICV injection (4 hours instead of 30 min), this difference is most likely a consequence of dissimilar pharmacokinetics and targeting efficiencies of intranasally versus ICV-administered drugs (Thorne et al., 1995, 2008; Shi et al., 2010). This assumption is supported by the fact that at 30 min after intranasal application, a much weaker signal was observed than after ICV application. Therefore, although NPS reaches the brain rapidly after intranasal administration, additional time may be necessary for the substance to reach its brain target cells in the full concentration required to produce behavioral effects. In combination with the results describing NPS-induced changes in expression levels of candidate proteins up to 24 hours after treatment, future studies characterizing an even more extended timeline of NPS effects will be helpful.

As shown here for the first time, NPS treatment also exerts anxiolytic effects in HAB mice, a mouse model of pathological anxiety. These effects become apparent in HAB mice only in the dark-light test and not in the EPM as well, where reduced anxiety was also apparent in C57BL/6N mice. This may be the consequence of different neurobiological mechanisms underlying the general condition of trait anxiety

represented by the HAB mice versus the temporary condition of state anxiety (Krömer et al., 2005; Bunck et al., 2009). Moreover, the HAB mice are selected according to their behavior on the EPM (Krömer et al., 2005; Hamsch et al., 2010), which means that they have already been exposed to this test once. This prior exposure may additionally sensitize them towards this test and may contribute to making their behavior particularly resistant against pharmacologically induced changes in this test, as shown by others in the case of benzodiazepine treatment (Gonzalez and File, 1997). NPS-elicited anxiolytic effects in HAB mice are highly promising, since they show that NPS may mitigate the phenotypic consequences of a genetic predisposition to high anxiety-related behavior.

These results represent a starting point for future studies exploring the precise pharmacokinetics of intranasally applied NPS. Additionally, this application method will most likely facilitate animal experiments studying NPS effects, since it considerably reduces the stress the animals are exposed to during treatment as compared to the surgery-dependent intracerebral injection used in previous studies (Xu et al., 2004; Jüngling et al., 2008; Leonard et al., 2008; Fendt et al., 2010).

4.2. Identification of target brain regions and target neurons of NPS by NPSR-mediated internalization of Cy3-NPS

Here, the brain target regions and target neurons of NPS were identified with a high specificity by application of Cy3-NPS. Fluorescently labeled neuropeptides have been previously used by others both to study specific receptor-ligand interactions and to identify target cells both *in vitro* (Bunnett et al., 1995; Grady et al., 1995) and *in vivo* (Hubbard et al., 2009). The work at hand is however the first one to combine *in vitro* use of fluorophore-coupled ligands with intracerebral tracking after intranasal application *in vivo*.

The cell culture results presented here prove that intracellular Cy3-NPS uptake is receptor-mediated and takes place only in those cells that express NPSR at the membrane. This GPCR-dependent internalization process occurs upon highly specific interaction between the ligand and its respective receptor and represents a cellular desensitization mechanism described also for other neuropeptide receptors (Grady et al., 1995; Hökfelt et al., 2003; Reyes et al., 2006). However, in the case of

NPS, this phenomenon had not yet been explicitly demonstrated. The only work in this direction so far had been performed using vasopressin stimulation of a chimeric construct of vasopressin and NPS receptor elements (Gupte et al., 2004). Therefore, the physiological significance of those findings was limited. The results obtained in the course of the study presented here constitute the first evidence for agonist-induced internalization of wild-type murine NPSR. Although it is known that some neuropeptides can directly cross the plasma membrane and exert effects in a receptor-independent manner (Saban et al., 2002; Prochiantz and Joliot, 2003; Marinova et al., 2005), this does not seem to be the case here, since the only uptake observed occurs in cells expressing the tagged NPSR-construct. Moreover, Cy3-NPS is highly apparent at the membrane immediately following stimulation, in contrast to cell-penetrating neuropeptides, such as dynorphin, which are located mainly in the cytoplasm (Marinova et al., 2005). Finally, the Cy3-NPS signal colocalized exclusively with the signal of the receptor-specific immunostaining (Figures 10, 11). This is quite compelling evidence for the fact that NPS internalization is dependent upon expression of active NPSR at the cell membrane.

These cell culture results permit the assumption that the internalization of Cy3-NPS in single cells of various brain regions upon ICV and intranasal administration *in vivo* also represents a receptor-mediated process. Besides proving the feasibility of targeting the brain by intranasal administration, this approach led to another major finding, namely the identification of the hitherto unknown NPS target brain regions and target neurons. The validity of these results is supported by publications which link some of the brain regions identified here with NPS-mediated effects. This is the case for the basolateral and lateral amygdaloid nuclei; here, not only were anxiolytic effects described upon local NPS injection, but also NPSR mRNA expression was found in the mouse (Jüngling et al., 2008). This also holds true for the hypothalamus (Smith et al., 2006; Fedeli et al., 2009; Yoshida et al., 2010). Moreover, the target brain regions of NPS were identified here by two different application methods, intranasal and ICV administration. Since the distribution pathways of substances vary according to the delivery approach used, the overlap between NPS target brain regions identified by these two methods very much strengthens the conclusion that these brain regions are indeed the physiological targets of NPS (see Table 11). These results partly contradict previous NPSR expression studies, as for instance in

the case of the hippocampus, where Cy3-NPS uptake is observed in the work at hand but where no NPSR mRNA seems to be expressed in the rat brain (Xu et al., 2007). This is most likely the consequence of differential NPSR expression patterns between rat and mouse, a fact that has already been proven in the case of the basolateral amygdala, where abundant NPSR mRNA expression was detected only in the mouse (Jüngling et al., 2008). Additionally, control experiments in which Cy3-NPS uptake was blocked using NPSR-specific antagonists strongly indicate that this uptake is NPSR-dependent. Furthermore, the internalization pattern of Cy3-NPS in brain neurons after intranasal administration coincides with that observed in cell culture upon internalization of the receptor-ligand complex (see Figures 10, 11, 19). Finally, it is known that, in NPSR-KO mice, NPS treatment no longer exerts its described effects (Zhu et al., 2010), thus proving that NPSR is the only mediator of NPS actions. The ultimate confirmation, which could result from an immunostaining against NPSR and investigation of the signal compared to the Cy3-NPS signal, represents an important future experimental approach.

The novelty of these findings consists in the identification of the physiological target brain regions and target cells of NPS. In contrast to current NPSR expression studies using ISH and immunostaining, the NPS target cells identified here are the ones where NPSR is expressed not only on mRNA level or within the cytoplasm, but is actually present at the membrane and can therefore bind to its ligand and most likely as a consequence activate the signaling cascade. Furthermore, using a fluorescent conjugate of NPS it was possible, for the first time, to track intranasally administered substances at the single cell level. This much improves the anatomical resolution of intracerebral distribution patterns hitherto available with radioactively labeled ligands (Thorne et al., 2004, 2008).

4.3. The hippocampus: A novel player in NPS-mediated anxiolytic effects

Most important, both intranasal and ICV administration of Cy3-NPS led to identification of the hippocampus as a novel NPS target region. NPSR mRNA and protein expression studies contain contradictory results with respect to the hippocampus. In the rat, no NPSR mRNA expression was detected in the CA1, CA2 and CA3 regions and in the dentate gyrus by ISH (Xu et al., 2007); immunostaining against NPSR on the other hand revealed sparse immunoreactivity in these same

hippocampal regions (Leonard and Ring, 2011). In the study at hand, however, abundant Cy3-NPS uptake was observed in the ventral as well as throughout the dorsal hippocampus, spanning all CA regions and the dentate gyrus.

As far as NPS effects in the hippocampus are concerned, there was until now no direct link between NPS treatment and modulation of hippocampal function with regard to NPS-elicited anxiolytic effects. The only observations so far relating NPS to the hippocampus presented only an indirect link between NPS actions and the hippocampal region by showing that NPS treatment increases phosphorylation of cAMP-response element binding protein (CREB) in the hippocampus, which the authors of the study hypothesized to play a role in reversing impairment of spatial memory after rapid eye movement (REM) sleep deprivation (Zhao et al., 2010).

The work at hand demonstrates that NPS injection specifically into the ventral hippocampus is sufficient to elicit anxiolytic effects similar to those observed after intra-amygdala and ICV injection (Xu et al., 2004; Jüngling et al., 2008). As shown in the present study, these behavioral changes are initiated only within the ventral CA1 region (the site of injection), since it was shown here additionally that Cy3-NPS distribution upon intrahippocampal injection remains locally restricted and does not reach the amygdala. Moreover, electrophysiological data obtained in parallel to this work show modulation of basal synaptic transmission, of transmitter release probability and of short- and long-term plasticity in the ventral hippocampus 2 hours after slice incubation with NPS (Ionescu et al., 2012). Interestingly, these electrophysiological results could be replicated in slices from the ventral hippocampus prepared 4 hours after intranasal NPS treatment in C57BL/6N mice (Dine*, Ionescu* et al., in preparation). This strongly supports the conclusion that the observed NPS-elicited activity changes are of physiological relevance and pertain to the endogenous brain network activity.

Here is shown that NPS treatment upregulates hippocampal synapsin Ia-b/IIa protein expression in mice 24 hours after application. This observation strengthens the electrophysiologically identified increase in neurotransmitter release probability after NPS treatment. As synapsin has been shown to be involved in modulation of neurotransmitter release by regulation of synaptic vesicles availability (Humeau et al., 2001; Baldelli et al., 2007; Cesca et al., 2010), increased synapsin expression may

mirror an increased number of synaptic vesicles at presynaptic terminals. Furthermore, the protein data obtained 24 hours after NPS treatment suggest that the effects observed 2 hours after slice incubation with NPS may continue in the long-term. More detailed investigation of NPS effects over an extended period of time, as well as high-resolution microscopy, for instance electron microscopy, to accurately quantify potential changes in the synaptic vesicle pools will be needed for verifying this hypothesis.

The anxiolytic effects elicited by NPS injection into the ventral CA1 region and the synapsin upregulation upon intranasal NPS treatment together with the electrophysiological data showing NPS-induced modulation of hippocampal activity strongly point towards the hippocampus as a novel major player in NPS-mediated anxiolytic effects (Figure 40). This is especially important since hitherto, the main focus has been on the amygdala as the key mediator of the anxiolytic NPS effects (Meis et al.; Jüngling et al., 2008; Fendt et al., 2010; Pape et al., 2010). The findings presented here do not contradict this model; rather, they complement it. The ventral hippocampus and especially the ventral CA1 region are associated with the amygdaloid nuclei by extensive bidirectional connections (Fanselow and Dong, 2010) (green arrows in Figure 40). Moreover, during the past decade, the role of the ventral hippocampus in regulating anxiety and fear formation and expression has emerged more and more clearly (Kjelstrup et al., 2002; Bannerman et al., 2004; McHugh et al., 2004). Therefore, the data presented here strongly suggest that upon NPS stimulation, the ventral hippocampus modulates the activity of amygdaloid nuclei to decrease anxiety in addition to the direct effects of NPS in the amygdala.

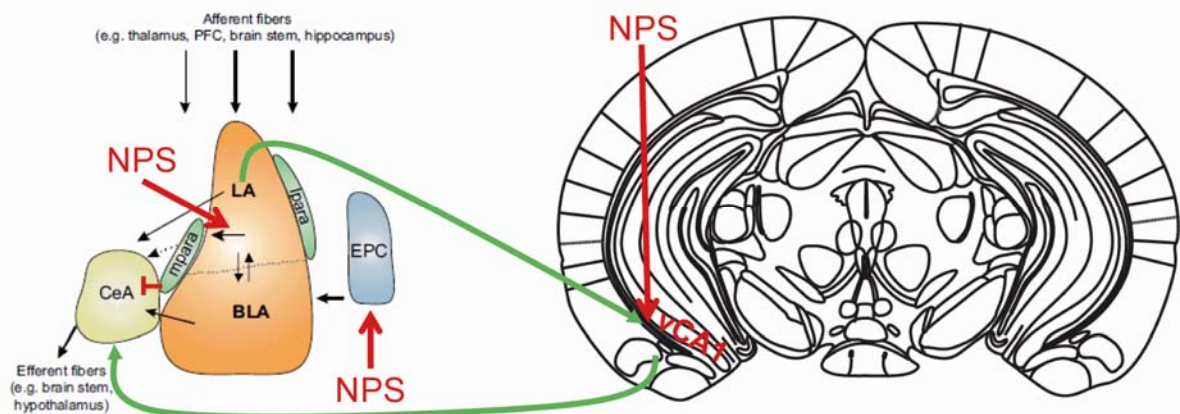


Figure 40. Effects of NPS in amygdaloid structures (Pape et al., 2010) and in the ventral CA1 region (Franklin and Paxinos, 2007). Red arrows show identified targets of NPS. Green arrows show input connections from the lateral amygdala to the ventral CA1 region and output connections from the ventral CA1 region to the central amygdala. LA: lateral amygdala; BLA: basolateral amygdala; EPC: endopiriform cortex; CeA: central amygdala; vCA1: ventral CA1 region; mpara: medial paracapsular interneurons; lpara: lateral paracapsular interneurons.

4.4. NPS and the glutamatergic system in C57BL/6N and HAB mice

In addition to hippocampal regulation of synapsin expression, NPS treatment also led to regulation of protein and mRNA expression of proteins associated with the glutamatergic system.

Although NPS actions have been previously linked to the glutamatergic system (Han et al., 2009; Okamura et al., 2010, 2011), there was hitherto no data available on regulatory effects of NPS *in vivo*. This work provides evidence that NPS treatment differentially regulates cerebral expression of GluR1, GluR2 and Glt-1 on both mRNA and protein level in C57BL/6N mice as well as in HAB mice in a region- and strain-dependent manner (see Figures 25-27, 33, 34). This is especially relevant since the glutamatergic system is known to be affected in psychiatric disorders like PTSD, where toxically increased glutamate release is thought to play a role in hippocampal shrinkage, as well as in consolidation of traumatic memories (Ravindran and Stein, 2009; Rossi et al., 2009).

GluR1 protein expression is increased in the prefrontal cortex of NPS-treated C57BL/6N mice, whereas GluR2 expression remains unaffected. This process might

result in an increased GluR1:GluR2 ratio, which reflects an enhancement of AMPA receptor function (Isaac et al., 2007). As acute potentiation of AMPA receptors in the prefrontal cortex has been shown to facilitate fear extinction (Zushida et al., 2007), specific upregulation of GluR1 by NPS treatment might provide a hint towards long-term NPS-mediated fear extinction following chronic NPS treatment. This speculation is supported by results showing that NPS treatment can facilitate fear extinction upon intra-amygdala injection (Jüngling et al., 2008). To further test this hypothesis, investigation of GluR1 and GluR2 expression specifically at the membrane as well as an AMPA binding assay will have to be performed in order to check whether the observed increase in total-cell GluR1 protein expression is also mirrored on a functional level.

In HAB mice, in contrast to C57BL/6N mice, NPS treatment upregulates protein expression of both GluR1 and GluR2. This might be the consequence of a different baseline activity of the glutamatergic system in the two strains, especially since the HAB mice represent a model of pathologically enhanced trait anxiety. In anxiety disorders and PTSD, hyperactivity of the glutamate system might lead to chronic potentiation of AMPA receptors and thereby to glutamate excitotoxicity (Tanaka et al., 2000). It has been noted that affected neurons express a reduced amount of GluR2 subunits. Therefore, it can be speculated that NPS actions under pathological conditions are capable of restoring homeostasis in the glutamate system.

In C57BL/6N mice, NPS also upregulates cerebral Glt-1 mRNA and protein expression in the prefrontal cortex in addition to the expression of AMPA receptor subunits. Since glutamate excitotoxicity has been reported in PTSD (Ravindran and Stein, 2009; Rossi et al., 2009), increase in Glt-1 levels may represent a possible damage-limiting mechanism of NPS actions. Moreover, since Glt-1 is expressed exclusively by astrocytes (Huang and Bergles, 2004), these data show that NPS, although it targets only neurons, can ultimately impact the entire cellular brain network.

The changes in protein expression described here represent valuable starting points for further investigation of the mechanisms underlying complex NPS-mediated effects, especially in the context of the behavioral and electrophysiology results. These changes in protein expression only become apparent 24 hours after treatment.

However, regulation of membrane transport and insertion mechanisms may occur already at an earlier time point and lead to the electrophysiological and behavioral effects described at 2 and 4 hours after NPS administration, respectively. Further studies on protein levels of cellular subfractions and on protein dynamics are needed to clarify this aspect. The fact that the cerebral expression of the examined candidates is differentially modulated at protein and mRNA levels, as well as the fact that these processes seem to be time-, region- and strain-dependent, suggest that NPS-mediated regulation of protein expression taps into a variety of posttranscriptional and posttranslational mechanisms to exert its effects.

Taken together, these expression analyses provide new insights into potential regulatory mechanisms of NPS *in vivo*, which have hitherto been explored *in vitro* and at the RNA level only (Vendelin et al., 2006).

4.5. Effects of NPS treatment on cerebral protein expression in a mouse model of PTSD

Regulatory effects of NPS on protein expression were also described in a mouse model of PTSD (Siegmund and Wotjak, 2007). Previous screening of protein expression in this mouse model revealed the synapsin isoforms I and II to be downregulated in the hippocampus at day 28 post-shock (Herrmann et al., submitted). Upon intranasal NPS treatment at day 28, treated mice displayed increased synapsin I and II mRNA expression in the hippocampus compared to vehicle-treated controls, as well as a trend towards increased synapsin Ia-b/IIa protein expression. This finding is most interesting, since it shows that NPS treatment has the potential to reverse molecular changes that can be attributed to the PTSD pathology.

Moreover, 24 hours after application, NPS treatment trendwise increased corticosterone levels in plasma of treated mice as compared to vehicle-treated controls. This observation confirms findings that show stimulatory effects of NPS on the HPA axis and increased plasma corticosterone 10 to 40 min after NPS ICV injection (Smith et al., 2006). It adds to the previous data by showing that NPS effects on blood corticosterone levels are robust enough to last up to 24 hours after treatment. Additionally, it provides valuable support in favor of the applicability of

NPS as an alternative treatment for PTSD, since in PTSD patients, cortisol plasma levels have been found to be decreased (Yehuda et al., 1995; Gill et al., 2008; Vythilingam et al., 2010). Upon successful treatment cortisol levels increased in responders (Olff et al., 2007). Therefore, these results may point towards an incipient success of NPS therapy that might, in time, attenuate at least part of the PTSD symptoms. Finally, elevated corticosterone levels after NPS treatment very nicely relate to NPS-induced upregulation of hippocampal synapsin expression, since it has been shown in cell culture of hippocampal neurons that corticosterone stimulation increases synapsin Ia-b expression on the protein level (Revest et al., 2010). Moreover, corticosterone has been shown to contribute to synaptic plasticity by regulating AMPA receptor trafficking differentially via the glucocorticoid receptor (GR) and the mineralocorticoid receptor (MR) (Avital et al., 2006; Krugers et al., 2010). Indeed, NPS treatment also evokes changes in expression of AMPA receptor subunits GluR1 and GluR2, as described here.

NPS treatment in the PTSD mouse model elicited no behavioral phenotype. This may however be due to the fact that at day 28, the mice already exhibit a full-blown PTSD phenotype (Siegmund and Wotjak, 2007) which may be difficult to alleviate by acute treatment only. Chronic treatment would have to be attempted at this time-point in order to better characterize the curative effects of NPS in the case of PTSD. However, the results presented here show that this mouse model could be appropriate to study the therapeutic and potential curative effects of NPS on PTSD symptoms. Traumatized mice treated with NPS respond to treatment as far as corticosterone plasma levels are concerned and they additionally show restoration in levels of synapsin, newly identified as a potential biomarker of PTSD (Herrmann et al., submitted).

4.6. Summary

To sum up, the work presented here establishes a non-invasive procedure for NPS administration in mice whereby anxiolytic and HPA axis-regulating effects of NPS are preserved, and that may be implemented in patients. Intranasal application of Cy3-NPS allowed visualization of NPS target cells at a single-cell resolution, thus establishing for the first time the use of fluorophore-coupled ligands for substance tracking after intranasal application. By this technique, the hippocampus was

identified as a novel target brain region of NPS which contributes to mediating its anxiolytic effects. Together with results on the regulatory effects of NPS on protein and mRNA expression in various brain regions associated with anxiety, these findings give new insights into the molecular basis of NPS-elicited effects. Finally, therapeutic actions of NPS are shown here for the first time in a high anxiety mouse model, the HAB mice, and trauma-counteracting effects of NPS treatment on hippocampal expression of synaptic proteins are described here in a mouse model of PTSD. This study therefore provides a solid basis for developing an NPS-based therapy for patients suffering from anxiety disorders like PD and PTSD.

5. Supplementary Material

Supplementary Table 1. List of devices used in this work.

Device	Firm
Bio-Rad DNA Subcell system (agarose gel electrophoresis)	Bio-Rad, Munich, Germany
Cell culture incubator Heraeus 240i	Thermo Scientific, Waltham, MA, USA
Confocal microscope Olympus IX81	Olympus Soft Imaging Systems GmbH, Münster, Germany
Cryostat Microm HM 500 OM	Thermo Scientific, Walldorf, Germany
Dynatech MR5000 plate reader	Dynatech Laboratories, Denkendorf, Germany
Epifluorescence microscope Olympus BX61	Olympus Soft Imaging Systems GmbH, Münster, Germany
Kodak M35 X-OMAT Processor	Carestream Health Inc, Rochester, NY, USA
LightCycler®2.0	Roche Diagnostics, Mannheim, Germany
Mini-Protean Electrophoresis System (SDS-PAGE)	Bio-Rad, Munich, Germany
Nanophotometer	Implen, Munich, Germany
PCR thermocycler TProfessional	Biometra, Göttingen, Germany
Plate centrifuge 5804 R	Eppendorf, Hamburg, Germany
Protean GelDoc 2000 system (agarose gel analysis)	Bio-Rad, Munich, Germany
Shaker Gyro-Rocker SSL3	Stuart, Staffordshire, UK
Sonifier Cell Disruptor B15	Branson, USA
Stereotact	TSE Systems, Bad Homburg, Germany
Table centrifuge 5415 R	Eppendorf, Hamburg, Germany
Turrax homogenizer VDI12	VWR, Darmstadt, Germany

Supplementary Table 2. List of materials used in this work.

Material	Firm
0.2 ml PCR tubes	Eppendorf, Hamburg, Germany
1.5 ml tubes	Eppendorf, Hamburg, Germany
10 µl Hamilton syringe	Hamilton Bonaduz AG, Bonaduz, Switzerland
2 ml tubes	Eppendorf, Hamburg, Germany
23 gage guide cannulas	Josef Peske GmbH & Co. KG, Aindling-Arnhofen, Germany
30 gage injection cannulas	VWR, Darmstadt, Germany
Cell culture vessels (10 cm dishes, 6/24/96-well plates)	Josef Peske GmbH & Co. KG, Aindling-Arnhofen, Germany
Cover slips 12 mm	Marienfeld GmbH & Co. KG, Lauda-Königshofen
Dual-Cement Basis + Katalysator	Pluradent AG & Co. KG, Munich, Germany
EDTA 1.5 ml tubes for blood	Josef Peske GmbH & Co. KG, Aindling-Arnhofen, Germany
FujiFilm X-Ray 18x24 100NF	Röntgen Bender GmbH & Co. KG, Baden-Baden, Germany
Gloves SemperGuard latex/nitrile powder-free	Semperit Technische Produkte, Vienna, Austria
LightCycler capillaries (20 µl)	Roche Diagnostics, Mannheim, Germany
Netwells for immunostainings	VWR, Darmstadt, Germany
Neubauer Counting Chamber improved	Carl Roth GmbH + Co., Karlsruhe, Germany
Nitrocellulose membrane	Carl Roth GmbH + Co., Karlsruhe, Germany
Parafilm	Josef Peske GmbH & Co. KG, Aindling-Arnhofen, Germany
Research pipettes	Eppendorf, Hamburg, Germany
RNase/DNase-free 0.5 ml tubes	Eppendorf, Hamburg, Germany
RNase-free 2 ml tubes	Eppendorf, Hamburg, Germany
Screws DIN84 1.0x2	Paul Korth GmbH, Lüdenscheid, Germany
Slides Superfrost® Plus	Thermo Scientific, Waltham, MA, USA
Surgical instruments	TSE Systems, Bad Homburg, Germany
Tygon tube	VWR, Darmstadt, Germany

Supplementary Table 3. List of substances used in this work (sorted alphabetically).

Substance	Firm
(R)-SHA 68	Generous gift from A. Sailer, Novartis Basel, Switzerland
[D-Cys(tBu) ₅]NPS	Generous gift from N. Singewald, University of Innsbruck, Austria
10x PCR Reaction Buffer (- MgCl ₂)	Invitrogen, Grand Island, NY, USA
25x Protease Inhibitor Cocktail	Roche, Grenzach-Wyhlen, Germany
4',6-diamidino-2-phenylindole (DAPI)	Carl Roth GmbH + Co., Karlsruhe, Germany
Acrylamide	Carl Roth GmbH + Co., Karlsruhe, Germany
Agar-Agar, Kobe I	Carl Roth GmbH + Co., Karlsruhe, Germany
Ammonium persulfate (APS)	RheinPerChemie GmbH, Hamburg, Germany
Ampicillin	Carl Roth GmbH + Co., Karlsruhe, Germany
Antibiotic-antimycotic solution	Gibco, Darmstadt, Germany
BamHI	New England Biolabs, Ipswich, MA, USA
Borate	Merck KGaA, Darmstadt, Germany
Bovine serum albumin (BSA): Albumin fraction V	Carl Roth GmbH + Co., Karlsruhe, Germany
Bromphenolblue	Merck KGaA, Darmstadt, Germany
Chloroform	Carl Roth GmbH + Co., Karlsruhe, Germany
Cy3-NPS	Phoenix Pharmaceuticals, Karlsruhe, Germany
Diethylpyrocarbonate (DEPC)	Carl Roth GmbH + Co., Karlsruhe, Germany
Dimethylsulfoxide (DMSO)	Invitrogen, Grand Island, NY, USA
dNTPs	Invitrogen, Grand Island, NY, USA
Dulbecco's modified Eagle's medium (DMEM)	Gibco, Darmstadt, Germany
Ethanol	Sigma-Aldrich, St Louis, MA, USA
Ethidium bromide (EtBr)	Sigma-Aldrich, St Louis, MA, USA
Ethylene glycol	Carl Roth GmbH + Co., Karlsruhe, Germany
Ethylenediaminetetraacetic acid (EDTA)	VWR, Darmstadt, Germany

ExGen 500 <i>in vitro</i> Transfection Reagent	Fermentas, St Leon-Rot, Germany
Fetal calf serum (FCS)	Gibco, Darmstadt, Germany
Fluorescein	Invitrogen, Grand Island, NY, USA
Forene 100 % (V/V)	Abbott, Wiesbaden, Germany
Formaldehyde min. 37 %	Merck KGaA, Darmstadt, Germany
Gelatin	Carl Roth GmbH + Co., Karlsruhe, Germany
Glucose	Carl Roth GmbH + Co., Karlsruhe, Germany
Glycerin ≥ 86 %	Carl Roth GmbH + Co., Karlsruhe, Germany
Glycin	Carl Roth GmbH + Co., Karlsruhe, Germany
Goat serum	Sigma-Aldrich, St Louis, MA, USA
Hank's Balanced Salt Solution with phenol red	Gibco, Darmstadt, Germany
Isopropanol	VWR, Darmstadt, Germany
Kanamycin	Carl Roth GmbH + Co., Karlsruhe, Germany
Ketamine hydrochloride	Essex Pharma GmbH, Munich, Germany
LB Broth EZMix™ Powder	Sigma-Aldrich, St Louis, MA, USA
Metacam	Boehringer Ingelheim, Biberach, Germany
Methanol	Carl Roth GmbH + Co., Karlsruhe, Germany
Methylbutane	Carl Roth GmbH + Co., Karlsruhe, Germany
MgCl ₂ (50 mM)	Invitrogen, Grand Island, NY, USA
Milk powder	Carl Roth GmbH + Co., Karlsruhe, Germany
TFM Tissue Freezing Medium	TBS Triangle Biomdeical Sciences, Inc, Durham, NC, USA
NEBuffer 3	New England Biolabs, Ipswich, MA, USA
NPS (rat)	Bachem, Weil am Rhein, Germany
PageRuler Prestained Protein Ladder	Invitrogen, Grand Island, NY, USA
peqGold Ladder-Mix (100-1000 bp)	PeqLab, Erlangen, Germany
peqGold Universal Agarose	PeqLab, Erlangen, Germany
Phosphate buffered saline (PBS)	Gibco, Darmstadt, Germany
Ponceau S	AppliChem, Darmstadt, Germany
Reaction Buffer for T4 ligase	New England Biolabs, Ipswich, MA, USA

Rhodamine B	Sigma-Aldrich, St Louis, MA, USA
Rhodamine-NPS	Phoenix Pharmaceuticals, Karlsruhe, Germany
Shandon Immu-Mount	Thermo Scientific, Waltham, MA, USA
Sodium pyruvate	Gibco, Darmstadt, Germany
Sulfosalicylic acid	Carl Roth GmbH + Co., Karlsruhe, Germany
T4 ligase	New England Biolabs, Ipswich, MA, USA
<i>Taq</i> polymerase	Invitrogen, Grand Island, NY, USA
Tetraethylmethylenediamine (TEMED)	Carl Roth GmbH + Co., Karlsruhe, Germany
Trichloroacetic acid	Carl Roth GmbH + Co., Karlsruhe, Germany
Tris	Carl Roth GmbH + Co., Karlsruhe, Germany
Triton X-100	Carl Roth GmbH + Co., Karlsruhe, Germany
Trypan blue	Sigma-Aldrich, St Louis, MA, USA
Trypsin	Gibco, Darmstadt, Germany
Tween 20	Carl Roth GmbH + Co., Karlsruhe, Germany
XhoI	New England Biolabs, Ipswich, MA, USA
Xylazin hydrochloride	Bayer Vital GmbH, Lederhosen, Germany
β -mercaptoethanol	Carl Roth GmbH + Co., Karlsruhe, Germany

Supplementary Table 4. List of kits used in this work.

Kit	Firm
BCA Protein Assay Reagent	Thermo Scientific, Waltham, MA, USA
Corticosterone (Rat/Mouse) ELISA	DRG Instruments GmbH, Marburg, Germany
NucleoSpin RNA II Kit	Macherey-Nagel, Düren, Germany
Omniscript Reverse Transcription Kit	Qiagen, Hilden, Germany
PureYield Plasmid Midiprep System	Promega, Madison, WI, USA
QIAquick Gel Extraction Kit	Qiagen, Hilden, Germany
QuantiFast SYBR Green PCR Kit	Qiagen, Hilden, Germany

Supplementary Table 5. Buffer recipes used in this work.

Buffer recipes

Ampicillin 50 mg/ml

- 1 g in 20 ml H₂O
- sterile filtration, aliquots of 1 ml at -20 °C

Ammoniumpersulfate (APS) 10 %

- 1 g in 10 ml H₂O, aliquots of 1 ml at -20 °C

Agar plates for bacterial growth

- 20 g LB broth
- 15 g Agar-Agar (1.5 %)
- 1 l H₂O
- add antibiotic (ampicillin at a final concentration of 100 µg/ml)
- cast plates

DEPC H₂O

- 2 ml DEPC in 2 l H₂O, mix overnight at RT
- autoclave twice

Freezing buffer for free-floating brain sections

- 25 % ethylene glycol
- 25 % glycerin
- 50 % PBS

HRP substrate solution

- luminol stock 250 mM (266 mg in 6 ml DMSO)
- coumaric acid stock 90 mM (38 mg in 2.5 ml DMSO)

LB medium

- 20 g LB broth in 1 l dH₂O
- autoclave

Kanamycin 30 mg/ml

- 300 mg in 10 ml H₂O
- concentration for agar plates: 30 µg/µl

Ketamine-rompun

- 2% rompun 2%
- xylazin – xylazin hydrochloride
- 5% ketamine 10% (ketamine hydrochloride)
- in NaCl

Laemmli dilution buffer (LAP+) for protein dilutions, 5x

- 5 % SDS
- 40 % glycin
- 160 mM Tris, pH = 6.8
- 5 % β-mercaptoethanol
- pinch of bromphenolblue
- H₂O ad 10 ml
- aliquots of 0.5 ml at -20 °C

Laemmli running buffer, 10x

- 25 mM Tris
- 192 mM glycin
- 0.5 % SDS
- H₂O ad 1 l

4 % PFA

- 100 ml Stock Solution A (27,6 g NaH₂PO₄ in 1000 ml ddH₂O) + 400 ml Stock Solution B (35,6 g Na₂HPO₄ in 1000 ml ddH₂O)
- 100 ml formaldehyde 37 % diluted with ddH₂O up to 500 ml
- filter formaldehyde with two filters to remove calcium and prevent salt formation
- together: 1 l 4 % PFA in phosphate buffer

Ponceau S solution

- 0.2 % Ponceau S
- 3 % trichloroacetic acid
- 3 % sulfosalicylic acid

-- dH₂O ad 1 l

TBS 10x

-- 100 mM Tris

-- 1.5 mM NaCl

-- H₂O ad 1 l, pH = 7.6

-- for TBS-T: 1 l 10x TBS + 10 ml Tween-20, H₂O ad 10 l, mix well

Trypsin EDTA

-- 1600 ml H₂O

-- 200 ml HBSS (10x with phenol red)

-- 200 ml 10x trypsin

-- mix and filter

TBE 10x

-- 90 mM Tris

-- 90 mM borate

-- 2.5 mM EDTA, pH = 8

WetBlot Buffer 10x

-- 250 mM Tris

-- 1900 mM glycin

-- H₂O ad 1 l

-- for 1x WetBlot Buffer ready-to-use: 100 ml 10x WetBlot Buffer + 700 ml H₂O + 200 ml methanol

Supplementary Table 6. List of software used in this work.

Software	Firm
ImageJ software	http://rsbweb.nih.gov/ij/ , Rasband, W.S., ImageJ, U.S. National Institutes of Health Bethesda, Maryland, USA
Adobe Photoshop CS5	Adobe
LightCycler software 2.0	Roche Diagnostics, Mannheim, Germany
Confocal microscope: FluoView FV 1000 2.1.2.5	Olympus Soft Imaging Systems GmbH, Münster, Germany
Statistical analysis: GraphPad Prism 5.03	GraphPad Software, La Jolla, CA, USA
ANY-maze 4.30	Stoelting, Wood Dale, IL, USA
Epifluorescence microscope: cell [^] F 2.8	Olympus Soft Imaging Systems GmbH, Münster, Germany

6. References

- Acheson, D.T., Gresack, J.E., and Risbrough, V.B. (2011). Hippocampal dysfunction effects on context memory: Possible etiology for posttraumatic stress disorder. *Neuropharmacology*.
- Afifi, T.O., Asmundson, G.J.G., Taylor, S., and Jang, K.L. (2010). The role of genes and environment on trauma exposure and posttraumatic stress disorder symptoms: a review of twin studies. *Clin Psychol Rev* 30, 101–112.
- Alfarez, D.N., Wiegert, O., and Krugers, H.J. (2006). Stress, corticosteroid hormones and hippocampal synaptic function. *CNS Neurol Disord Drug Targets* 5, 521–529.
- American Psychiatric Association (2000). *Diagnostic and Statistical Manual of Mental Disorders DSM-IV-TR Fourth Edition* (Amer Psychiatric Pub).
- Asami, T., Hayano, F., Nakamura, M., Yamasue, H., Uehara, K., Otsuka, T., Roppongi, T., Nihashi, N., Inoue, T., and Hirayasu, Y. (2008). Anterior cingulate cortex volume reduction in patients with panic disorder. *Psychiatry Clin. Neurosci.* 62, 322–330.
- Autry, A.E., Adachi, M., Nosyreva, E., Na, E.S., Los, M.F., Cheng, P., Kavalali, E.T., and Monteggia, L.M. (2011). NMDA receptor blockade at rest triggers rapid behavioural antidepressant responses. *Nature* 475, 91–95.
- Avital, A., Segal, M., and Richter-Levin, G. (2006). Contrasting roles of corticosteroid receptors in hippocampal plasticity. *J. Neurosci.* 26, 9130–9134.
- Bachmann, A.W., Sedgley, T.L., Jackson, R.V., Gibson, J.N., Young, R.M., and Torpy, D.J. (2005). Glucocorticoid receptor polymorphisms and post-traumatic stress disorder. *Psychoneuroendocrinology* 30, 297–306.
- Bailey, K.R., Pavlova, M.N., Rohde, A.D., Hohmann, J.G., and Crawley, J.N. (2007). Galanin receptor subtype 2 (GalR2) null mutant mice display an anxiogenic-like phenotype specific to the elevated plus-maze. *Pharmacol. Biochem. Behav.* 86, 8–20.
- Baldelli, P., Fassio, A., Valtorta, F., and Benfenati, F. (2007). Lack of synapsin I reduces the readily releasable pool of synaptic vesicles at central inhibitory synapses. *J. Neurosci* 27, 13520–13531.
- Bannerman, D.M., Rawlins, J.N.P., McHugh, S.B., Deacon, R.M.J., Yee, B.K., Bast, T., Zhang, W.-N., Pothuizen, H.H.J., and Feldon, J. (2004). Regional dissociations within the hippocampus—memory and anxiety. *Neurosci Biobehav Rev* 28, 273–283.
- van den Berg, M.P., Romeijn, S.G., Verhoef, J.C., and Merkus, F.W.H.M. (2002). Serial cerebrospinal fluid sampling in a rat model to study drug uptake from the nasal cavity. *J. Neurosci. Methods* 116, 99–107.

- Bernier, V., Stocco, R., Bogusky, M.J., Joyce, J.G., Parachoniak, C., Grenier, K., Arget, M., Mathieu, M.-C., O'Neill, G.P., Slipetz, D., et al. (2006). Structure-function relationships in the neuropeptide S receptor: molecular consequences of the asthma-associated mutation N107I. *J. Biol. Chem* 281, 24704–24712.
- Binder, E.B., Bradley, R.G., Liu, W., Epstein, M.P., Deveau, T.C., Mercer, K.B., Tang, Y., Gillespie, C.F., Heim, C.M., Nemeroff, C.B., et al. (2008). Association of FKBP5 polymorphisms and childhood abuse with risk of posttraumatic stress disorder symptoms in adults. *Jama* 299, 1291–1305.
- Blanco, E., Bilbao, A., Luque-Rojas, M.J., Palomino, A., Bermúdez-Silva, F.J., Suárez, J., Santín, L.J., Estivill-Torrús, G., Gutiérrez, A., Campos-Sandoval, J.A., et al. (2011). Attenuation of cocaine-induced conditioned locomotion is associated with altered expression of hippocampal glutamate receptors in mice lacking LPA1 receptors. *Psychopharmacology*.
- Boeck, C.R., Martinello, C., de Castro, A.A., Moretti, M., Dos Santos Casagrande, T., Guerrini, R., Calo', G., and Gavioli, E.C. (2010). Blockade of adenosine A2A receptor counteracts neuropeptide-S-induced hyperlocomotion in mice. *Naunyn Schmiedebergs Arch. Pharmacol* 381, 153–160.
- Born, J., Lange, T., Kern, W., McGregor, G.P., Bickel, U., and Fehm, H.L. (2002). Sniffing neuropeptides: a transnasal approach to the human brain. *Nat. Neurosci* 5, 514–516.
- Bremner, J.D. (2007). Functional neuroimaging in post-traumatic stress disorder. *Expert Rev Neurother* 7, 393–405.
- Brothers, S.P., and Wahlestedt, C. (2010). Therapeutic potential of neuropeptide Y (NPY) receptor ligands. *EMBO Mol Med* 2, 429–439.
- Bunck, M., Czibere, L., Horvath, C., Graf, C., Frank, E., Kessler, M.S., Murgatroyd, C., Müller-Myhsok, B., Gonik, M., Weber, P., et al. (2009). A hypomorphic vasopressin allele prevents anxiety-related behavior. *PLoS ONE* 4, e5129.
- Bunnett, N.W., Dazin, P.F., Payan, D.G., and Grady, E.F. (1995). Characterization of receptors using cyanine 3-labeled neuropeptides. *Peptides* 16, 733–740.
- Camarda, V., Rizzi, A., Ruzza, C., Zucchini, S., Marzola, G., Marzola, E., Guerrini, R., Salvadori, S., Reinscheid, R.K., Regoli, D., et al. (2009). In vitro and in vivo pharmacological characterization of the neuropeptide s receptor antagonist [D-Cys(tBu)⁵]neuropeptide S. *J. Pharmacol. Exp. Ther* 328, 549–555.
- Cannon, W.B. (1932). *Wisdom Of The Body* (W. W. Norton and Company, Inc.).
- Cao, J., de Lecea, L., and Ikemoto, S. (2011). Intraventricular administration of neuropeptide S has reward-like effects. *Eur. J. Pharmacol.* 658, 16–21.
- Cesca, F., Baldelli, P., Valtorta, F., and Benfenati, F. (2010). The synapsins: key actors of synapse function and plasticity. *Prog. Neurobiol* 91, 313–348.

- Chalmers, D.T., Lovenberg, T.W., Grigoriadis, D.E., Behan, D.P., and De Souza, E.B. (1996). Corticotrophin-releasing factor receptors: from molecular biology to drug design. *Trends Pharmacol. Sci.* 17, 166–172.
- Chrousos, G.P., and Gold, P.W. (1992). The concepts of stress and stress system disorders. Overview of physical and behavioral homeostasis. *Jama* 267, 1244–1252.
- Clark, S.D., Duangdao, D.M., Schulz, S., Zhang, L., Liu, X., Xu, Y., and Reinscheid, R.K. (2011). Anatomical characterization of the neuropeptide S system in the mouse brain by in situ hybridization and immunohistochemistry. *The Journal of Comparative Neurology* 519, 1867–1893.
- Cloos, J.-M., and Ferreira, V. (2009). Current use of benzodiazepines in anxiety disorders. *Curr Opin Psychiatry* 22, 90–95.
- Cohen, H., Liu, T., Kozlovsky, N., Kaplan, Z., Zohar, J., and Mathé, A.A. (2011). The Neuropeptide Y (NPY)-ergic System is Associated with Behavioral Resilience to Stress Exposure in an Animal Model of Post-Traumatic Stress Disorder. *Neuropsychopharmacology: Official Publication of the American College of Neuropsychopharmacology*.
- Dannlowski, U., Kugel, H., Franke, F., Stuhrmann, A., Hohoff, C., Zwanzger, P., Lenzen, T., Grotegerd, D., Suslow, T., Arolt, V., et al. (2011). Neuropeptide-S (NPS) Receptor Genotype Modulates Basolateral Amygdala Responsiveness to Aversive Stimuli. *Neuropsychopharmacology*.
- Deuschle, M., Schweiger, U., Weber, B., Gotthardt, U., Körner, A., Schmider, J., Standhardt, H., Lammers, C.H., and Heuser, I. (1997). Diurnal activity and pulsatility of the hypothalamus-pituitary-adrenal system in male depressed patients and healthy controls. *J. Clin. Endocrinol. Metab.* 82, 234–238.
- Dhuria, S.V., Hanson, L.R., and Frey, W.H. (2009). Intranasal drug targeting of hypocretin-1 (orexin-A) to the central nervous system. *J Pharm Sci* 98, 2501–2515.
- Dhuria, S.V., Hanson, L.R., and Frey, W.H. (2010). Intranasal delivery to the central nervous system: mechanisms and experimental considerations. *J Pharm Sci* 99, 1654–1673.
- Domschke, K., Ohrmann, P., Braun, M., Suslow, T., Bauer, J., Hohoff, C., Kersting, A., Engelien, A., Arolt, V., Heindel, W., et al. (2008). Influence of the catechol-O-methyltransferase val158met genotype on amygdala and prefrontal cortex emotional processing in panic disorder. *Psychiatry Res* 163, 13–20.
- Domschke, K., Reif, A., Weber, H., Richter, J., Hohoff, C., Ohrmann, P., Pedersen, A., Bauer, J., Suslow, T., Kugel, H., et al. (2010). Neuropeptide S receptor gene - converging evidence for a role in panic disorder. *Mol. Psychiatry*.
- Dufes, C., Olivier, J.-C., Gaillard, F., Gaillard, A., Couet, W., and Muller, J.-M. (2003). Brain delivery of vasoactive intestinal peptide (VIP) following nasal administration to rats. *Int J Pharm* 255, 87–97.

- Ehlert, U., Gaab, J., and Heinrichs, M. (2001). Psychoneuroendocrinological contributions to the etiology of depression, posttraumatic stress disorder, and stress-related bodily disorders: the role of the hypothalamus-pituitary-adrenal axis. *Biol Psychol* 57, 141–152.
- Endler, N.S., and Kocovski, N.L. (2001). State and trait anxiety revisited. *J Anxiety Disord* 15, 231–245.
- Fanselow, M.S., and Dong, H.-W. (2010). Are the dorsal and ventral hippocampus functionally distinct structures? *Neuron* 65, 7–19.
- Fedeli, A., Braconi, S., Economidou, D., Cannella, N., Kallupi, M., Guerrini, R., Calò, G., Cifani, C., Massi, M., and Ciccocioppo, R. (2009). The paraventricular nucleus of the hypothalamus is a neuroanatomical substrate for the inhibition of palatable food intake by neuropeptide S. *Eur. J. Neurosci* 30, 1594–1602.
- Fendt, M., Imobersteg, S., Bürki, H., McAllister, K.H., and Sailer, A.W. (2010). Intra-amygdala injections of neuropeptide S block fear-potentiated startle. *Neurosci. Lett* 474, 154–157.
- Filiou, M.D., and Turck, C.W. (2012). Psychiatric disorder biomarker discovery using quantitative proteomics. *Methods Mol. Biol.* 829, 531–539.
- Filiou, M.D., Zhang, Y., Teplytska, L., Reckow, S., Gormanns, P., Maccarrone, G., Frank, E., Kessler, M.S., Hambusch, B., Nussbaumer, M., et al. (2011). Proteomics and metabolomics analysis of a trait anxiety mouse model reveals divergent mitochondrial pathways. *Biol. Psychiatry* 70, 1074–1082.
- Franklin, K.B.J., and Paxinos, G. (2007). *The Mouse Brain in Stereotaxic Coordinates with CDROM* (Academic Press).
- Furukawa, T.A., Watanabe, N., and Churchill, R. (2006). Psychotherapy plus antidepressant for panic disorder with or without agoraphobia: systematic review. *Br J Psychiatry* 188, 305–312.
- van Gaalen, M.M., and Steckler, T. (2000). Behavioural analysis of four mouse strains in an anxiety test battery. *Behav. Brain Res.* 115, 95–106.
- Garcia, L.S., Comim, C.M., Valvassori, S.S., Réus, G.Z., Andreazza, A.C., Stertz, L., Fries, G.R., Gavioli, E.C., Kapczinski, F., and Quevedo, J. (2008). Chronic administration of ketamine elicits antidepressant-like effects in rats without affecting hippocampal brain-derived neurotrophic factor protein levels. *Basic Clin. Pharmacol. Toxicol.* 103, 502–506.
- Gilbertson, M.W., Shenton, M.E., Ciszewski, A., Kasai, K., Lasko, N.B., Orr, S.P., and Pitman, R.K. (2002). Smaller hippocampal volume predicts pathologic vulnerability to psychological trauma. *Nat. Neurosci.* 5, 1242–1247.
- Gill, J., Vythilingam, M., and Page, G.G. (2008). Low cortisol, high DHEA, and high levels of stimulated TNF-alpha, and IL-6 in women with PTSD. *J Trauma Stress* 21, 530–539.

- Golub, Y., Kaltwasser, S.F., Mauch, C.P., Herrmann, L., Schmidt, U., Holsboer, F., Czisch, M., and Wotjak, C.T. (2011). Reduced hippocampus volume in the mouse model of Posttraumatic Stress Disorder. *J Psychiatr Res* 45, 650–659.
- Gonzalez, L.E., Andrews, N., and File, S.E. (1996). 5-HT_{1A} and benzodiazepine receptors in the basolateral amygdala modulate anxiety in the social interaction test, but not in the elevated plus-maze. *Brain Res.* 732, 145–153.
- Gonzalez, L.E., and File, S.E. (1997). A five minute experience in the elevated plus-maze alters the state of the benzodiazepine receptor in the dorsal raphe nucleus. *J. Neurosci.* 17, 1505–1511.
- Gozes, I., Giladi, E., Pinhasov, A., Bardea, A., and Brenneman, D.E. (2000). Activity-dependent neurotrophic factor: intranasal administration of femtomolar-acting peptides improve performance in a water maze. *J. Pharmacol. Exp. Ther* 293, 1091–1098.
- Grady, E., Garland, A., Gamp, P., Lovett, M., Payan, D., and Bunnett, N. (1995). Delineation of the endocytic pathway of substance P and its seven-transmembrane domain NK1 receptor. *Mol. Biol. Cell* 6, 509–524.
- Groc, L., Choquet, D., and Chaouloff, F. (2008). The stress hormone corticosterone conditions AMPAR surface trafficking and synaptic potentiation. *Nat. Neurosci.* 11, 868–870.
- Guastella, A.J., Einfeld, S.L., Gray, K.M., Rinehart, N.J., Tonge, B.J., Lambert, T.J., and Hickie, I.B. (2010). Intranasal oxytocin improves emotion recognition for youth with autism spectrum disorders. *Biol. Psychiatry* 67, 692–694.
- Gupte, J., Cutler, G., Chen, J.-L., and Tian, H. (2004). Elucidation of signaling properties of vasopressin receptor-related receptor 1 by using the chimeric receptor approach. *Proc. Natl. Acad. Sci. U.S.A* 101, 1508–1513.
- Hambusch, B., Chen, B.-G., Brenndörfer, J., Meyer, M., Avrabos, C., Maccarrone, G., Liu, R.H., Eder, M., Turck, C.W., and Landgraf, R. (2010). Methylglyoxal-mediated anxiolysis involves increased protein modification and elevated expression of glyoxalase 1 in the brain. *J. Neurochem* 113, 1240–1251.
- Han, R.-W., Yin, X.-Q., Chang, M., Peng, Y.-L., Li, W., and Wang, R. (2009). Neuropeptide S facilitates spatial memory and mitigates spatial memory impairment induced by N-methyl-D-aspartate receptor antagonist in mice. *Neurosci. Lett* 455, 74–77.
- Heim, C., and Nemeroff, C.B. (2009). Neurobiology of posttraumatic stress disorder. *CNS Spectr* 14, 13–24.
- Heinrichs, S.C., Lapsansky, J., Lovenberg, T.W., De Souza, E.B., and Chalmers, D.T. (1997). Corticotropin-releasing factor CRF1, but not CRF2, receptors mediate anxiogenic-like behavior. *Regul. Pept.* 71, 15–21.
- Hökfelt, T., Bartfai, T., and Bloom, F. (2003). Neuropeptides: opportunities for drug discovery. *Lancet Neurol* 2, 463–472.

- Holsboer, F. (1999). The rationale for corticotropin-releasing hormone receptor (CRH-R) antagonists to treat depression and anxiety. *J Psychiatr Res* 33, 181–214.
- Huang, Y.H., and Bergles, D.E. (2004). Glutamate transporters bring competition to the synapse. *Curr. Opin. Neurobiol* 14, 346–352.
- Hubbard, C.S., Dolence, E.K., Shires, J.A., and Rose, J.D. (2009). Identification of brain target neurons using a fluorescent conjugate of corticotropin-releasing factor. *J. Chem. Neuroanat* 37, 245–253.
- Humeau, Y., Doussau, F., Vitiello, F., Greengard, P., Benfenati, F., and Poulain, B. (2001). Synapsin controls both reserve and releasable synaptic vesicle pools during neuronal activity and short-term plasticity in Aplysia. *J. Neurosci* 21, 4195–4206.
- Ionescu, I.A., Dine, J., Yen, Y.-C., Buell, D.R., Herrmann, L., Holsboer, F., Eder, M., Landgraf, R., and Schmidt, U. (2012). Intranasally Administered Neuropeptide S (NPS) Exerts Anxiolytic Effects Following Internalization Into NPS Receptor-Expressing Neurons. *Neuropsychopharmacology: Official Publication of the American College of Neuropsychopharmacology*.
- Isaac, J.T.R., Ashby, M., and McBain, C.J. (2007). The role of the GluR2 subunit in AMPA receptor function and synaptic plasticity. *Neuron* 54, 859–871.
- Jansson, B., and Björk, E. (2002). Visualization of in vivo olfactory uptake and transfer using fluorescein dextran. *J Drug Target* 10, 379–386.
- Ježek, K., Lee, B.B., Kelemen, E., McCarthy, K.M., McEwen, B.S., and Fenton, A.A. (2010). Stress-Induced Out-of-Context Activation of Memory. *PLoS Biol* 8, e1000570.
- Jüngling, K., Seidenbecher, T., Sosulina, L., Lesting, J., Sangha, S., Clark, S.D., Okamura, N., Duangdao, D.M., Xu, Y.-L., Reinscheid, R.K., et al. (2008). Neuropeptide S-mediated control of fear expression and extinction: role of intercalated GABAergic neurons in the amygdala. *Neuron* 59, 298–310.
- Karst, H., Berger, S., Turiault, M., Tronche, F., Schütz, G., and Joëls, M. (2005). Mineralocorticoid receptors are indispensable for nongenomic modulation of hippocampal glutamate transmission by corticosterone. *Proc. Natl. Acad. Sci. U.S.A.* 102, 19204–19207.
- Kessler, R.C., Chiu, W.T., Demler, O., Merikangas, K.R., and Walters, E.E. (2005). Prevalence, severity, and comorbidity of 12-month DSM-IV disorders in the National Comorbidity Survey Replication. *Arch. Gen. Psychiatry* 62, 617–627.
- Kessler, R.C., Sonnega, A., Bromet, E., Hughes, M., and Nelson, C.B. (1995). Posttraumatic stress disorder in the National Comorbidity Survey. *Arch. Gen. Psychiatry* 52, 1048–1060.

- Kim, S.C., Jo, Y.S., Kim, I.H., Kim, H., and Choi, J.-S. (2010). Lack of medial prefrontal cortex activation underlies the immediate extinction deficit. *J. Neurosci* 30, 832–837.
- Kjelstrup, K.G., Tuvnes, F.A., Steffenach, H.-A., Murison, R., Moser, E.I., and Moser, M.-B. (2002). Reduced fear expression after lesions of the ventral hippocampus. *Proc. Natl. Acad. Sci. U.S.A.* 99, 10825–10830.
- de Kloet, C.S., Vermetten, E., Geuze, E., Kavelaars, A., Heijnen, C.J., and Westenberg, H.G.M. (2006). Assessment of HPA-axis function in posttraumatic stress disorder: pharmacological and non-pharmacological challenge tests, a review. *J Psychiatr Res* 40, 550–567.
- Kozlovsky, N., Matar, M.A., Kaplan, Z., Kotler, M., Zohar, J., and Cohen, H. (2007). Long-term down-regulation of BDNF mRNA in rat hippocampal CA1 subregion correlates with PTSD-like behavioural stress response. *Int. J. Neuropsychopharmacol.* 10, 741–758.
- Kozlovsky, N., Matar, M.A., Kaplan, Z., Zohar, J., and Cohen, H. (2009). The role of the galaninergic system in modulating stress-related responses in an animal model of posttraumatic stress disorder. *Biol. Psychiatry* 65, 383–391.
- Krömer, S.A., Kessler, M.S., Milfay, D., Birg, I.N., Bunck, M., Czibere, L., Panhuysen, M., Pütz, B., Deussing, J.M., Holsboer, F., et al. (2005). Identification of glyoxalase-I as a protein marker in a mouse model of extremes in trait anxiety. *J. Neurosci* 25, 4375–4384.
- Krugers, H.J., Hoogenraad, C.C., and Groc, L. (2010). Stress hormones and AMPA receptor trafficking in synaptic plasticity and memory. *Nat. Rev. Neurosci.* 11, 675–681.
- Landgraf, R., Kessler, M.S., Bunck, M., Murgatroyd, C., Spengler, D., Zimbelmann, M., Nussbaumer, M., Czibere, L., Turck, C.W., Singewald, N., et al. (2007). Candidate genes of anxiety-related behavior in HAB/LAB rats and mice: focus on vasopressin and glyoxalase-I. *Neurosci Biobehav Rev* 31, 89–102.
- Lennertz, L., Quednow, B.B., Schuhmacher, A., Petrovsky, N., Frommann, I., Schulze-Rauschenbach, S., Landsberg, M.W., Steinbrecher, A., Höfels, S., Pukrop, R., et al. (2011). The functional coding variant Asn107Ile of the neuropeptide S receptor gene (NPSR1) is associated with schizophrenia and modulates verbal memory and the acoustic startle response. *The International Journal of Neuropsychopharmacology / Official Scientific Journal of the Collegium Internationale Neuropsychopharmacologicum (CINP)* 1–11.
- Leonard, S.K., Dwyer, J.M., Sukoff Rizzo, S.J., Platt, B., Logue, S.F., Neal, S.J., Malberg, J.E., Beyer, C.E., Schechter, L.E., Rosenzweig-Lipson, S., et al. (2008). Pharmacology of neuropeptide S in mice: therapeutic relevance to anxiety disorders. *Psychopharmacology (Berl.)* 197, 601–611.
- Leonard, S.K., and Ring, R.H. (2011). Immunohistochemical localization of the neuropeptide S receptor in the rat central nervous system. *Neuroscience* 172, 153–163.

- Lister, R.G. (1987). The use of a plus-maze to measure anxiety in the mouse. *Psychopharmacology (Berl.)* 92, 180–185.
- Liu, X., Zeng, J., Zhou, A., Theodorsson, E., Fahrenkrug, J., and Reinscheid, R.K. (2011). Molecular fingerprint of neuropeptide S-producing neurons in the mouse brain. *J. Comp. Neurol.* 519, 1847–1866.
- Livak, K.J., and Schmittgen, T.D. (2001). Analysis of relative gene expression data using real-time quantitative PCR and the 2(-Delta Delta C(T)) Method. *Methods* 25, 402–408.
- Maren, S., and Holt, W.G. (2004). Hippocampus and Pavlovian fear conditioning in rats: muscimol infusions into the ventral, but not dorsal, hippocampus impair the acquisition of conditional freezing to an auditory conditional stimulus. *Behav. Neurosci.* 118, 97–110.
- Marinova, Z., Vukojevic, V., Surcheva, S., Yakovleva, T., Cebers, G., Pasikova, N., Usynin, I., Hugonin, L., Fang, W., Hallberg, M., et al. (2005). Translocation of dynorphin neuropeptides across the plasma membrane. A putative mechanism of signal transmission. *J. Biol. Chem.* 280, 26360–26370.
- Martin, S., Henley, J.M., Holman, D., Zhou, M., Wiegert, O., van Spronsen, M., Joëls, M., Hoogenraad, C.C., and Krugers, H.J. (2009). Corticosterone alters AMPAR mobility and facilitates bidirectional synaptic plasticity. *PLoS ONE* 4, e4714.
- Mathew, S.J., Price, R.B., and Charney, D.S. (2008). Recent advances in the neurobiology of anxiety disorders: Implications for novel therapeutics. *American Journal of Medical Genetics Part C: Seminars in Medical Genetics* 148C, 89–98.
- McHugh, S.B., Deacon, R.M.J., Rawlins, J.N.P., and Bannerman, D.M. (2004). Amygdala and ventral hippocampus contribute differentially to mechanisms of fear and anxiety. *Behav. Neurosci.* 118, 63–78.
- Meis, S., Bergado-Acosta, J.R., Yanagawa, Y., Obata, K., Stork, O., and Munsch, T. (2008). Identification of a neuropeptide S responsive circuitry shaping amygdala activity via the endopiriform nucleus. *PLoS ONE* 3, e2695.
- Meis, S., Bergado-Acosta, J.R., Yanagawa, Y., Obata, K., Stork, O., and Munsch, T. Identification of a Neuropeptide S Responsive Circuitry Shaping Amygdala Activity via the Endopiriform Nucleus. *PLoS ONE* 3,.
- Mochizuki, T., Kim, J., and Sasaki, K. (2010). Microinjection of neuropeptide S into the rat ventral tegmental area induces hyperactivity and increases extracellular levels of dopamine metabolites in the nucleus accumbens shell. *Peptides* 31, 926–931.
- Ohkubo, K., Okuda, M., and Kaliner, M.A. (1994). Immunological localization of neuropeptide-degrading enzymes in the nasal mucosa. *Rhinology* 32, 130–133.

- Okamura, N., Garau, C., Duangdao, D.M., Clark, S.D., Jüngling, K., Pape, H.-C., and Reinscheid, R.K. (2011). Neuropeptide S enhances memory during the consolidation phase and interacts with noradrenergic systems in the brain. *Neuropsychopharmacology* 36, 744–752.
- Okamura, N., Habay, S.A., Zeng, J., Chamberlin, A.R., and Reinscheid, R.K. (2008). Synthesis and pharmacological in vitro and in vivo profile of 3-oxo-1,1-diphenyl-tetrahydro-oxazolo[3,4-a]pyrazine-7-carboxylic acid 4-fluorobenzylamide (SHA 68), a selective antagonist of the neuropeptide S receptor. *J. Pharmacol. Exp. Ther.* 325, 893–901.
- Okamura, N., Hashimoto, K., Iyo, M., Shimizu, E., Dempfle, A., Friedel, S., and Reinscheid, R.K. (2007). Gender-specific association of a functional coding polymorphism in the Neuropeptide S receptor gene with panic disorder but not with schizophrenia or attention-deficit/hyperactivity disorder. *Prog. Neuropsychopharmacol. Biol. Psychiatry* 31, 1444–1448.
- Okamura, N., Reinscheid, R.K., Ohgake, S., Iyo, M., and Hashimoto, K. (2010). Neuropeptide S attenuates neuropathological, neurochemical and behavioral changes induced by the NMDA receptor antagonist MK-801. *Neuropharmacology* 58, 166–172.
- Olf, M., de Vries, G.-J., Güzelcan, Y., Assies, J., and Gersons, B.P.R. (2007). Changes in cortisol and DHEA plasma levels after psychotherapy for PTSD. *Psychoneuroendocrinology* 32, 619–626.
- Ozsoy, Y., Gungor, S., and Cevher, E. (2009). Nasal delivery of high molecular weight drugs. *Molecules* 14, 3754–3779.
- Pape, H.-C., Jüngling, K., Seidenbecher, T., Lesting, J., and Reinscheid, R.K. (2010). Neuropeptide S: a transmitter system in the brain regulating fear and anxiety. *Neuropharmacology* 58, 29–34.
- Perisic, T., Zimmermann, N., Kirmeier, T., Asmus, M., Tuorto, F., Uhr, M., Holsboer, F., Rein, T., and Zschocke, J. (2010). Valproate and amitriptyline exert common and divergent influences on global and gene promoter-specific chromatin modifications in rat primary astrocytes. *Neuropsychopharmacology* 35, 792–805.
- Pini, S., Cassano, G.B., Simonini, E., Savino, M., Russo, A., and Montgomery, S.A. (1997). Prevalence of anxiety disorders comorbidity in bipolar depression, unipolar depression and dysthymia. *J Affect Disord* 42, 145–153.
- Pitman, R.K., Gilbertson, M.W., Gurvits, T.V., May, F.S., Lasko, N.B., Metzger, L.J., Shenton, M.E., Yehuda, R., and Orr, S.P. (2006). Clarifying the origin of biological abnormalities in PTSD through the study of identical twins discordant for combat exposure. *Ann. N. Y. Acad. Sci.* 1071, 242–254.
- Pitman, R.K., Shin, L.M., and Rauch, S.L. (2001). Investigating the pathogenesis of posttraumatic stress disorder with neuroimaging. *J Clin Psychiatry* 62 Suppl 17, 47–54.

- Posener, J.A., DeBattista, C., Williams, G.H., Chmura Kraemer, H., Kalehzan, B.M., and Schatzberg, A.F. (2000). 24-Hour monitoring of cortisol and corticotropin secretion in psychotic and nonpsychotic major depression. *Arch. Gen. Psychiatry* 57, 755–760.
- Praag, H.M. van, Kloet, E.R. de, and Os, J. van (2004). *Stress, the Brain and Depression* (Cambridge University Press).
- Prochiantz, A., and Joliot, A. (2003). Can transcription factors function as cell-cell signalling molecules? *Nat. Rev. Mol. Cell Biol.* 4, 814–819.
- Raadsheer, F.C., van Heerikhuize, J.J., Lucassen, P.J., Hoogendijk, W.J., Tilders, F.J., and Swaab, D.F. (1995). Corticotropin-releasing hormone mRNA levels in the paraventricular nucleus of patients with Alzheimer's disease and depression. *Am J Psychiatry* 152, 1372–1376.
- Raczka, K.A., Gartmann, N., Mechias, M.-L., Reif, A., Büchel, C., Deckert, J., and Kalisch, R. (2010). A neuropeptide S receptor variant associated with overinterpretation of fear reactions: a potential neurogenetic basis for catastrophizing. *Mol. Psychiatry* 15, 1045, 1067–1074.
- Raiteri, L., Luccini, E., Romei, C., Salvadori, S., and Calò, G. (2009). Neuropeptide S selectively inhibits the release of 5-HT and noradrenaline from mouse frontal cortex nerve endings. *Br. J. Pharmacol* 157, 474–481.
- Rasmusson, A.M., Hauger, R.L., Morgan, C.A., Bremner, J.D., Charney, D.S., and Southwick, S.M. (2000). Low baseline and yohimbine-stimulated plasma neuropeptide Y (NPY) levels in combat-related PTSD. *Biol. Psychiatry* 47, 526–539.
- Rauch, S.L., Shin, L.M., and Phelps, E.A. (2006). Neurocircuitry models of posttraumatic stress disorder and extinction: human neuroimaging research—past, present, and future. *Biol. Psychiatry* 60, 376–382.
- Ravindran, L.N., and Stein, M.B. (2009). Pharmacotherapy of PTSD: premises, principles, and priorities. *Brain Res* 1293, 24–39.
- Ravindran, L.N., and Stein, M.B. (2010a). Pharmacotherapy of post-traumatic stress disorder. *Curr Top Behav Neurosci* 2, 505–525.
- Ravindran, L.N., and Stein, M.B. (2010b). The pharmacologic treatment of anxiety disorders: a review of progress. *J Clin Psychiatry* 71, 839–854.
- Reinscheid, R.K. (2007). Phylogenetic appearance of neuropeptide S precursor proteins in tetrapods. *Peptides* 28, 830–837.
- Reinscheid, R.K., Xu, Y.-L., Okamura, N., Zeng, J., Chung, S., Pai, R., Wang, Z., and Civelli, O. (2005). Pharmacological characterization of human and murine neuropeptide s receptor variants. *J. Pharmacol. Exp. Ther* 315, 1338–1345.
- Revest, J.-M., Kaouane, N., Mondin, M., Le Roux, A., Rougé-Pont, F., Vallée, M., Barik, J., Tronche, F., Desmedt, A., and Piazza, P.V. (2010). The

- enhancement of stress-related memory by glucocorticoids depends on synapsin-Ia/Ib. *Mol. Psychiatry* 15, 1125, 1140–1151.
- Reyes, B.A.S., Fox, K., Valentino, R.J., and Van Bockstaele, E.J. (2006). Agonist-induced internalization of corticotropin-releasing factor receptors in noradrenergic neurons of the rat locus coeruleus. *Eur. J. Neurosci* 23, 2991–2998.
- Rizzi, A., Vergura, R., Marzola, G., Ruzza, C., Guerrini, R., Salvadori, S., Regoli, D., and Calo, G. (2008). Neuropeptide S is a stimulatory anxiolytic agent: a behavioural study in mice. *Br. J. Pharmacol* 154, 471–479.
- Rodrigues, H., Figueira, I., Gonçalves, R., Mendlowicz, M., Macedo, T., and Ventura, P. (2011). CBT for pharmacotherapy non-remitters-a systematic review of a next-step strategy. *J Affect Disord* 129, 219–228.
- Rossi, S., De Capua, A., Tavanti, M., Calossi, S., Polizzotto, N.R., Mantovani, A., Falzarano, V., Bossini, L., Passero, S., Bartalini, S., et al. (2009). Dysfunctions of cortical excitability in drug-naïve posttraumatic stress disorder patients. *Biol. Psychiatry* 66, 54–61.
- Roth, A.L., Marzola, E., Rizzi, A., Arduin, M., Trapella, C., Corti, C., Vergura, R., Martinelli, P., Salvadori, S., Regoli, D., et al. (2006). Structure-activity studies on neuropeptide S: identification of the amino acid residues crucial for receptor activation. *J. Biol. Chem* 281, 20809–20816.
- Rudolph, U., and Knoflach, F. (2011). Beyond classical benzodiazepines: novel therapeutic potential of GABAA receptor subtypes. *Nat Rev Drug Discov* 10, 685–697.
- Saban, R., Gerard, N.P., Saban, M.R., Nguyen, N.-B., DeBoer, D.J., and Wershil, B.K. (2002). Mast cells mediate substance P-induced bladder inflammation through an NK1 receptor-independent mechanism. *American Journal of Physiology - Renal Physiology* 283, F616 -F629.
- Sah, R., Ekhtor, N.N., Strawn, J.R., Sallee, F.R., Baker, D.G., Horn, P.S., and Geraciotti, T.D., Jr (2009). Low cerebrospinal fluid neuropeptide Y concentrations in posttraumatic stress disorder. *Biol. Psychiatry* 66, 705–707.
- Santini, E., Ge, H., Ren, K., Peña de Ortiz, S., and Quirk, G.J. (2004). Consolidation of fear extinction requires protein synthesis in the medial prefrontal cortex. *J. Neurosci* 24, 5704–5710.
- Schmidt, U., Holsboer, F., and Rein, T. (2011). Epigenetic aspects of posttraumatic stress disorder. *Dis. Markers* 30, 77–87.
- Selye, H. (1956). *The stress of life* (New York, NY, US: McGraw-Hill).
- Shea, A., Walsh, C., Macmillan, H., and Steiner, M. (2005). Child maltreatment and HPA axis dysregulation: relationship to major depressive disorder and post traumatic stress disorder in females. *Psychoneuroendocrinology* 30, 162–178.

- Shi, C., Wang, L., Wu, Y., Wang, P., Gan, Z., Lin, K., Jiang, L., Xu, Z., and Fan, M. (2010). Intranasal administration of nerve growth factor produces antidepressant-like effects in animals. *Neurochem. Res* 35, 1302–1314.
- Shin, L.M., and Liberzon, I. (2009). The Neurocircuitry of Fear, Stress, and Anxiety Disorders. *Neuropsychopharmacology* 35, 169–191.
- Shin, L.M., Orr, S.P., Carson, M.A., Rauch, S.L., Macklin, M.L., Lasko, N.B., Peters, P.M., Metzger, L.J., Dougherty, D.D., Cannistraro, P.A., et al. (2004). Regional cerebral blood flow in the amygdala and medial prefrontal cortex during traumatic imagery in male and female Vietnam veterans with PTSD. *Arch. Gen. Psychiatry* 61, 168–176.
- Shin, L.M., Rauch, S.L., and Pitman, R.K. (2006). Amygdala, medial prefrontal cortex, and hippocampal function in PTSD. *Ann. N. Y. Acad. Sci* 1071, 67–79.
- Shiromani, P., Keane, T., and LeDoux, J.E. (2009). *Post-Traumatic Stress Disorder: Basic Science and Clinical Practice* (Humana Press).
- Si, W., Aluisio, L., Okamura, N., Clark, S.D., Fraser, I., Sutton, S.W., Bonaventure, P., and Reinscheid, R.K. (2010). Neuropeptide S stimulates dopaminergic neurotransmission in the medial prefrontal cortex. *J. Neurochem* 115, 475–482.
- Siegmund, A., Langnaese, K., and Wotjak, C.T. (2005). Differences in extinction of conditioned fear in C57BL/6 substrains are unrelated to expression of alpha-synuclein. *Behav. Brain Res* 157, 291–298.
- Siegmund, A., and Wotjak, C.T. (2007). A mouse model of posttraumatic stress disorder that distinguishes between conditioned and sensitised fear. *J Psychiatr Res* 41, 848–860.
- Smith, K.L., Patterson, M., Dhillo, W.S., Patel, S.R., Semjonous, N.M., Gardiner, J.V., Ghatei, M.A., and Bloom, S.R. (2006). Neuropeptide S stimulates the hypothalamo-pituitary-adrenal axis and inhibits food intake. *Endocrinology* 147, 3510–3518.
- Southwick, S.M., Bremner, J.D., Rasmusson, A., Morgan, C.A., 3rd, Arnsten, A., and Charney, D.S. (1999a). Role of norepinephrine in the pathophysiology and treatment of posttraumatic stress disorder. *Biol. Psychiatry* 46, 1192–1204.
- Southwick, S.M., Paige, S., Morgan, C.A., 3rd, Bremner, J.D., Krystal, J.H., and Charney, D.S. (1999b). Neurotransmitter alterations in PTSD: catecholamines and serotonin. *Semin Clin Neuropsychiatry* 4, 242–248.
- Steckler, T., Kalin, N.H., and Reul, J.M.H.M. (2005). *Handbook of Stress and the Brain (Two-Volume Set)* (Elsevier Science).
- Steckler, T., and Risbrough, V. (2011). Pharmacological treatment of PTSD - Established and new approaches. *Neuropharmacology*.

- Stenzel-Poore, M.P., Heinrichs, S.C., Rivest, S., Koob, G.F., and Vale, W.W. (1994). Overproduction of corticotropin-releasing factor in transgenic mice: a genetic model of anxiogenic behavior. *J. Neurosci.* *14*, 2579–2584.
- Tan, K.R., Brown, M., Labouèbe, G., Yvon, C., Creton, C., Fritschy, J.-M., Rudolph, U., and Lüscher, C. (2010). Neural bases for addictive properties of benzodiazepines. *Nature* *463*, 769–774.
- Tanaka, H., Grooms, S.Y., Bennett, M.V., and Zukin, R.S. (2000). The AMPAR subunit GluR2: still front and center-stage. *Brain Res.* *886*, 190–207.
- Thorne, R.G., Emory, C.R., Ala, T.A., and Frey, W.H. (1995). Quantitative analysis of the olfactory pathway for drug delivery to the brain. *Brain Res* *692*, 278–282.
- Thorne, R.G., and Frey, W.H. (2001). Delivery of neurotrophic factors to the central nervous system: pharmacokinetic considerations. *Clin Pharmacokinet* *40*, 907–946.
- Thorne, R.G., Hanson, L.R., Ross, T.M., Tung, D., and Frey, W.H. (2008). Delivery of interferon-beta to the monkey nervous system following intranasal administration. *Neuroscience* *152*, 785–797.
- Thorne, R.G., Pronk, G.J., Padmanabhan, V., and Frey, W.H. (2004). Delivery of insulin-like growth factor-I to the rat brain and spinal cord along olfactory and trigeminal pathways following intranasal administration. *Neuroscience* *127*, 481–496.
- Trapella, C., Pela, M., Del Zoppo, L., Calo, G., Camarda, V., Ruzza, C., Cavazzini, A., Costa, V., Bertolasi, V., Reinscheid, R.K., et al. (2011). Synthesis and separation of the enantiomers of the neuropeptide S receptor antagonist (9R/S)-3-oxo-1,1-diphenyl-tetrahydro-oxazolo[3,4-a]pyrazine-7-carboxylic acid 4-fluoro-benzylamide (SHA 68). *J. Med. Chem.* *54*, 2738–2744.
- True, W.R., Rice, J., Eisen, S.A., Heath, A.C., Goldberg, J., Lyons, M.J., and Nowak, J. (1993). A twin study of genetic and environmental contributions to liability for posttraumatic stress symptoms. *Arch. Gen. Psychiatry* *50*, 257–264.
- Tyrka, A.R., Price, L.H., Gelernter, J., Schepker, C., Anderson, G.M., and Carpenter, L.L. (2009). Interaction of childhood maltreatment with the corticotropin-releasing hormone receptor gene: effects on hypothalamic-pituitary-adrenal axis reactivity. *Biol. Psychiatry* *66*, 681–685.
- Uchida, R.R., Del-Ben, C.M., Busatto, G.F., Duran, F.L.S., Guimarães, F.S., Crippa, J.A.S., Araújo, D., Santos, A.C., and Graeff, F.G. (2008). Regional gray matter abnormalities in panic disorder: a voxel-based morphometry study. *Psychiatry Res* *163*, 21–29.
- Vendelin, J., Bruce, S., Holopainen, P., Pulkkinen, V., Ryttilä, P., Pirskanen, A., Rehn, M., Laitinen, T., Laitinen, L.A., Haahtela, T., et al. (2006). Downstream target genes of the neuropeptide S-NPSR1 pathway. *Hum. Mol. Genet* *15*, 2923–2935.

- Vythilingam, M., Gill, J.M., Luckenbaugh, D.A., Gold, P.W., Collin, C., Bonne, O., Plumb, K., Polignano, E., West, K., and Charney, D. (2010). Low early morning plasma cortisol in posttraumatic stress disorder is associated with comorbid depression but not with enhanced glucocorticoid feedback inhibition. *Psychoneuroendocrinology* 35, 442–450.
- Wignall, E.L., Dickson, J.M., Vaughan, P., Farrow, T.F.D., Wilkinson, I.D., Hunter, M.D., and Woodruff, P.W.R. (2004). Smaller hippocampal volume in patients with recent-onset posttraumatic stress disorder. *Biol. Psychiatry* 56, 832–836.
- Xu, Y.-L., Gall, C.M., Jackson, V.R., Civelli, O., and Reinscheid, R.K. (2007). Distribution of neuropeptide S receptor mRNA and neurochemical characteristics of neuropeptide S-expressing neurons in the rat brain. *J. Comp. Neurol* 500, 84–102.
- Xu, Y.-L., Reinscheid, R.K., Huitron-Resendiz, S., Clark, S.D., Wang, Z., Lin, S.H., Brucher, F.A., Zeng, J., Ly, N.K., Henriksen, S.J., et al. (2004). Neuropeptide S: A Neuropeptide Promoting Arousal and Anxiolytic-like Effects. *Neuron* 43, 487–497.
- Yamamoto, S., Morinobu, S., Fuchikami, M., Kurata, A., Kozuru, T., and Yamawaki, S. (2008). Effects of single prolonged stress and D-cycloserine on contextual fear extinction and hippocampal NMDA receptor expression in a rat model of PTSD. *Neuropsychopharmacology* 33, 2108–2116.
- Yehuda, R., Brand, S., and Yang, R.-K. (2006). Plasma neuropeptide Y concentrations in combat exposed veterans: relationship to trauma exposure, recovery from PTSD, and coping. *Biol. Psychiatry* 59, 660–663.
- Yehuda, R., Cai, G., Golier, J.A., Sarapas, C., Galea, S., Ising, M., Rein, T., Schmeidler, J., Müller-Myhsok, B., Holsboer, F., et al. (2009). Gene expression patterns associated with posttraumatic stress disorder following exposure to the World Trade Center attacks. *Biol. Psychiatry* 66, 708–711.
- Yehuda, R., Kahana, B., Binder-Brynes, K., Southwick, S.M., Mason, J.W., and Giller, E.L. (1995). Low urinary cortisol excretion in Holocaust survivors with posttraumatic stress disorder. *Am J Psychiatry* 152, 982–986.
- Yehuda, R., Koenen, K.C., Galea, S., and Flory, J.D. (2011). The role of genes in defining a molecular biology of PTSD. *Dis. Markers* 30, 67–76.
- Yehuda, R., and LeDoux, J. (2007). Response variation following trauma: a translational neuroscience approach to understanding PTSD. *Neuron* 56, 19–32.
- Yoshida, K., Kim, J., Nakajima, K., Oomura, Y., Wayner, M.J., and Sasaki, K. (2010). Electrophysiological effects of neuropeptide S on rat ventromedial hypothalamic neurons in vitro. *Peptides* 31, 712–719.
- Zhang, Y., Filiou, M.D., Reckow, S., Gormanns, P., Maccarrone, G., Kessler, M.S., Frank, E., Hamsch, B., Holsboer, F., Landgraf, R., et al. (2011). Proteomic

- and metabolomic profiling of a trait anxiety mouse model implicate affected pathways. *Mol. Cell Proteomics* 10, M111.008110.
- Zhao, Z., Huang, L., Wu, H., Li, Y., Zhang, L., Yin, Y., Xiang, Z., and Zhao, Z. (2010). Neuropeptide S mitigates spatial memory impairment induced by rapid eye movement sleep deprivation in rats. *Neuroreport* 21, 623–628.
- Zhu, H., Mingler, M.K., McBride, M.L., Murphy, A.J., Valenzuela, D.M., Yancopoulos, G.D., Williams, M.T., Vorhees, C.V., and Rothenberg, M.E. (2010). Abnormal response to stress and impaired NPS-induced hyperlocomotion, anxiolytic effect and corticosterone increase in mice lacking NPSR1. *Psychoneuroendocrinology* 35, 1119–1132.
- Zushida, K., Sakurai, M., Wada, K., and Sekiguchi, M. (2007). Facilitation of extinction learning for contextual fear memory by PEPA: a potentiator of AMPA receptors. *J. Neurosci* 27, 158–166.

Acknowledgments

This work could not have existed in its current form without contributions from many wonderful people, all of whom I wish to acknowledge at this point.

First and foremost, my thanks go to Dr. Ulrike Schmidt (Ulli), the head of my research group and the greatest supervisor I could ever have wanted for myself. Hers were the ideas from which this work developed. I owe her much for giving me the opportunity to work with her; for everything she has taught me about science and life; for her unfaltering support and patience; and for keeping everything she promised. I would like to thank my PhD advisor, Professor Rainer Landgraf, for his support, teaching and wonderful collaboration during my project. I gratefully acknowledge all the members of my defense committee for having taken the time to read and evaluate my work.

I am also most grateful to Professor Florian Holsboer for giving me the opportunity to do my PhD thesis at his institute, and for his continued and kind support of my work.

My entire research group deserves to be gratefully mentioned here: Leonie Herrmann and Dr. Dominik Büll for their great input and feedback; Bozidar Novak and Christine Huber for all the technical assistance they have given me over the past two years; and all my wonderful office colleagues for their emotional support and for making this the nicest workplace I have yet known.

Much of the work presented here was performed within collaborations at my institute. From Professor Landgraf's group I would like to thank Markus Nussbaumer for all the help with almost every single animal experiment; and Yi-Chun Yen for the great collaboration. I am most grateful to Drs. Matthias Eder and Julien Dine for the very fruitful and ongoing collaboration and for the great input on my projects. I am indebted to PD Dr. Carsten T. Wotjak for providing us with the animal model of PTSD and for contributing his expertise on the design of behavioral experiments and on statistical evaluation; and to Kathrin Henes for her help with the behavioral experiments.

Last but not least, exceptional credit goes to my friends and most especially to my family, for having borne with me through the many ups and downs of my work, for

having encouraged and supported me, and for their belief that I would, in the end, finally make it to this point.

Curriculum vitae

Name: Irina Alexandra Ionescu

Date of birth: 30.08.1985

Nationality: Romanian

EDUCATION

- 08/2009-07/2012 **PhD** at the Max Planck Institute of Psychiatry, Munich, Germany, within the International Max Planck Research School (IMPRS) for Molecular and Cellular Life Sciences
- 2007-2009 **MSc Neurosciences**, IMPRS of Neurosciences and Molecular Biology, Georg-August-University, Göttingen, Germany
- 2004-2007 **BSc Biomedicine**, Julius-Maximilians-University, Würzburg, Germany
- 2004 **Abitur** at the German Goethe-Gymnasium, Bucharest, Romania

RESEARCH PROJECTS

- **PhD thesis:** “Characterization of Neuropeptide S (NPS) in view of its potential as a novel anxiolytic therapy” – final grade: 0.79 (= magna cum laude = very good)
- **Master’s thesis:** „Inducing the early-onset, inflammatory phenotype of demyelinating cerebral childhood adrenoleukodystrophy (CCALD) in mice lacking ABCD1”, Max Planck Institute of Experimental Medicine, Göttingen, Germany – final grade: 1.15 (= A = excellent)
- **Bachelor’s thesis:** „Purification and viral vector-mediated transduction of murine hematopoietic stem cells”, Institute of Virology and Immunobiology, Würzburg, Germany – final grade: 1.0 (= A = excellent)

SCHOLARSHIPS AND AWARDS

- 07/2012 **Travel grant from the German Neuroscience Society** for attending the 8th FENS Forum of Neuroscience, Barcelona, Spain
- 10/2004-08/2009 **Scholarship for highly qualified graduates of German high-schools abroad, DAAD (German Academic Exchange Service)**

ACADEMIC ENGAGEMENT

- 05/2011-03/2012 **Organiser of the PhD student symposium Interact 2012** (area of responsibility: Group Speaker of the Scientific Programme Team)
- 06-08/2011 **Mentoring of a Canadian undergraduate student within the DAAD program Research in Science and Engineering (RISE)**

MEETING ABSTRACTS

- 07/2012 **8th FENS Forum of Neuroscience, Barcelona, Spain**
 Poster: "Intranasal application of Neuropeptide S (NPS) identifies the hippocampus as a novel NPS target region that mediates NPS-elicited anxiolytic effects"
- 10/2011 **Biomarkers, Functional Genomics & Novel Antidepressants**
 – Part III: Drug Development and Biomarker Identification, Schloss Ringberg, Germany
 Talk: "The NPS-NPSR pathway – towards a novel anxiolytic therapy"

List of publications

1. Touma C, Gassen NC, Herrmann L, Cheung-Flynn J, Büll DR, **Ionescu IA**, Heinzmann JM, Knapman A, Siebertz A, Depping AM, Hartmann J, Hausch F, Schmidt MV, Holsboer F, Ising M, Cox MB, Schmidt U*, and Rein T*. (2011). FK506 binding protein shapes stress responsiveness: modulation of neuroendocrine reactivity and coping behavior. *Biol Psychiatry* 70, 928-36.

2. **Ionescu IA**, Dine J*, Yen YC*, Buell DR, Herrmann L, Holsboer F, Eder M, Landgraf R, and Schmidt U. (2012). Intranasally administered Neuropeptide S (NPS) exerts anxiolytic effects following internalization into NPS receptor-expressing neurons. *Neuropsychopharmacology* 37, 1323-37. #

3. Herrmann L, **Ionescu IA**, Henes K, Golub Y, Wang NXR, Buell DR, Holsboer F, Wotjak CT, and Schmidt U. (2012). Long-Lasting Hippocampal Synaptic Protein Loss in a Mouse Model of Posttraumatic Stress Disorder. *PLoS One*, in press.

4. Dine J*, **Ionescu IA***, Stepan J, Yen YC, Holsboer F, Landgraf R, Eder M*, and Schmidt U*. (submitted). Identification of a significant role for the ventral hippocampus in neuropeptide S-elicited anxiolysis. *Cereb Cortex*. #

*: These authors contributed equally to this work.

#: Parts of this thesis were published or will be published in these articles.

Declaration / Erklärung

Hiermit versichere ich, dass ich die vorliegende Arbeit selbstständig und nur mit den angegebenen Quellen und Hilfsmitteln angefertigt habe. Alle Ausführungen, die wörtlich oder sinngemäß übernommen wurden, sind als solche gekennzeichnet. Weiterhin erkläre ich, dass diese Dissertation nicht ganz oder in wesentlichen Teilen einer anderen Prüfungskommission vorgelegt wurde. Auch versichere ich, dass ich mich nicht anderweitig ohne Erfolg einer Doktorprüfung unterzogen habe.

München, 28. Februar 2012

Irina Ionescu.